1-1-2011

# Dynamics of nanoparticles in complex fluids.

Rami Ahmad Saleh Omari
*Wayne State University,*

# DYNAMICS OF NANOPARTICLES IN COMPLEX FLUIDS

by

**RAMI A. OMARI**

**DISSERTATION**

Submitted to the Graduate School

of Wayne State University,

Detroit, Michigan

in partial fulfillment of the requirements

for the degree of

**DOCTOR OF PHILOSOPHY**

2011

MAJOR: PHYSICS (Condensed Matter)

Approved by:

_____

Advisor Date

_____

_____

_____

_____

## DEDICATION

*To my parents whose support motivated me to continue my graduate education and to my brothers: Rabie, Wadie, and Ehsan.who surrounded me with love and encouragement.*

## ACKNOWLEDGEMENTS

I have been fortunate to be surrounded by many great people and it is my great pleasure to thank them for their support, motivation and encouragement during my academic career. First, I would like to express my sincere gratitude towards my advisor Prof. Ashis Mukhopadhyay, for his endless support and valuable guidance throughout the route of my Ph.D. degree. He introduced me to the fascinating world of soft matter physics, which has been my primary research focus for the past four years. I surely benefited and learnt a lot from his knowledge in soft condensed matter field and from his method of research work supervision.. His guidance during my experiments and the preparation of our manuscripts was of critical importance. In addition, he is considerate to the students working in his research group. Many thanks also go to my senior lab colleague, Chris Grabowski for his patience in guiding me in the lab and teaching me to work on different experimental techniques availabe in the lab including Fluorescence Correlation Spectroscopy (FCS), ellipsometry , and Langmuir-Blodget trough. He also taght me how to use different softwares that we were using to analyse the data collected during the experiments including: DIAdem, Igor, Origin, and Labview. In addition, I would like to thank Venkatesh Sabbo Rao for being such an interesting lab colleague and for the many useful disscution on FCS. I would like to thank Indermeet Kohli, Andrew Aneese, and Laura Gunther for being such an interesting lab partners. Special consideration goes out to my dissertation committee as a whole. They have taken time out of their busy schedules to ensure my thesis meets the standards for publication. Finally, special thanks go out to my family for their support and love throughout all of my academic pursuits.

## TABLE OF CONTENTS

## LIST OF TABLES

## LIST OF FIGURES

# CHAPTER 1

## Introduction

Soft condensed matter is a subfield of condensed matter comprising materials in states of matter that are neither simple liquids nor crystalline solids. These materials are extremely soft, it can be destroyed easily by mechanical means, and that is why we call it soft. These materials are familiar from our everyday life- glues, paints, soaps, and plastics are examples of soft materials. Much of the food we eat and indeed ourselves classed as soft matter[1].

Soft matter materials include colloidal dispersions, polymers, amphiphiles, and liquid crystals. Although these materials seem to be very different, they have common structural and dynamical properties that we can consider them as a class. One of these properties is their intermediate mesoscopic length scales. Colloidal dispersions are less than 1μm in size, polymer chains and the self-assembled structures formed by amphiphilic molecules have dimensions in the range of 10 nm which is larger than the atomic size (> 0.1 nm) and smaller than the macroscopic objects (<10 μm). Another feature of soft matter is that they undergo Brownian motion. This means that they are subjected to random forces from thermal motion of the surrounding molecules[2]. The small size of soft matter structures allow them to fluctuate in any thermal system and the typical energies between the bonds of the structures are comparable to thermal energies. Therefore, soft matter systems can be considered as a constant state of random motion; polymer chains in solution or melt are continually writhing and turning and the colloidal particles diffuse in solutions due to Brownian motion[1].

Soft matter systems have a tendency to self-assemble. These systems move toward equilibrium to minimize the free energy. The balance of the energy and the entropy lead to

complex structures of soft matter systems. This self-assembly can occur at the levels of molecules such as the block co-polymer systems[3], or on the mesoscopic level such as amphiphilic molecules. These amphiphilic molecules consist of hydrophilic "water loving" part and hydrophobic "water hating" part; therefore when immersed in aqueous solution, the molecules assemble themselves to form remarkable structures such as micelles which may be spherical or cylindrical in shape, bilayers, and vesicles. Moreover, these aggregates may themselves associate in ordered arrangements to produce complex phases.

Condensed matter is held together by intermolecular forces, which determine their bulk and macroscopic properties. In solids, each molecule is locked on crystal lattice point and there is a direct relationship between the energy of the bonds and the stiffness. In liquids, on the contrary, the molecules are not locked rigidly into specific positions, but its position relative to its neighbor's, changes on a characteristic relaxation time. In soft matter, characteristic relaxation times fall into a range of values perceptible to the human senses, and these materials behave in a way that is neither solid-like nor liquid like-they are viscoelastic. In many systems, the relaxation time diverge as the temperature is lowered leading to a non-equilibrium state of matter-a glass-in which liquid-like property such as lack of order and solid-like elastic property appeared at the same time[1]. The term 'soft' originate from macroscopic mechanical properties. Many soft materials have weak ordering on the contrary of the three-dimensional atomic long-range order found in crystalline solid. However, there is a degree of local order similar to that one in liquid. The intermolecular force is responsible for the ordering of soft materials. These forces are a balance of repulsive interactions at short distances and attractive interactions that predominate at larger length-scale. Repulsive force results from the overlap of the electrons when atoms approach another. The origin of this repulsion is essentialy quantum mechanical due to Pauli's

exclusion principle. Attractive interactions in uncharged molecules result from van der Waals forces, which arise from interactions between dipoles. All such molecules can be thought of as having constantly fluctuating random dipole moment. This interaction has the same order of magnitude as thermal energy $k_B$T at room temperature. Therefore, there is a probability that the bond energy may be broken and subsequently reformed by thermal agitation.

Understanding condensed matter systems' behavior depends on accurate models of the microscopic behavior of its components at the molecular and atomic scale, obtained to understand the macrosopic properties. To access the microscopic behavior of these systems, adequate probes are required. There are two aspects of interest related to soft matter systems. The first one is related to the sample structure, which can be accessed by direct microscopy, but with visible light, this access is limited in resolution to a few hundred of nanometer and restricted to transparent samples. However, progress in electron microscopy provides structural information to subnanometer resolution, but the gained information is limited to a few atomic layers on the sample surface[4]. The real space images obtained using such direct imaging techniques give us structural information that can be understood in terms of atomic positions. The second aspect of interest is related to the dynamics of the sample, which can be accessed by scattering methods that can reveal the characteristic microscopic excitations in the sample. Compared to imaging, the information obtained by scattering methods cannot be directly interpreted in real space. However, the detailed description is not that important to understand the microscopic properties but instead the typical correlations in the atomic positions and motions. The advantage of the scattering methods is that they can reveal these correlations over a huge range both of length and time scales including at the microscopic scales relevant for the intrinsic particle interaction[4]. In scattering experiment, particles or waves emitted by a source,

are deflected by the sample to inspect, and the scattered intensity is collected by a detector. Examples of the scattering techniques are dynamic light scattering (DLS) and fluorescence correlation spectroscopy (FCS) which is the counterpart to DLS where the former use incoherent (fluorescence) light while the latter uses coherent light. Other types of scattering are X-ray and neutron beams, which have much smaller wavelength than light so it can be used to probe much smaller features than visible light.

A brief description of the major classes of soft matter is introduced here before progressing further. Colloidal dispersions can be defined as a microscopically heterogeneous system where particles of solids or droplet of liquid with dimensions in the range between 1 nm to 1 μm are dispersed in a liquid medium[1, 2]. Paint, ink, mayonnaise, and ice cream are familiar examples of such systems. Moreover, milk and blood, which are biological fluids, are considered as colloidal dispersions. Because of the small size of the colloidal particles, their surface to volume ratio is large, and many molecules lie close to the interface between one phase and another[2]. Therefore, they are characterized with high area of interface associated with a substantial amount of interfacial energy. Despite this large energy, colloidal dispersions are characterized by their stability, which prevent colloidal particles to combine forming larger aggregates in order to reduce the interfacial energy. Gravity is one force that may destabilize a dispersion. If the dispersed particles are denser than the dispersing fluid, the particles have the tendency to sediment. Opposing this tendency is the Brownian motion of the particles. As the dispersed particles become smaller, the Brownian motion overcomes gravity. At small enough size, the effect of gravity is minimized to destabilize the dispersion. If the particles encounter one another and come into contact, they will stick irreversibly forming larger assembly in a process known as aggregation. The process of reversible aggregation is called flocculation. To prevent

colloidal aggregation, the forces between the colloidal particles, which are normally the attractive van der Waals interactions, must be changed to make the particles repel each other. This can be achieved by exploiting electrostatic forces in charge stabilization, or by attaching polymers chains to the surface of them in steric stabilization[1]. Phase transitions and critical phenomena such as critical slowing down of diffusion and critical opalescence are some of the phenomena that colloidal systems have in common with molecular systems. Due to their large size and slow dynamics, the experimental study of colloids is much simpler than for molecular systems. For example, instead of using X-ray or neutron scattering, light scattering and microscopy can be used in many cases. The slow dynamics of colloids gives rise to non-equilibrium phenomena including shear thinning which is a very useful property in paint. At high shear rates, the viscosity of the paints should be small so that the paint can be brought to the wall. After that, the paint should stay on the wall and not slide off the wall under gravity. Hence, at low shear rates the viscosity of the paint should be large[4].

The technology of preparing and processing colloids is of industrially importance since long time ago. However, it is recently that physical chemists and physicists have started to probe the physical chemical basis of colloidal stability. Better knowledge of the nature of interpaticle interactions have led to profound understanding of the behavior of colloids. This knowledge is leading to a new era of colloid science, where materials can be designed for specific applications. For example, a group of researchers presented a novel method for creating asymmetrical particles with unusual, flattened shapes from colloidal latex microspheres pinned at an oil−water interface[5]. “The shape and degree of asymmetry are controlled by incubating particles for minutes to tens of minutes at an elevated temperature. Fluid interfaces also provide interesting possibilities for tuning the chemistry and shape of the particles further. By changing the surface

wetting properties, it should be possible to generate an even greater variety of shapes by controlling the relative portions of the particle in each phase" (Fig.1.1).

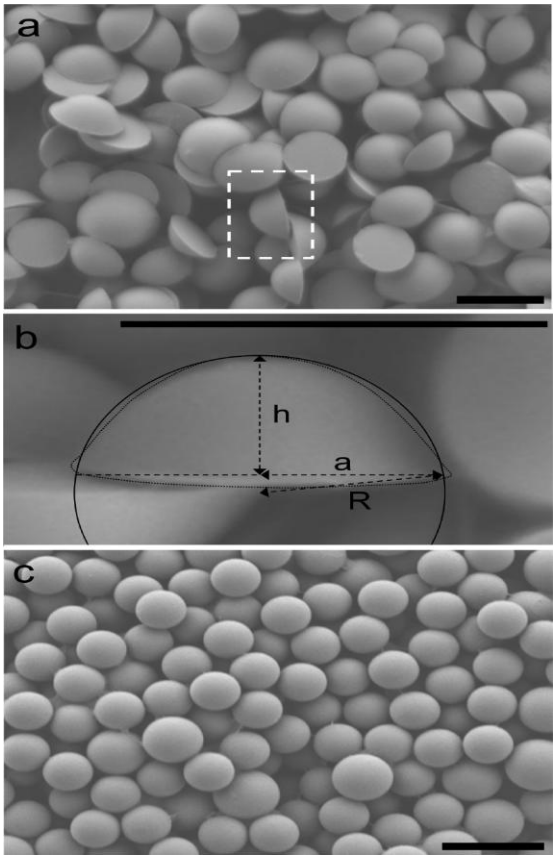


Fig. 1.1 (a) SEM image of asymmetric particles formed at an oil-water interface. (b)Magnified image of a single particle. (c) Original spherical particles. The scale bars are 5 μm.(Park 2010)

The second large class of soft matter is polymers. A polymer is a large molecule composed of many repeating elementary units, called monomers. These monomers are connected to each other by covalent bonds. In the simplest case, polymers are long, linear chain molecules. Such polymers are linear homopolymers. The entire structure of a polymer is generated during a process by which the monomers are covalently bonded together called polymerization, or by the variation of the polymer architecture. On large distances compared to the size of a monomer, the chemical structure of the building block play a minor role, and the properties of the chain are

determined by the statistical mechanics of the chain, essentially the chain entropy. Many properties of polymers are direct consequences of the *central limit theorem*, which is the law of large numbers. This theorem states that Gaussian distribution governs the most probable spatial conformation of large number of monomers. Therefore, the laws of statistics are universally valid[4]. One of the universal characteristic of polymers is the fact that two molecules cannot cross each other; this introduces the effect of entanglement, which gives striking viscoelastic effects in polymer melts and solutions. In addition, properties derived from specific chemical structure of the monomers play a role in determine the properties of the chain. For example, the microstructure of polymer, which can be regular or random, determines whether the polymer crystallizes or not. Moreover, the miscibility of polymer systems is very sensitive to the chemical structure of the chain. In addition, transport properties such as diffusion are determined by friction coefficient, which is specific for a given polymer. The interplay between universal and specific properties is one of the major challenges of polymer science[4].

The development of methods for the controlled synthesis of polymers is one of the most important technological advances of this century. Polymer materials are used everywhere because they are durable, simple to produce and easy to process, and because their mechanical properties are very versatile; the same polymer can flow viscously, react like a rubber, or show a pronounced brittleness. More recently, polymers can be modified to have specific properties such as high strength (in fibers) or electrical conductivity. For example, the synthesis of a conjugated organic polymer has been widely used as a conductive material in devices such as light-emitting diodes, televisions and solar cells. In a paper published in PNAS[6]., a group of researchers succeed in synthesizing highly structured short chains of polymer poly(3,4-ethylenedioxythiophene), or PEDOT (Fig 1.2) could potentially have an impact on everyday

electronic products. PEDOT has been used in electronic application for its transparency, ductility, and stability of its conducting, or doped state. Therefore, it is used in organic light emitting diodes, which is found in many electronic devices such as televisions and computer monitors. It may soon be possible to build integrated circuits from polymers. Moreover, our developing knowledge of the structure and the properties of synthetic polymers will be important to our exploration and exploitation of biopolymers such as DNA and proteins. Engineering of biomaterials is expected to be the next important technological advances to humankind[6].

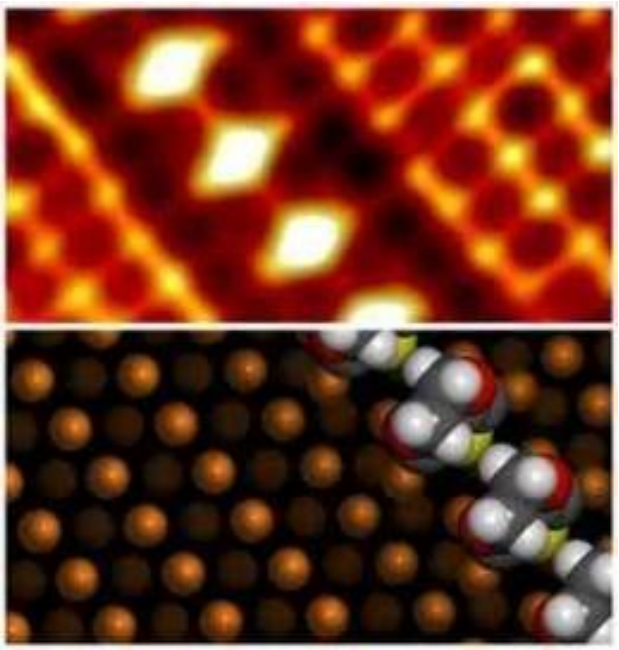

Fig 1.2 A high-resolution scanning tunneling microscope image (top) and density functional theory-calculated structures (bottom) reveal the formation of a well-organized PEDOT polymer. (Lipton-Duffin 2010)[6]

Liquid crystal state is a new state of matter, which was discovered in the nineteenth century. The term liquid crystal refers to a phase formed between a crystal and a liquid with a degree of order intermediate between the molecular disorder of the liquid and the regular structure of a crystal[1]. The most important property of liquid crystal phases is that the molecules can have long-range orientational order. This will be possible if the molecules are anisotropic,

whether this results from rod-like or disc-like shape. Molecules that are able to form liquid crystal phases are called mesogens. Liquid crystal phases can be divided into two classes: thermotropic and lyotropic. The former exhibit a phase transition into the liquid crystal phase as the temperature is changed while the latter exhibit transitions as a function of both temperature and concentration of liquid crystal molecules in a solvent. Thermotropic liquid crystal phases are formed by pure mesogens in a certain temperature range, in which heat is generated or consumed. Lyotropic liquid crystal phases form in solution, and the concentration controls the liquid crystallinity. Thermotropic liquid crystal phase are formed by anisotropic molecules with long-range oriental order, and some degree of translational order[2]. Understanding the correlation between the molecular structure and the physical properties of thermotropic liquid crystals are important, and they are exploited in liquid crystal displays (LCDs), digital watches, and other electronic equipments. The simplest phase of liquid crystal phases is the nematic phase-here, the molecules have no long-range positional order, but they possess long-rang orientational order. Thus, the nematic phase can be considered to be anisotropic liquid. The nematc phases formed by chiral molecules are called chiral nematics or more commonly cholestrerics. A more ordered phase is the smectic phase – here, the molecules maintain the orientational order and they gain long-range positional order in one dimension. Phases with two-dimensional positional order can be formed by disc-like molecules then being termed as columnar phase.

Recently, the previously largely independent research fields of colloids, membranes, microemulsions, and polymers have been integrated in the new research field soft matter. Many phenomena in these systems have the same underlying physical mechanics. Moreover, it has been recognized that combinations of these systems, like for example polymers and colloids, exhibit new properties which are found in each system separately. These mixed systems have a

higher degree of complexity than the separate systems. In order to understand their behavior, knowledge from each subfields of soft matter has to be put together. An important part of this complexity is the effective interactions between the macromolecules which, in complex systems, are not limited to the coulomb and quantum-mechanical interactions. Instead, it depends on the many degrees of freedom of the solvent, and it is already the result of a thermodynamic average. One of these complex systems is the mixture of nanoparticles with macromolecules such as polymers, proteins, etc. Understanding the interactions in these systems is essential for solving various problems in technological and medical fields, such as developing high performance polymeric materials, chromatography, and drug delivery vehicles. Many experimental and theoretical studies have been done to understand the structural, mechanical and rheological properties of macromolecules at and near flat surfaces. Several experiments have indicated that the local density, segmental packing, conformation, and mobility of the chains close to an interface are significantly different compared to the bulk[7-14]. However, very little is known at the molecular level about the interaction of macromolecules with nanoparticles, whose size approaches to the average size of the molecule. Lack of such knowledge is an important problem, because it hinders progress in fields as diverse as soft matter, biotechnology and nanomedicine. Therefore, a detailed understanding of the interactions of nanoparticles in solutions of macromolecules is required to make important technological advances. The first part of the thesis has investigated the dynamics of colloidal particles in semi dilute and entangled polymer solution. The second part of this research has studied another complex system, which are the colloidal dispersions in binary liquid mixtures. Recently, there has been a great interest in colloidal dispersions and the dynamics of colloids. If colloidal particles are immersed in a solvent consisting of a binary liquid mixture, one of the fluid components may preferentially

adsorb onto the bodies because of the difference in their affinity for the fluid components[15]. Near the critical point of the liquid mixture, the enhancement of the adsorption of the preferred component, which is so-called "critical adsorption", becomes particularly pronounced due to the correlation effects induced by the critical composition fluctuations of the solvent[16-19]. Critical adsorption on a spherical nanoparticle is expected to exhibit important differences in behavior due to the effect of surface curvature[19]. It has been demonstrated experimentally that critical adsorption is highly related to thermally-induced reversible colloidal aggregation. This so-called flocculation phenomena is observed in binary liquid mixtures (2,6 lutidine + water, isobutyric acid + water, etc.) in the presence of a small volume fraction of silica or polystyrene colloidal particle[20-23]. Many theoretical and experimental studies have tried to explain this phenomenon; however, none of them can explain all of the experimental observations[24, 25]. Therefore, to properly address the aggregation phenomena, the knowledge of the adsorption profiles at the surface of a single sphere near the critical temperature of the liquid mixture will be useful. As far as I know, this is the first experimental study in which the critical adsorption on spherical particles was measured. In the broader framework, the results presented here will help in understanding the interaction of liquids with surfaces possessing geometric structure[26], the phase behavior of multi-component fluids[27, 28], and wetting phenomena[20, 29-31].

This dissertation shall be organized as follows. Chapter 2 will present background information pertinent to the thesis. It will cover polymers, while special attention will be paid to polymer solutions . In addition, it will cover critical adsorption on colloidal dispersions in binary liquid mixture. Chapter 3 outlines the experimental techniques employed during my research: fluorescence correlation spectroscopy and ellipsometry. Chapters 4-6 include the results of my experiments. Particularly, Chapter 4 covers gold nanoparticles diffusion in different semidilute

and entangled polymer solutions. Chapter 5 covers the investigation of critical adsorption on spherical colloidal particles in binary mixtures, and chapter 6 discus the results of gold nanoparticles adsorption on solid surfaces.

# CHAPTER 2

# BACKGROUND

## 2.1 INTRODUCTION

This chapter presents the background information pertinent to the thesis. First, it will cover polymers with special attention to polymer diffusion in semidilute and entangled solutions. Next, a brief discussion of phase transition and critical phenomena will be introduced. As an example of a phase transition, binary mixtures will be treated mathematically to calculate the phase diagram. Finally, critical adsorption in binary mixtures on planar and spherical surfaces will be addressed and some of the theoretical results will be introduced.

## 2.2 POLYMERS

### 2.2.1 INTRODUCTION TO POLYMERS

Polymers refer to a large class of soft matter comprising natural and synthetic materials with wide variety of different physical and chemical properties arising from the different arrangements and chemical identity of the molecules that make them up. They play an essential and ubiquitous role in everyday life, ranging from familiar synthetic plastics and fibers to natural biopolymers such as DNA and proteins that are essential for life. Although polymers have a wide variety of different properties, which arise from the different chemistry that makes them up, many of their physical properties have universal characteristics resulting from the generic properties of long, string-like, molecules[1].

### 2.2.2 POLYMER MICROSTRUCTURE

A polymer is a large molecule (macromolecule) that is built from many elementary units, called monomers. These structural repeating units are connected to each other by covalent bonds in the form of a long chain. In other long-chain objects, the subunits are not joined by covalent bonds, but by physical ones. Examples of this are the long chains of compact protein molecules, which constitute actin filaments. Such objects are sometimes called 'living polymers'; they can change their length in response to changes in the environment. This contrasts with the more usual covalently linked polymers, in which the length of the molecules is fixed during the polymerization[1].

The entire structure of polymer is generated during a process by which chemical monomers are covalently bonded together called polymerization[32]. The number of monomers in a polymer molecule is called the degree of polymerization N, and the molar mass M of a polymer is equal to its degree of polymerization N times the molar mass $M_{mon}$ of its chemical monomer

$$M = NM_{mon} \qquad 2.1$$

The conventional way to describe the mass of a polymer is the molar mass, which is the mass of one mole of these molecules. Most polymers are based on carbon with a huge variety of possible structures, and from these different structures, we have different properties. The general structure of vinyl monomers and polymers are shown in Fig 2.1, where R represents different possible chemical moities. If the R group is hydrogen, we have the simplest chemical structure with a carbon main chain and two hydrogen atoms per carbon. The repeating unit is $–CH_2–CH_2–$, and the polymer is named after the monomer used in their synthesis (ethylene, $CH_2= CH_2$). The

chemical identity of the monomers and the polymer's microstructure are the two main factors that determine the physical properties of a polymer. Polymer's microstructure is the organization of atoms along the chain, which is fixed during polymerization process, and it cannot be changed without breaking covalent bonds[32].

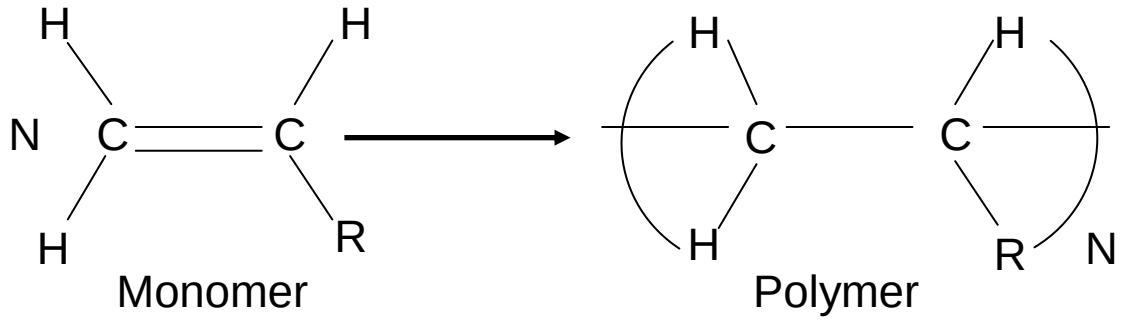


Fig 2.1: Polymerization of vinyl monomers (Rubinstein 2003).

Polymers with more than one type of chemical group attached to each main chain carbon atom can have different arrangements of the groups in three dimensions. There are two regular arrangements of side groups called: isotactic and syndiotactic arrangements (Fig 2.2)- these have similar side groups appearing on the same side of the chain or on alternative sides, respectively. If the arrangement of the groups is random, then we have an atactic polymer (Fig. 2.2). The atactic arrangement has very large energy barriers to rotation of the side groups preventing any rearrangement of the groups once the arrangement is set in place during the synthesis of the polymer. This is called 'quenched disorder' and it is the reason why these molecules usually cannot crystallize- they form glasses at low temperatures.

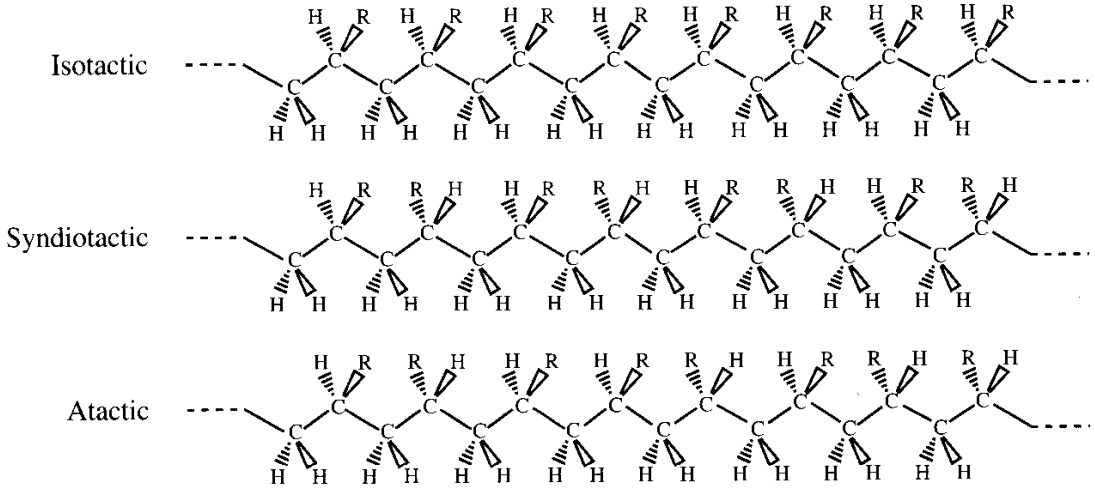


Fig. 2.2 Tacticities of vinyl polymers, illustrated with all backbone carbons with H and R groups (Rubinstein 2003).

In many polymers, the molecule contains only one type of monomer - such molecules are called homopolymers. However, polymers containing more than one type of monomer are called copolymers. Copolymers can be alternating, random, block, or graft depending on the sequence in which their monomers are bonded together (Fig. 2.3). A pure random arrangement of monomers is called random copolymer. If the different monomers arranged in blocks, they are called block copolymers. Block copolymers can be diblock if they contain two blocks and triblock if they contain three blocks. Polymers with many alternating blocks are called multiblock copolymers. If a polymer contains a side chain that has a different composition or configuration than the main chain, the polymer is called a graft. One kind of graft copolymer is high-impact polystyrene (HIPS), which is produced by grafting chains of polybutadine onto a polystyrene backbone. The polystyrene gives the material strength, but the rubbery polybutadiene chains give it resilience to make it less brittle. Combining several different

monomers into a single chain leads to new macromolecules called heteropolymers. Many biopolymers are heteropolymers. DNA is a heteropolymer consisting of four different types of monomers (nucleotides), while natural proteins are heteropolymers consisting of 20 different types of monomers (amino acids).

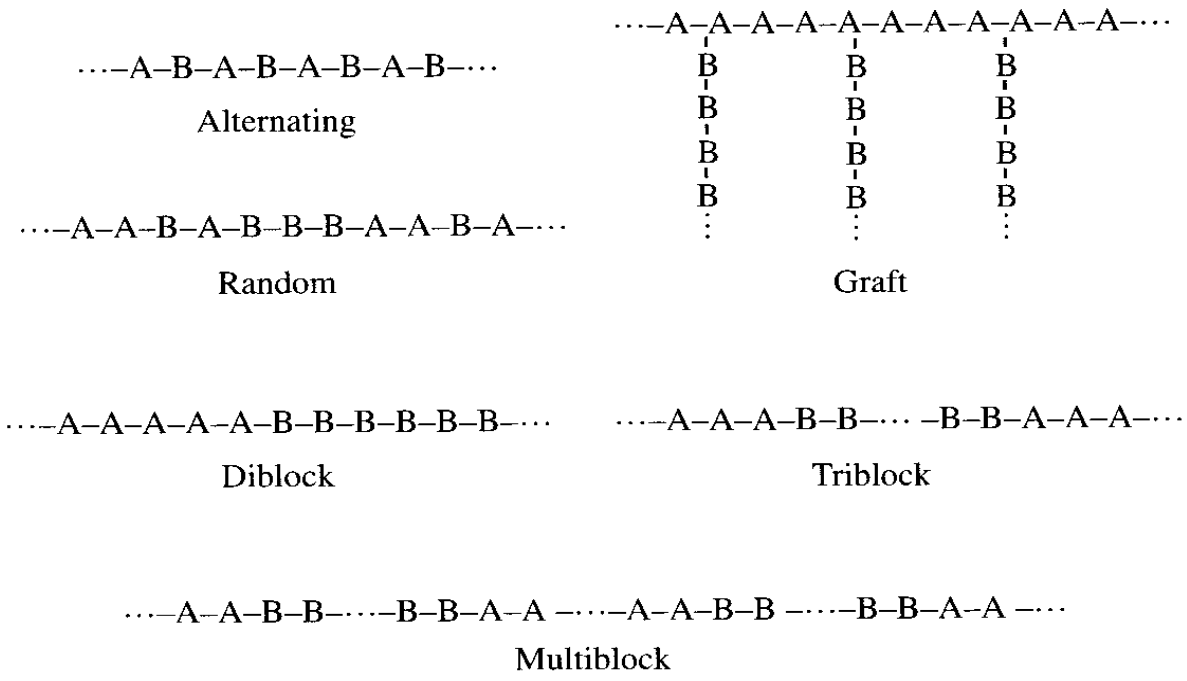


Fig. 2.3 Types of copolymers (Rubinstein 2003).

According to the way the polymer is synthesized, they have different architectures. This feature also controls the properties of polymers. Types of polymer architectures include: linear, ring, star-branched, H-branched, comb, ladder, dendrimer or randomly branched as sketched in Fig 2.4. Linear polymers are completely characterized by the number of monomers present in the chain, which is the degree of polymerization, N. Physical properties such as modulus, tensile strength, and the glass transition temperature follow a similar trend with increasing chain length.

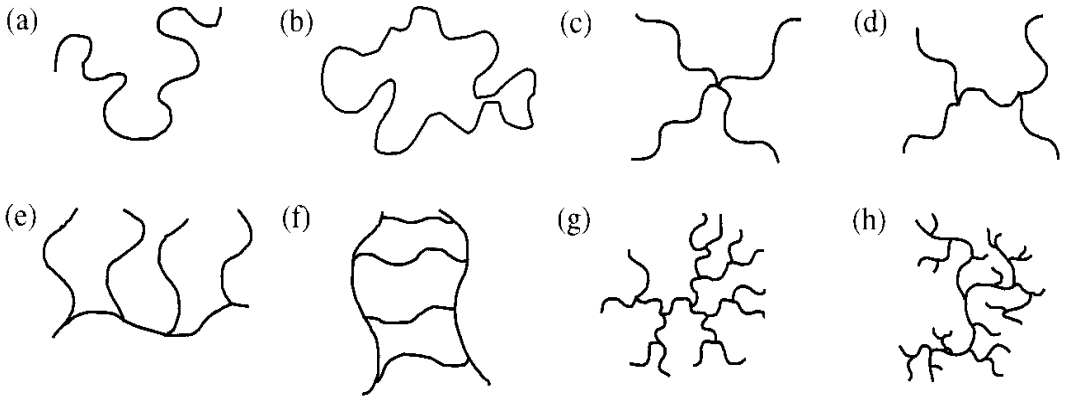


Fig. 2.4 Examples of Polymer architectures: (a) linear; (b) ring; (c) star; (d) H; (e) comb; (f) ladder; (g) dendrimer; (h) randomely branched. (Rubbinstien 2003).

Dendrimers are three-dimensional structures that branch outwards from a common center; therefore, the density of monomer units decreases when moving closer to the center of the dendrimer. This property provides potential medical applications, such as drug delivery.

### 2.2.3 POLYMER CONFORMATIONS

A conformation is the spatial structure of a polymer determined by the relative locations of its monomers in space. Polymer characteristics such as microstructure, architecture, degree of polymerization and chemical composition are fixed during polymerization and cannot be changed without breaking covalent bonds. However, after polymerization, a polymer molecule can adopt many different conformations, and it depends on rotations about the bonds that make up the polymer backbone. There are three characteristics that determine the conformation of a

polymer: the flexibility of the chain, interaction between monomers on the chain, and interactions with surroundings. Chains can be stiff or flexible depending on the inherent flexibility of the chain. The interaction between the monomers on the chain can be either attractive or repulsive. The monomers of a chain can also interact with their surrounding (other chains or the solvent) and the relative strength of these various interactions can change with temperature. Thus, chain conformations can be changed by tuning these effects.

### 2.2.4 PHYSICAL STATES OF POLYMERIC MATERIALS

#### 1) LIQUID POLYMERS

Polymer melts and solutions are two types of polymer liquids. Polymer solutions can be obtained by dissolving a polymer in a solvent. Interactions between polymer molecules in solution depend strongly on concentration. In dilute solution, the molecules are well separated and do not interact with each other, so each molecule can be considered as an isolated chain. However, as the concentration is increased the coils start to overlap. This is called the coil overlap concentration, c* where the coils are just in contact. The volume fraction, an alternative measure of the concentration, is the ratio of the occupied volume $nV_m$ of the polymer in the solution to the volume of the solution, so Ø* is the corresponding overlap volume fraction to c*. According to that, polymer solutions are classified as dilute or semidilute (Fig. 2.5). At volume fractions below overlap (Ø < Ø*) the solution is called dilute. In this regime, the average distance between chains in dilute solutions is larger than their size. Therefore, most of the properties of dilute solutions are very similar to pure solvent with slight modifications due to the presence of the polymer. At volume fractions above overlap (Ø > Ø*) the solution is called semi dilute. The solvent occupies most of the volume of a semi dilute solution. In this case, however,

polymer coils overlap and dominate most of the physical properties of semi dilute solutions (such as viscosity)[32].

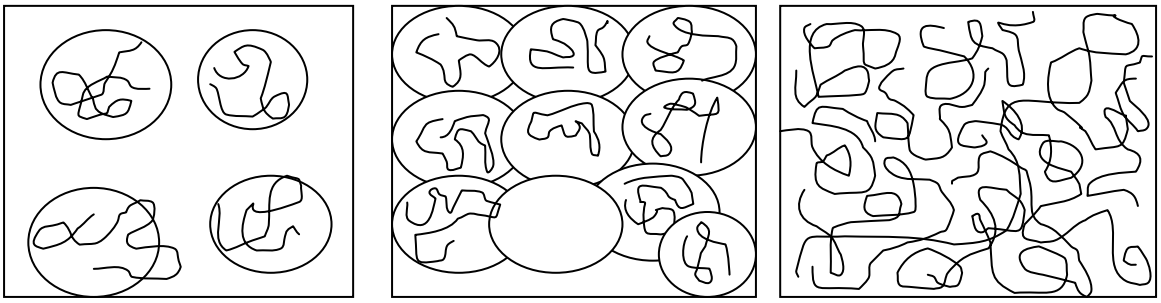

(a) (b) (c)

Fig. 2.5 Regimes of polymer solutions (a) Dilute Ø < Ø* (b) overlap Ø = Ø* (c) Semidilute Ø > Ø*

Polymer melts are neat polymeric liquids above their glass transition and melting temperatures. It is a bulk liquid state formed by polymers in the absence of a solvent. A macroscopic piece of a polymer melt remembers its shape and behaves elastically on short time scales, but it shows liquid flow behavior with high viscosity at long times. Such time dependent mechanical properties are termed viscoelastic because of the combination of viscous flow at long times and elastic response at short times[32]. Silly Putty is a familiar example of polymer melts. This will flow like a liquid out of a container, because pouring is a slow flow due to gravitational forces (long times). However, if it is formed into a ball and dropped on the floor, it bounces back, i.e., it behaves like an elastic material due to the brief impact of the ball with the floor (short times). In a polymer melt, there is a strong overlap with neighboring chains which lead to entanglement that greatly slows the motion of polymers. Rubber is a common and important example of polymer melt in which cross-links, randomly placed between adjacent chains, bond

the chains together to form a macroscopic network. The cross-links, however, prevent macroscopic bulk flow.

In polymer solution, a polymer chain is in continual motion because of thermal energy, and it will undergo many different conformations in rapid succession. In the dilute regime, the conformation of a polymer depends on the interaction between chain segments and solvent molecules. If the solvent is good, a chain expands from its unperturbed dimensions to maximize the number of segment-solvent contacts and the polymer chain adopts a swollen coil conformation in this situation, and solvent molecules are allowed to freely move through gaps and cavities created by the chain. If the solvent is poor, the chain will contract to minimize interactions with the solvent and the polymer chain adopts a compact globule conformation. An intermediate case, the θ-solvent, occurs when these two effects are perfectly balanced; the polymer molecule will adopt unperturbed dimensions. Since solvent quality is dependent upon temperature (higher temperatures yield better quality), the θ state is achieved at one particular temperature (the θ-temperature). A θ solvent has properties most closely related to an ideal system due to the elimination of monomer-monomer interactions.

The simplest model of a polymer chain is the ideal chain where there are no interactions between monomers separated by many bonds along the chain. Linear polymer melts and concentrated solutions have practically ideal chain conformations because the interactions between the monomers are almost completely screened by surrounding chains. In addition, chains are nearly ideal in polymer solutions at θ temperature. In this case, the size of linear chains can be characterized by their mean-square end-to-end distance. For a linear ideal chain made up of $N$ monomers, each of length $a$ and having different orientations the mean-square end-to-end distance is:

$$\langle R^2 \rangle = Na^2 \qquad 2.2$$

The path of the polymer in space can be imagined as a random walk. This implies that the overall size of a random walk is proportional to the square root of the number of steps. However, for branched or ring polymers with too many ends or no ends at all, the size of polymers of any architecture can be characterized by the radius of gyration. The mean square radius of gyration $<R_g^2>$ is defined as the average square distance from all monomers to the center of mass of the polymer and is related to the mean-square end-to-end distance of an ideal linear chain:

$$\langle {R_g}^2 \rangle = \langle R^2 \rangle / 6 \qquad 2.3$$

Real chains interact with both their solvent and themselves. The relative strength of these interactions determines whether the monomers effectively attract or repel one another. The net two-body interaction between monomers in a solvent can be characterized by a parameter called the exclusion volume, v. The exclusion volume is that volume which each segment of a coil occupies which is not accessible to the other parts of the chain. The excluded volume is temperature dependent and makes a positive contribution to the free energy of the polymer coil. When the attraction between monomers just balances the effect of the hard core repulsion (which prevents monomers from overlapping), the net excluded volume is zero (v = 0) and the chain will

adopt a nearly ideal conformation. This situation corresponds to a particular temperature θ for a solvent and is called the *θ-condition*[32].

If the attraction between monomers is weaker than the hard-core repulsion, the excluded volume is positive and the chain swells. This happens at a temperature above the θ-temperature. The coil size is larger than the ideal size with radius $R \sim N^{3/5}$ (Fig 2.6 a). This is referred to as the good solvent behavior. If the attraction between monomers is stronger than the hard-core repulsion, the excluded volume is negative and the chain collapses. This occurs below the θ-temperature and corresponds to a poor solvent. In a poor solvent, the polymer is in a collapsed globular conformation corresponding to a dense packing of thermal blobs (Fig. 2.6b). The size of a globule is smaller than the ideal size: $R_{gl} \sim N^{1/3}$.

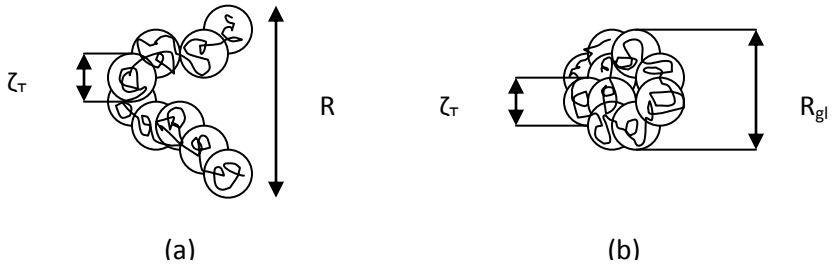


Fig. 2.6 Polymer chain conformations in (a) good solvent: self-avoiding walk of thermal blobs (b) poor solvent: collapsed globule of thermal blobs [24]

## 2) VISCOELASTIC POLYMERS

Polymers like most soft materials behave in a way that combines the viscous response of Newtonian liquids and the elastic response of Hookean solids, with an additional dependence on timescales. For a Hookean solid the application of a shear stress σ, to the material produces a strain e, that is proportional to applied stress with the constant of proportionality being the shear

modulus G as in the relation ($G = \sigma/e$). In a Newtonian liquid, the application of shear stress produces a time-dependent strain proportional to the applied stress with the constant of the proportionality being the viscosity of the liquid η and ė is the strain rate, as given by ($\sigma = \eta\dot{e}$). Viscoelastic materials respond to an applied stress in a time dependent way. A constant stress applied at time t = 0 causes the material to respond in an elastic way, with constant strain, but after a certain time τ it begins to flow like a liquid. This time τ is the relaxation time; it is the time that separates the solid-like behavior from the liquid-like behavior. For ideal simple liquid, $\eta \sim G_0\tau$, where $G_0$ is an instantaneous shear modulus which characterizes the elastic response at times much shorter than the relaxation time and η characterizes the viscous behavior at long times. However, for complex fluids like polymer melts, the viscoelastic response has a time dependence that is characterized by more than one relaxation time and the effective viscosity may depend on shear rate: $\sigma = \eta(\dot{e})\dot{e}$. In the dilute-solution limit, the polymer contribution to the viscoelastic properties is just that of a single coil in an infinite bath of solvent, multiplied by the number of such coils in solution. For polymer solutions that are dilute, there are hydrodynamic interactions that affect the viscoelastic properties of the solution. These hydrodynamic interactions are the disturbances in the solvent velocity field created by motion of one part of a polymer chain that then affect the drag exerted by the solvent on other parts of the same chain. In most concentrated solutions or melts, entanglements between the long polymer molecules greatly slow polymer relaxation. Polymer melts can have relaxation times of order of milliseconds or even seconds, resulting in very spectacular viscoeleastic properties.

## 3) SOLID POLYMERS

There are different types of polymeric solids. Upon cooling a polymer melt, it can either transform into a semicrystalline solid below its melting temperature $T_m$ or into a polymeric glass

below its glass transition temperature $T_g$. The semi-crystalline state consists of small crystalline regions called lamellae in a matrix of amorphous material, which can be in either a liquid-like or glassy state. The incomplete crystallization that leads to the semi-crystalline state is owing to kinetic limitations, branching and the presence of quenched disorder. A fully crystalline state is inaccessible on experimental timescales. Examples of semi-crystalline solid polymers include synthetic polymers such as polyethylene as well as natural materials like starch. Familiar examples of glass include polystyrene (PS) and poly(methyl methacrylate) (PMMA).

**4) GLASSY POLYMERS**

The transformation of a liquid into a glass on cooling is a common, yet mysterious process. When a liquid is cooled, the molecules composing it draw more closely together to maximize attractive interactions. If the molecules are bulky and of irregular shape, including most polymers, or if the liquid is cooled so fast that the liquid does not have time to crystallize, then at low temperatures it vitrifies into a rigid phase that retains the disordered molecular arrangements of the liquid. This rigid disordered material is called glass. Glasses are liquids whose molecules are so tightly packed, and hence are so sluggish, that they cannot relax to equilibrium even over long periods of time. Almost all polymers form glasses; everyday examples include poly(methyl methacrylate) and polycarbonates, which are extensively used for their transparency and good mechanical properties, and polystyrene in disposal plastic cups.

### 2.2.5 DIFFUSION IN POLYMER SOLUTION

Diffusion is the process responsible for the spread of particles through random motion from one part of a system to another. While diffusion in both gases and liquids can be

successfully predicted by theories, diffusion in polymers is complex and the diffusion rates should lie between those in liquids and in solids. There are different physical models and theories of diffusion used in describing the diffusion in polymer solutions. It depends mainly on the concentration and degree of swelling of polymers[33]. The diffusion was first treated mathematically by Fick who developed a law for diffusion in one dimension, the equation is known as Fick's first law. In the case of diffusion without convection, this equation can be written as:

$$J = -D\frac{\partial c}{\partial z} \qquad 2.4$$

where j is the flux per unit area, D is the diffusion coefficient, and $\frac{\partial c}{\partial z}$ is the gradient of the concentration along the z-axis. This equation is the starting point of numerous models of diffusion in polymer systems. In the study of solvent diffusion in polymer solutions, it is known that the diffusion of the solvent is linked to the physical properties of the polymer network and the interactions between the polymer and the solvent itself. The amount of solvent absorbed per unit area of polymer at time t, $M_t$, is represented by:

$$M_t = kt^n \qquad 2.5$$

where k is a constant and n a parameter related to the diffusion mechanism, the value of which lies between 1/ 2 and 1. This equation can be used to describe the solvent diffusional behaviors for any polymer-penetrant system. Alfrey *et al.* intoduced a classification according to the solvent diffusion rate and the polymer relaxation rate.

I. *Fickian diffusion (Case I)*: observed in polymer networks when the temperature is well above the glass transition temperature of the polymer (Tg). In this case, when the polymer is in the rubbery state, the polymer chains will have a higher mobility that allows an easier penetration of the solvent. As a result, Fickian diffusion is characterized by a solvent diffusion rate, $R_{diff}$, slower than the polymer relaxation rate, $R_{relax}$ ($R_{diff} << R_{relax}$), and a large gradient of solvent penetration is observed in the system. The solvent concentration profile shows an exponential decrease from the completely swollen region to the core of the polymer. The diffusion distance is proportional to the square root of time

$$M_t = kt^{1/2} \quad 2.6$$

II. Non-Fickian diffusion (Case II and anomalous): observed in glassy polymers, i.e. when the temperature of study is below $T_g$. In this case, the polymer chains are not mobile enough to permit immediate penetration of the solvent in the polymer core. There are two kinds of non-Fickian diffusion : Case II diffusion and anomalous diffusion. The main difference between these two diffusion categories depends on the solvent diffusion rate. In Case II diffusion, the solvent diffusion rate is faster than the polymer relaxation process ($R_{diff} >> R_{relax}$), whereas in anomalous diffusion, the solvent diffusion rate and the polymer relaxation are about the same order of magnitude ($R_{diff} \sim R_{relax}$). For case II, the diffusion distance is directly proportional time.

$$M_t = kt \quad 2.7$$

For anomalous diffusion, the diffusion distance is given by:

$$M_t = kt^n \quad 2.8$$

where $1/2 < n < 1$.

### 2.2.6 PREVIOUS EXPERIMENTS ON POLYMER DIFFUSION IN SOLUTION AND ANOMALOUS DIFFUSION

Liu *et. al.*[34] measured the self-diffusion coefficient $D_s$ of dye-labeled polystyrene chains having $M$w = 3.90 * $10^5$ g/mol over almost 4 decades of polymer concentration in toluene solution, from $10^{-4}$ to 0.4 g/mL, by fluorescence correlation spectroscopy (FCS). In the very dilute regime up to a concentration of 5 *$10^{-3}$ g/mL, the diffusion coefficient remains practically constant. Then there is a transition regime around 0.01 g/mL, which is the overlap concentration. In Fig.2.7a, the experimental results are compared with the predictions of scaling and reptation theory. Next, from 0.02 to 0.40 g/mL in the semidilute regime, the self-diffusion coefficient decreases with increasing polymer concentration as $D$s ~$c^{-1.75}$, in agreement with the theoretical prediction of scaling and reptation theory. In Figure 2.7b, the experimental data are fitted to the stretched-exponential equation $D$s = $D_0$ exp- (-15$c^{0.65}$), with $D_0$ =2 * $10^{-7}$ $cm^2/s$ and $c$ given in g/mL. The crossover is fitted rather well. On the other hand, in the higher concentration range the experimental concentration dependence of $D_s$ seems to be less curved than the fit function. There is an extensive discussion in the literature whether the experimental data support the scaling predictions, which are applicable in certain concentration regimes, or are better described by continuous function over the entire concentration range.

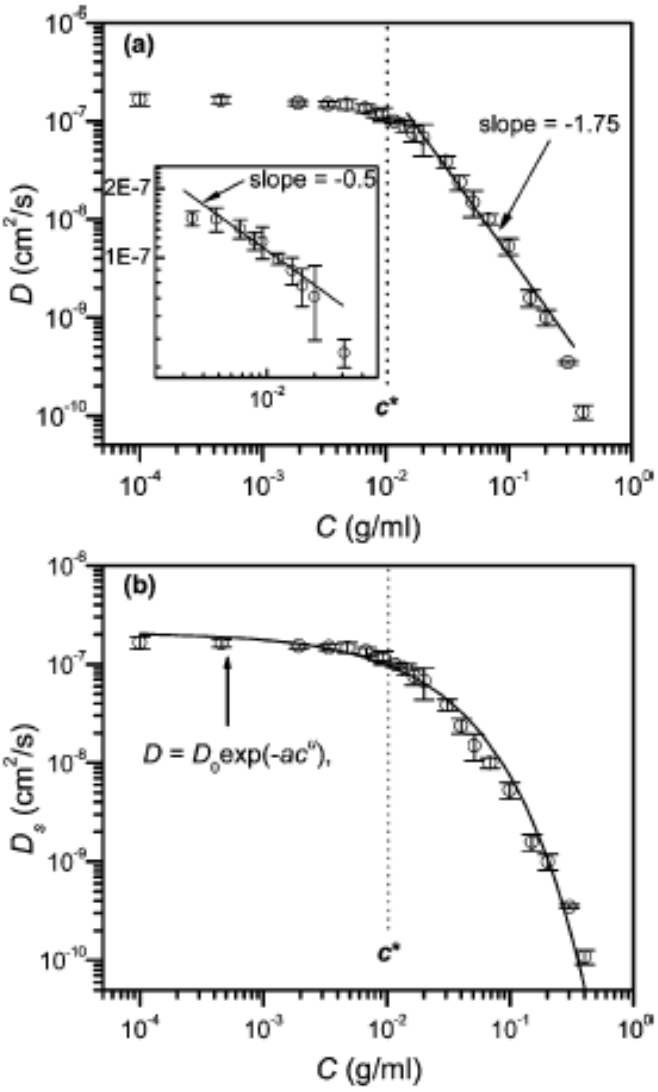


Fig. 2.7 Diffusion coefficient of labeled polystyrene in toluene as a function of polymer concentration: (a) showing predictions according to reptation and scaling theory; (b) showing a fit according to Phillies' equation (Liu 2005).

The tracer diffusion of spherical particles in polymer solutions has been studied widely to understand the diffusion in solutions containing mixtures of macromolecules of differing architectures. Won et. al.[35] have used dynamic light scattering (DLS) to follow the tracer diffusion of polystyrene spheres (R≈200 nm) in dilute, semidilute and entangled solution of poly (vinyl methyl ether) (PVME) ($M_w$ = 1.3 x $l0^6$). They found that the diffusivity drops by almost 5

orders of magnitude over the range of matrix concentration from dilute to entangled. In addition, they focus on the applicability of the reputation hypothesis. In general, the diffusivity of a sphere follows the Stokes-Einstein (SE) reation: $D=kT/6\pi\eta R$, where R is the radius of the sphere and $\eta$ is the zero-shear-rate viscosity of the medium in which it is suspended. This relation assume that the medium may be treated as a continuum on the length scale of R. SE Equation works perfectly for noninteracting spheres in a small-molecule solvent, but it is certainly not obvious that an arbitrary polymer solution will satisfy the continuum assumption. The product $D\eta /D_0\eta_s$ where $D_0$ is the infinite dilution diffusivity of the sphere and $\eta_s$ is the solvent viscosity may deviate from unity as the polymer concentration increases above c*. $D\eta /D_0\eta_s >1$ is referred as a positive deviation from SE behavior and $D\eta /D_0\eta_s<1$ as a negative deviation. A positive deviation corresponds to a diffusivity that decreases with increasing concentration less rapidly than the solution viscosity increases. The DLS diffusion data are presented as a function of matrix concentration in Fig. 2.8 in a double-logarithmic format. By the highest matrix concentration, the mobility of the spheres has decreased by well over 4 orders of magnitude; the largest drop reported previously has been less than 3 orders of magnitude. Significant decreases in mobility do not begin to appear until a matrix concentration of 0.006 g/mL.

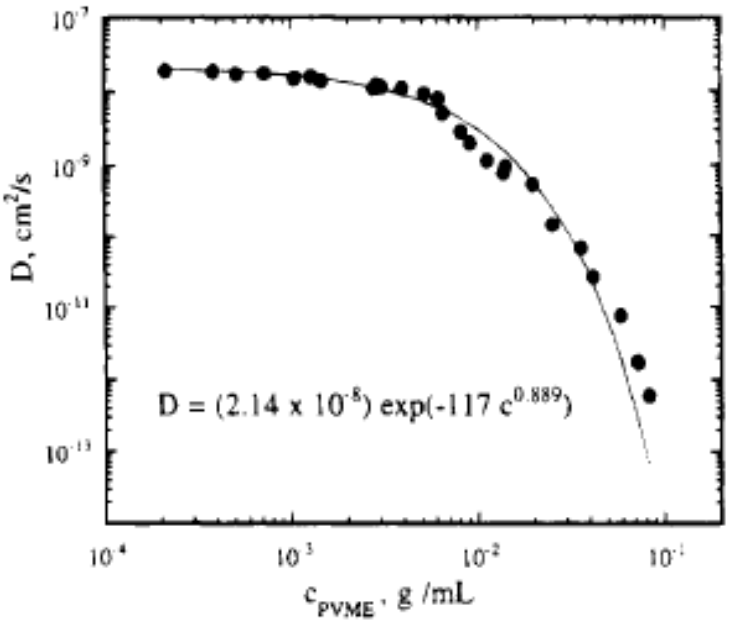


Fig 2.8 Tracer diffusion coefficient of PS spheres in PVME solutions as a function of matrix concentration. The smooth curve represents the equation shown on the plot (Won 1994).

Using previously measured solution viscosities, the data were compared with the Stokes-Einstein (SE) relation. The principal new result of this work is that although a positive deviation from SE behavior is observed near c* for the matrix, SE behavior is recovered once the matrix becomes sufficiently entangled. Possibly, previous studies of sphere diffusion were not extended to sufficiently high concentration (i.e., $c >> c^*$ and $R >> \xi$) to observe this phenomenon. This new result was confirmed via forced Rayleigh scattering. In addition, these data can reconcile measurements of sphere diffusion with reptation-based models for chain mobility in well-entangled systems. The behavior near c* is discussed in terms of the matrix correlation length, $\xi$, which has a maximum at $\xi \approx R_g$, for $c \approx c^*$. An explanation of the positive deviation for SE is that the fluid within a distance $\xi$ of the sphere surface may have different composition from the bulk, and this could certainly influence sphere diffusion over this length scale. For the system used in their study, in which the surface-matrix interaction is assumed neutral, a depletion layer would exist, leading to an enhanced short-time diffusion for the spheres.

## 2.3 PHASE TRANSITION AND CRITICAL PHENOMENA

Phase transition is a term used to describe the transition between three familiar phases of matter: solid, liquid, and gaseous phases. Ehrenfest classified phase transitions into first-order and second-order phase transitions. An order parameter can be defined for a phase transition, which typically takes a zero value in the disordered phase and a non-zero value in the ordered phase. The way the order parameter varies with temperature tells us about the nature of the transition. There is a fundamental difference between first-order phase transition, where the order parameter changes discontinuosly at the phase transition (e.g. melting of a crystal), and the second-order transitions, where the order parameter is continuous. The classic example of a second- order transition is the change from a liquid to a gas at a critical point, which is a particular combination of pressure, temperature, and density called the critical pressure, critical temperature, and critical density respectively. Near the critical point, the fluid is sufficiently hot and compressed that the distinction between the liquid and gaseous phases is almost non-existent. At low temperature, there is a large difference between the liquid and the gas densities, $\rho_L$ and $\rho_{G,}$ and as the critical temperature is approached this density difference tends to zero. Thus, $\rho_L$ - $\rho_G$ can be considered as the order parameter, since it has a non-zero value below the critical temperature and zero above it. A phase boundary separates different phases. A change in parameters such as the temperature across the phase boundary causes a sudden change in the phase of a material. This phase boundary sometimes disappears at a critical point, where the two phases become indistinguishable and the material shows anomalous behavior. The theory of critical phenomena explains this behavior. Binary mixtures of two liquids systems exhibit a critical temperature below which the two components do not mix homogeneously in all proportions.

Continuous phase transition can be characterized by parameters known as critical exponents, which describe the behavior near the critical point of the various quantities in interest. These exponents take the same values for very different systems. This phenomenon, called universality, is explained qualitatively and quantitatively by the renormalization group. The most important exponent is the one that describing the divergence of the correlation length while approaching the transition. The correlation length can be defined as a measure of the range over which fluctuations in one region of space are correlated with those in another region. In a physical system, any two points that are separated by a distance larger than the correlation length will each have fluctuations, which are relatively independent, that is, uncorrelated. Experimentally, the correlation length is found to diverge at the critical point. Thus near the critical point, the correlation length may be written as:

$$\xi \sim |t|^{-\nu} \text{ , where } t = \frac{T - T_c}{T} \qquad 2.8$$

The divergence of the correlation length at the critical point means that very far points become correlated. In other words, the long-wavelength fluctuations dominate. Thus, the system near a second-order phase transition ‘loses memory’ of its microscopic structure and begins to display new long-range macroscopic correlations. For a binary mixture system, the correlation length $\xi$ is a measure of the width of the range over which the concentration varies. Such a width increases with increasing nearness to the critical liquid–liquid point, so much so that, in the immediate vicinity of the critical point, the correlation length of a binary mixture at critical composition exhibits an anomalous behavior conforming to the exponential law (Eq. 2.8)

### 2.3.1 BINARY MIXTURES

Assume we have two miscible liquids in all proportions at high temperature, but separate into two distinct phases when the temperature is lowered[1]. Using the regular solution model which is a mean field theory, the free energy of mixing, $F_{mix}$ can be predicted. To calculate $F_{mix}$, we need to calculate the change in the entropy on mixing, $S_{mix}$ and the change of the energy on mixing, $U_{mix}$. To find $S_{mix}$, the molecules of the two liquids are imagined to be arranged on a lattice, where each lattice has a *z* neighbors, and the composition of the mixture is measured in terms of the volume fraction φ. if the volume fraction of A molecules is $\varphi_A$, and the volume fraction of B is $\varphi_B$, then we can use the Boltzmann formula to write down the entropy[1] :

$$S_{mix} = -k_B(\emptyset_A \ln \emptyset_A + \emptyset_B \ln \emptyset_B) \qquad 2.9$$

Here, we assume that the sites are independent of each other. To find $U_{mix}$, we assume that molecules interact only with their nearest neighbors in a way that is pairwise additive, then the energy of mixing can be written as:

$$U_{mix} = \frac{z}{2}\left[(\emptyset_A{}^2 - \emptyset_A)\epsilon_{AA} + (\emptyset_B{}^2 - \emptyset_B)\epsilon_{BB} + 2\emptyset_A\emptyset_B\epsilon_{AB}\right] \qquad 2.10$$

where, $\epsilon_{AA}$ is the energy interaction between two neighboring A molecules.

$\epsilon_{BB}$ is the energy interaction between two neighboring B molecules.

$\epsilon_{AB}$ is the energy interaction between A molecule and a neighboring B molecule.

For incompressible mixture, $\varphi_A + \varphi_B = 1$, then we introduce a single dimensionless parameter χ, which characterizes the strength of the energetic interaction between A and B relative to their self interaction.

$$\chi = \frac{z}{2k_BT}(2\epsilon_{AB} - \epsilon_{AA} - \epsilon_{BB}) \quad 2.11$$

Using this definition, we can write the energy of mixing as:

$$U_{mix} = \chi \emptyset_A \emptyset_B \quad 2.12$$

The free energy of mixing, F=U-TS can be written down as:

$$\frac{F_{mix}}{k_BT} = \emptyset_A \ln \emptyset_A + \emptyset_B \ln \emptyset_B + \chi \emptyset_A \emptyset_B \quad 2.13$$

The phase behavior of the mixture can be understood by looking at the shape of the curves of free energy against composition change with varying $\chi$. Fig. 2.8 shows examples of these curves. For $\chi < 0$, the curve has a single minimum at $\varphi_A = \varphi_B = 0.5$, and for $\chi \geq 2$, the curves has two minima and a maxima at $\varphi_A = \varphi_B = 0.5$.

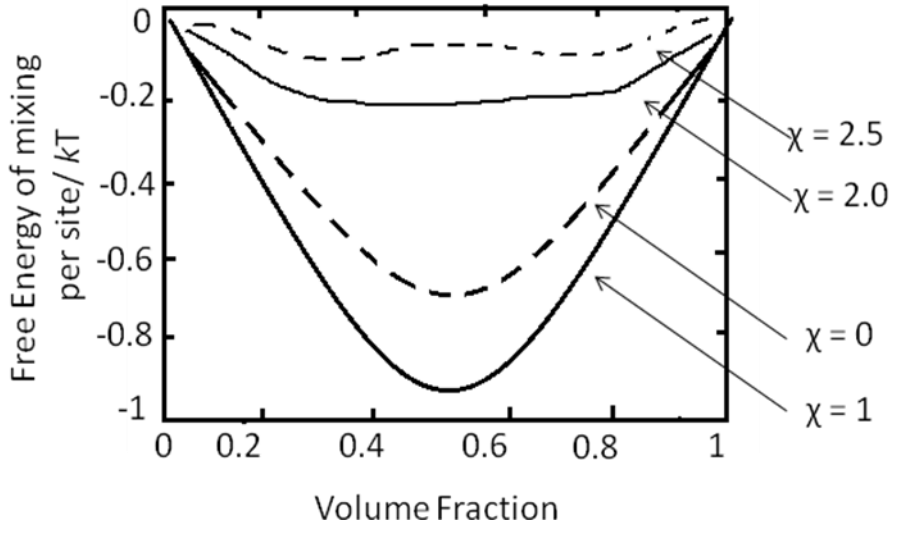


Fig. 2.9 The free energy of mixing devided by $k_B$T, as a function of the composition.

If the free energy resulting from phase separation into any pair of volume fraction $\varphi_1$ and $\varphi_2$ is always higher than the free energy of the starting composition, then the mixture is stable. On the other hand, if there is any region of composition in which the curve is convex, then there are some starting compositions, which can lead to a lowering free energy. These compositions are known as the coexisting compositions, and the locus of these compositions as the temperature is changed is called the coexistence curve. Within this curve, there are compositions that are unstable for small fluctuations in compositions and will immediately phase-separate. The curvature of the free energy $d^2F/d\varphi^2$ in this case is negative. On the other hand, there are compositions that are locally stable for small fluctuations in composition, but globally unstable with respect to separation in two coexisting curves. The curvature $d^2F/d\varphi^2$ in this case is negative, such compositions are said to be metastable. The limit for local stability is defined at $d^2F/d\varphi^2=0$. Finally, a critical temperature Tc separates the two types of compositions that are stable and those that are phase-separated. The phase diagram for the mixture is a plot that shows

on a plane of composition and temperature the regions where the mixture is stable, unstable, or metastable. By knowing the relationship between the free energy for mixing as a function of composition and the phase behavior, the phase diagram can be calculated. Fig. 2.10 shows an example of the calculated phase diagram for the regular solution model described.

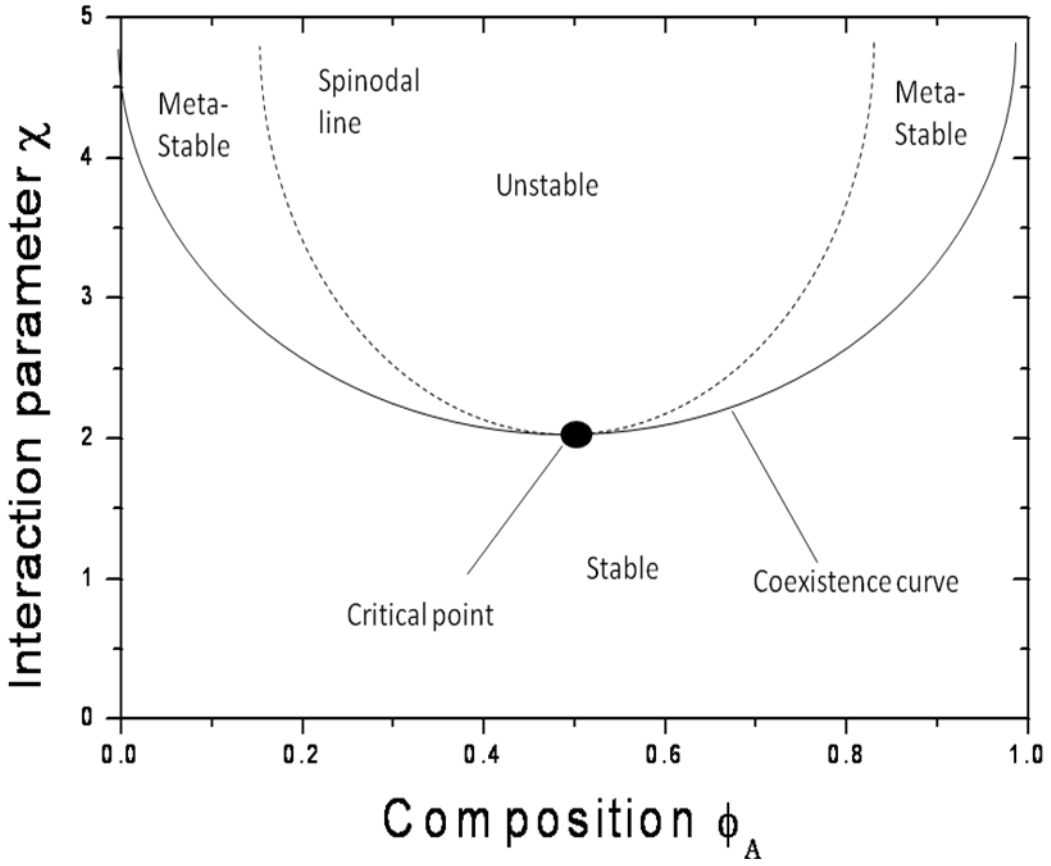


Fig 2.10: The phase diagram of a liquid mixture whose free energy of mixing is described by the regular solution model.

### 2.3.2 CRITICAL ADSORPTION IN COLLIDAL DISPERSION

If colloidal particles are immersed in a solvent consisting of a binary liquid mixture, one of the fluid components may preferentially adsorb onto the bodies because of the difference in their affinity for the fluid components[15]. This preferential adsorption layer has a width of the order of the solvent correlation length, which is a few angstroms, affecting only one or a few layers of liquid molecules next to the particles[36-38]. However, near the critical point of the liquid mixture, the enhancement of the adsorption of the preferred component is called "critical adsorption", and this becomes particularly long- ranged and pronounced due to the correlation effects induced by the critical composition fluctuations of the solvent. The critical adsorption of simple fluids at semi-infinite and planar liquid-vapor and liquid solid surfaces in many different systems has been studied in much detail and is well understood. The effect of a solid boundary on a simple fluid or binary fluid undergoing a continuous phase transition was studied by Fisher and de Gennes[39]. Next to a strongly adsorbing boundary, they predicted that the order parameter profile should decay away from the boundary as[38, 40]:

$$\rho(z) - \rho_c = Mt^{\beta} P(z/\xi, ht^{-\Delta}) \qquad 2.14$$

where $\rho(z)$ is the density a distance z from the boundary, $\rho_c$ is the critical density, $t=T/T_c-1$ is the reduced temperature, $\xi = \xi_o t^{-\nu}$ the bulk correlation length, $\Delta= 1.65$ is the gap exponent. $h= [\mu(\rho, T) - \mu(\rho_c, T)]/2k_BT$, where $\mu(\rho_c, T)$ is the chemical potential along the isochore. Equation 2.14

is obtained by taking the derivative with respect to h of the fundamental renormalization group scaling relation for the free energy . Below Tc , P(x,y) satisfies the constraint that, for $z\rightarrow\infty$ and

h→∞, the shape of the coexistence region in the bulk is described $\rho(z)-\rho_c = Mt^{\beta}P(z/\xi)$, and hence P(x,y)→1. Above Tc , for z→∞ and h→∞, it must be P(x,y)→0 s0 that $\rho(z)-\rho_c = 0$.

Binary fluid mixtures near their critical demixing point belong to the same universality class as the liquid-vapor critical point, where in eq. 2.14 the volume fraction φ is the appropriate order parameter. One of the primary advantages of studying adsorption near a binary liquid mixture critical point is that this adsorption is described by a universal function P(z/ξ), which is a function of the dimensionless depth x = z/ξ, where z is the depth away from the surface while ξ is the bulk correlation length given by $\xi = \xi_o t^{-\nu}$ . Here, $\xi_o$ is system dependent amplitude; ν ≈0.632 is a universal critical exponent. Therefore, the relationship between the local volume fraction φ(z) of the adsorbed component and the universal function P(z/ξ) can be written as:

$$\varphi_{\pm}(z) = \varphi_c + Mt^{\beta}P_{\pm}(z/\xi_{\pm}) \qquad 2.15$$

Another quantity, which is measured experimentally is the excess adsorption per unit area, which for a planar wall geometry is given by:

$$\Gamma_c = AM\xi_o t^{\beta-\nu} + B \qquad 2.16$$

where A and B are parameters depend on the size of the gap.

Compared to planner surfaces, critical adsorption on spherical particles is expected to behave differently because of the surface curvature[19]. The spherical particles with mesoscopic radius $R_0$ immersed in a binary liquid are characterized by the dimensionless variable $R_0/\xi$, where $R_0$ is the radius of the dissolved sphere and ξ is the bulk correlation length. The

corresponding adsorption profiles at the radial distance s from the surface are characterized by universal scaling functions $P_{\pm}(s/\xi_{\pm}, R_0/\xi_{\pm})$ for $T \neq T_c$. Close to Tc, critical adsorption on the surface of a sphere with radius $R_0$ is characterized by an order parameter

$$\langle \varphi(r) \rangle_t = a|t|^{\beta} P_{\pm}(s/\xi_{\pm}, R_0/\xi_{\pm}) \qquad 2.17$$

The scaling functions $P_{\pm}$ depend on two scaling variables $x_{\pm}=s/\xi_{\pm}$, $y_{\pm}=R_0/\xi_{\pm}$.

The excess adsorption $\Gamma$ $(t \to 0, R)$ describing the total enrichment of the preferred component of the fluid near criticality in proximity of a sphere has a curvature dependence characterized by universal scaling functions $G_{\pm}$ $(R_0/\xi_{\pm})$ obtained from integrating $P_{\pm}(s/\xi_{\pm}, R_0/\xi_{\pm})$ over $x_{\pm}=s/\xi_{\pm}$. In a theoretical result, this has been calculated as

$$\Gamma\ (t \to 0, R)\ \to \{g_{+} \frac{t^{\beta-\nu}-1}{\nu-\beta} + t^{\beta-\nu}\ G_{\pm}\ (y_{\pm})\} \qquad 2.18$$

In the limit $R_0/\xi_{\pm} \to 0$, the scaling functions $G_{\pm}$ $(y_{\pm})$ is given by

$$G_{\pm}\ (y_{\pm} \to 0)\ \to \omega_{\pm}\ y_{\pm}^{\ -3+1+\beta/\nu} \qquad 2.19$$

Fig. 2.10 shows numerical results for $G_{\pm}$ $(y_{\pm})$ corresponding to a sphere; $y_{\pm}G_{\pm}$ $(y_{\pm})$ is plotted as a function of $y_{\pm}^{-1} = \xi_{\pm} / R_0$. We note that $y_{\pm}G_{\pm}$ $(y_{\pm})$ diverges as $y_{\pm}^{-1} \to \infty$. In addition, the excess adsorption yields

$$\Gamma\ (t \to 0, R)\ \to |t|^{-\gamma} \qquad 2.20$$

where, γ is the bulk susceptibility critical exponent. One of the objectives of my thesis is to experimentally test these scaling predictions.

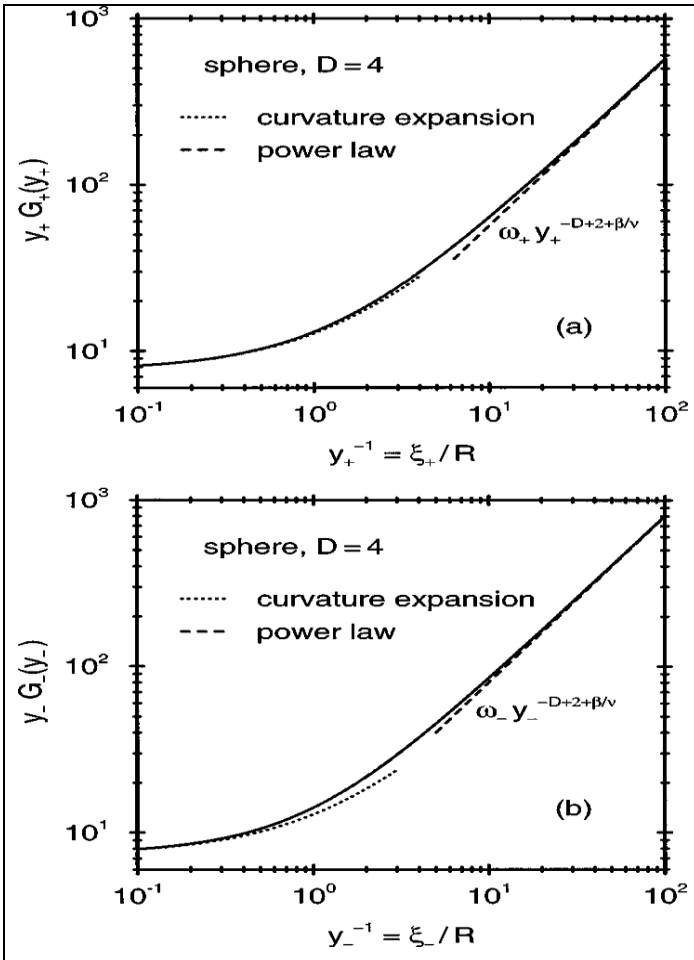


Fig. 2.11. Scaling functions $G_{\pm}(y_{\pm})$ for a sphere in mean- field approximation (i.e., $d$=$D$ with $D$=4) as a function of $y_{\pm}^{-1}$ =ξ± /$R$ for (a) $T$>$T_c$ and (b) $T$<$T_c$. for $D$=4 the exponent -$D$ +2+β/ν is equal to -1.(Hanke 1999)

Another motivation comes from the observation that the critical adsorption is highly related to thermally-induced reversible colloidal aggregation[21-23, 28]. Close to the critical demixing point of the binary liquid, the colloids were found to undergo a sharply defined reversible aggregation transition, termed flocculation, in contrast to the irreversible coagulation. This flocculation phenomena was first observed in the binary liquid mixtures (2,6 lutidine + water) in the presence of a small volume fraction of Stöber silica colloidal particles[13]. These silica particles are known

to adsorb lutidine preferentially, yet flocculation occurs on the water-rich side of the binary phase diagram. Subsequently, particle aggregation phenomena have been reported in several other phase-separating binary mixtures.

These findings have been discussed in terms of the wetting behavior of the colloidal materials with respect to the two components of the binary mixture; in particular, the flocculation transition has been tentatively associated with the prewetting line, which extends from the wetting transition (at coexistence) into the one-phase region as shown in the phase digram in fig. 2.11. The bold solid line on this diagram represents the two-phase coexistence curve for lutidine and water, which possesses a lower consolute point with a critical lutidine mass fraction $C_c$ ( $\approx$0.29) and a critical temperatue $T_c(\approx 34^0 C)$. Below the coexistence curve the liquid mixture is in the one phase region, while above the coexistence curve, the liquid mixture separated into two phases, one lutidine rich and the other lutidine poor. The light solid line represents a typical colloidal aggregation line for the colloidal particles in the mixture. Prior to aggregation, there is a strong increase in lutidine adsorption on the surface the particles as seen from turbidity measurements and the adsorption layer can be seen to increase with temperature up to the aggregation[20].

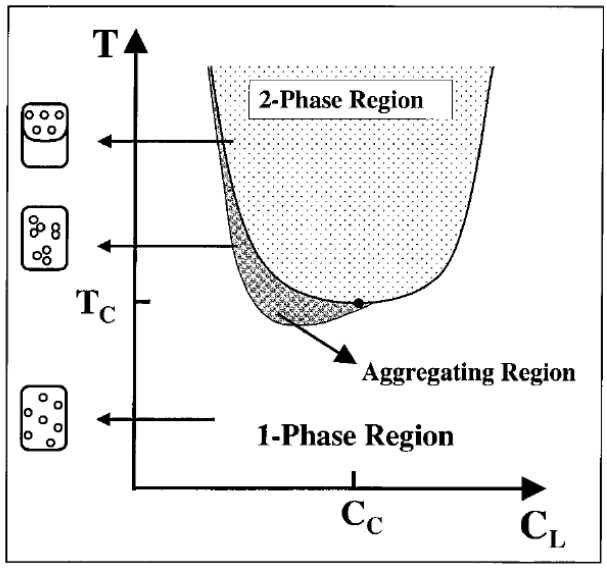


Fig. 2.12 The schematic phase diagram of 2,6 lutidine and water mixture containing small amounts of silica colloids. Here $C_L$ is the bulk lutidine concentration (weight fraction), with $C_c$~0.29 and $T_C$~34%C. (Beysens 1998)

The colloidal particles used in many of these experiments have surface hydroxyl groups which dissolve in the binary mixture. Therefore, the surface becomes negatively charged. If one of the components of the mixture preferentially adsorbs onto the particles, an adsorbed film of the phase rich in that component can develop onto them. If the phase separation temperature of the liquid mixture is approached, the thickness of the adsorbed layer around the colloidal particles will increase. This leads to wetting films of the preferred phase coating the colloidal particles. These wetting films result in the presence of effective surface fields, which could lead to flocculation in these systems.

There are numerous theoretical and experimental studies attempting to explain this thermally-induced reversible colloidal aggregation phenomenon. Unfortunately, most of these explanations have not provided definitive predictions that could be compared directly with experimental results. Law, Petit, and Beysens modified and improved the DLVO theory to include the presence of an adsorbed layer around the colloidal particles[24]. They described the

attractive dispersion interactions by the Dzyaloshinskii-Lifshitz-Pitaevskii (DLP) potential. They found that a shorter screening length inside the adsorption layer screens the charge of the particles so they get close to each other. Once they are close, the adsorption layers come together, and the coalescence energy and the repulsion form the secondary minimum. They found that for particles with a diameter of 100 nm an adsorbed layer thickness of about 12 nm is necessary for aggregation to take place.

Sluckin argues that the aggregation is an equilibrium phase separation of a three component system, two solvents and colloids[41]. Following this idea, Jayalakshmi and Kaler has been suggested that if a high concentration of particles is used, it can alter the solvent phase diagram. In this case, flocculation may be linked to phase separation in the ternary mixture [27]. Comparing their results with earlier aggregation studies strongly support their suggestions that the aggregation phenomena observed for colloidal particles in binary liquid mixtures is in fact a true phase separation in the ternary mixture.

Fisher and de Gennes predicted that the confinement of critical fluctuations of the order parameter in a binary liquid mixture near its critical demixing point Tc gives rise to long-ranged forces between immersed plates or particles, the so-called “critical Casimir effect”. In particular, they pointed out that these long-ranged forces would lead to the flocculation of colloidal particles which are dissolved in a near-critical binary liquid mixture. If the liquid mixture is near the critical point, the interference of critical adsorption on neighboring particles can give rise to an attractive critical Casimir force. This has also been argued to contribute to flocculation for a near-critical solvent mixture[42, 43].

# CHAPTER 3

# EXPERIMENTAL TECHNIQUES

## 3.1 FLUORESCENCE CORRELATION SPECTROSCOPY

### 3.1.1 FLUORESCENCE

Luminescence is the emission of light from electronically excited states. It is divided into two types, fluorescence and phosphorescence, depending upon the nature of the ground states and the excited states. In a singlet excited state, the electron in the excited orbital has the opposite spin orientation as the second electron in the ground-state orbital. These two electrons are said to be paired. Consequently, return to the ground state is spin allowed and occurs rapidly by emission of a photon. This emission is called fluorescence and the emission rates of fluorescence are typically $10^{-8}$ $s^{-1}$, so that a typical fluorescence lifetime is near 10 ns. The lifetime is the average period of time a fluorescent substance (fluorophores) remains in the excited state. In a triplet state these electrons are unpaired, that is, their spins have the same orientation. Therefore, a change in the spin orientation is needed to return to the singlet ground state. Phosphorescence is the emission which results from a triplet excited state returning to a singlet ground state. Such transitions are not allowed and the emission rates are slow ($10^{3}$-$10^{0}$ $s^{-1}$), so that phosphorescence lifetimes are typically milliseconds to seconds[44].

Substances, which display significant fluorescence generally, possess delocalized electrons formally present in conjugated double bonds. Some typical fluorophores are shown in Fig.3.1. The first known fluorophore is quinine, which was responsible for stimulating the development of the first spectrofluorometers. Many other fluorophores are encountered in daily

life. The green or red-orange glows seen in antifreeze are due to fluorescein or rhodamine, respectively.

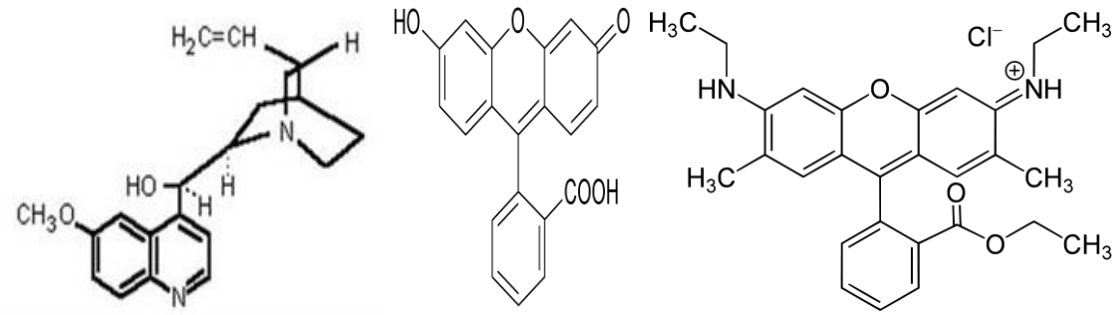


Quinine Fluorescein Rhodamine b

Fig. 3.1 Structures of typical fluorophores [44] ( Lakowicz 1999)

Fluorescence spectral data are presented as emission spectra. A fluorescence emission spectrum is a plot of the fluorescence intensity versus wavelength (nanometers) or wavenumber ($cm^{-1}$). Emission spectra vary widely and depend upon the chemical structure of the fluorophore and the solvent in which it is dissolved. One characteristic that are displayed by fluorophores is Stokes' shift, which is a shift to lower wavelength (i.e., a loss of energy) of the emission relative to the absorption Fig.3.2. This energy loss between excitation and emission are observed universally for fluorescing molecules in solution. Another characteristic is that the same fluorescence emission spectra are usually independent of the excitation length.

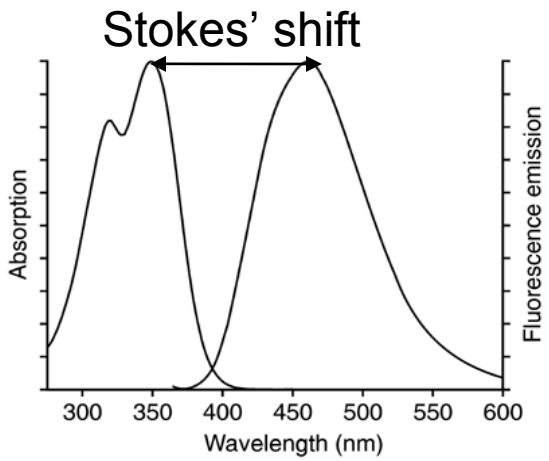


Fig. 3.2 Absorption and fluorescence emission spectrum of quinine (Lakowicz 1999)[44]

### 3.1.2 Luminance of metal nanoparticles

Optical techniques for detecting single molecules open new windows at the nanoscale in the fields of material science and cell biology. Early work has used aromatic dye molecules, whose fluorescence can be detected with high signal to noise ratio. Nevertheless, the finite photochemical lifetime of dyes limit their uses to probe very slow (~100 s) dynamics[45, 46]. In addition, the small size of the dye molecules (≈1 nm) makes it difficult to extend this method in measuring the dynamics at larger length scale. Semiconductor nanocrystals, which resist bleaching for longer times, have recently been introduced as labels. The random interruption of their luminescence by long off-times is, however, a serious drawback for many applications. Tracking biomolecules requires chemically and photochemically stable labels, ideally no larger than a few nanometers[45, 46]. It has been shown in the recent years that metal nanoparticles have a highly efficient photoluminescence upon multi-photon excitation, which can provide sufficient contrast against background even in dense condensed matter environment[47-49]. Noble metals, in particular gold, interact strongly with light although they are chemically inert, and they resist

high illumination levels and do not saturate, and they can be attached to biomolecules. Therefore gold nanoparticles are used for optical labels in FCS experiments (Fig 3.3a)[50]. By plotting of emission intensity versus incident power, the excitation of nanoparticles can be determined if it is a three-photon process or a two-photon process. Fig. 3.3b shows the dependence of the emission intensity on the incident power. The two-photon induced luminescence is forbidden for a perfect spherical particle, so here in the graph, the particles are deviated from perfectly spherical shape, or they have some surface defects. In general, gold nanoparticles are photostable under hours of continuous excitation and do not blink like semiconductor quantum dots. [50]

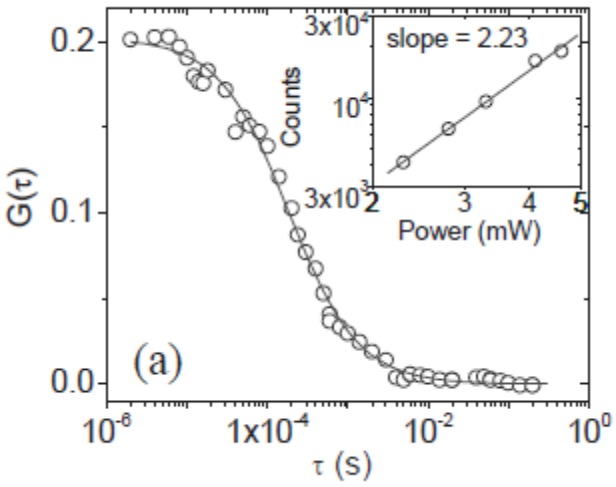


Fig.3.3 (a) Intensity-intensity autocorrelation function of gold colloid diffusion in water. (Inset) Photon counts plotted as a function laser power on a log-log scale for a single gold colloid embedded in the polymer melt.(Grabowski 2009)

### 3.1.3 FLUORESCENCE CORRELATION SPECTROSCOPY (FCS) TECHNIQUE

Thermally induced diffusion is one of the fundamental properties exhibited by molecules within a solution. This diffusion is directly related to the hydrodynamic radius of the molecules via the Stokes-Einstein relation[4, 51, 52]. Any change in that radius will change the associated diffusion coefficient of the molecules. Such changes occur to molecules when interacting with

their environment. The ability of precisely measuring the diffusion coefficient is important in many systems. Standard methods for diffusion coefficient measurements are dynamic light scattering (DLS)[53], pulsed field gradient NMR[54], or size exclusion electrophoresis[55]. All of these methods work at high sample concentrations, far away from the limit of infinite dilution. To obtain the correct infinite-dilution limit and thus a correct estimate of the hydrodynamic radius, one has to take measurements at different concentrations and to extrapolate the concentration/diffusion coefficient curve toward zero concentration[56]. In contrast to the above techniques, fluorescence correlation spectroscopy (FCS) was invented for measuring diffusion, concentration, and chemical biochemical interactions/reactions of fluorescent or fluorescently labeled molecules at nanomolar concentrations in solution.

Fluorescence correlation spectroscopy (FCS) is an experimental technique used to obtain temporal fluctuations of moving fluorescent molecules in a sample. These fluctuations can be quantified in their strength and duration by temporally autocorrelating the recorded intensity signal, a mathematical procedure after which the technique is named. The autocorrelation analysis provides a measure for the self-similarity of a time series signal by analyzing the temporal fluctuations data. Consequently, one can measure the translational diffusion, the rotational diffusion, the flow, or the chemical reactions of the molecules. FCS was first introduced by Madge, Elson and Webb in 1972 to measure the diffusion and chemical dynamics of DNA-drug interaction[57, 58]. Although the principal ideas behind FCS, as well as its applications, were already well established at that time, the technique suffered from poor signal-to-noise ratios, mainly because of low detection efficiency, large ensemble numbers and insufficient background suppression. Introducing the confocal illumination scheme in FCS in 1993 by Rigler *et. al* have generated important technical improvements and pushed the

sensitivity of the technique to the single- molecule level, thus increasing the signal- to-noise ratio dramatically[59]. Moreover, using efficient fluorescent dyes to label the molecules of interest, strong and stable light sources like lasers, and ultrasensitive detectors, e.g. avalanche photodiodes with single-photon sensitivity, the detection of the fluorescence signal coming from individual molecules in highly dilute samples has become practical[60]. Therefore, FCS experiments can be conducted in a wide variety of specimens, ranging from materials science to biology[60].

In FCS experiments, the number of fluorescent molecules which emitted photons from the focal volume element in equilibrium is monitored as a function of time. The recorded fluorescence emission signal is proportional to the number of fluorescent molecules in the probe volume[61]. Fluctuations in the fluorescence signal are induced by molecules entering and leaving the illuminated region and as fluorescent molecules chemically transform to and from non-fluorescent forms. This technique works properly if the signal fluctuates and the fluorescence intensity has a characteristic time behavior. Since the measured intensity fluctuation always contains some noise, information about different processes occurring in a given focal volume is obtained from the characteristic spectrum of that noise.

FCS is a single molecule sensitive technique. For observing molecular behavior to be effective, the fluctuations have to be detectable. Moreover, the number of molecules in the detection volume has to be small enough so that the contribution of each individual molecule is identifiable[62]. At the same time, the signal from these molecules has to be strong enough for the information to be useful. Therefore, it is obvious that FCS can only function properly if one somehow manages to reduce the concentrations and observation volumes such that only few molecules are simultaneously detected, and at the same time increase the fluorescence photon

yield per single molecule. Experimentally, one can obtain small open volumes, often less than a femtoliter, by strong focusing of the illumination into a double cone with a waist 1 μm in diameter plus selection of the fluorescence emitted only from this region by inserting a pinhole in the image plane. This is achieved by the use of a confocal laser-scanning microscope, reducing background from out-of-focus excitation. In addition, the signal strength can be improved by using efficient fluorescent dyes to label the molecules of interest.

The single molecule sensitivity of FCS allows the detection of fluorescent molecules (fluorophores) in the small focal volume of the laser beam (of order of 0.1 fL). These fluorophores keep diffusing into and out of the laser focus and the number of them will fluctuate[60]. Since the laser focus maintains a constant volume, this implies using grand canonical ensemble to better understand the theoretical foundation of FCS. These fluctuations can be the result of Brownian diffusion, chemical reactions, externally induced flows, and other such processes[57, 62]. The autocorrelation function (ACF) of a fluctuation F(t) measured with respect to time. The measured fluctuations F(t) will be treated mathematically by calculating the autocorrelation function (ACF) G (τ) which is given by:

$$G(\tau) = \frac{\langle \delta F(t).\delta F(t-\tau) \rangle}{\langle F(t) \rangle^2} \qquad 3.1$$

Where < > denotes a time average and $\tau$ is the time lag. G (τ) decays from a maximum value at τ =0 to zero at large lag times. Fig 3 shows the development of an autocorrelation curve. The amplitude of G (τ) and the characteristic delay time provides multiple parameters on single molecule scale with high spatial and temporal resolution such as local concentration, mobility coefficients.

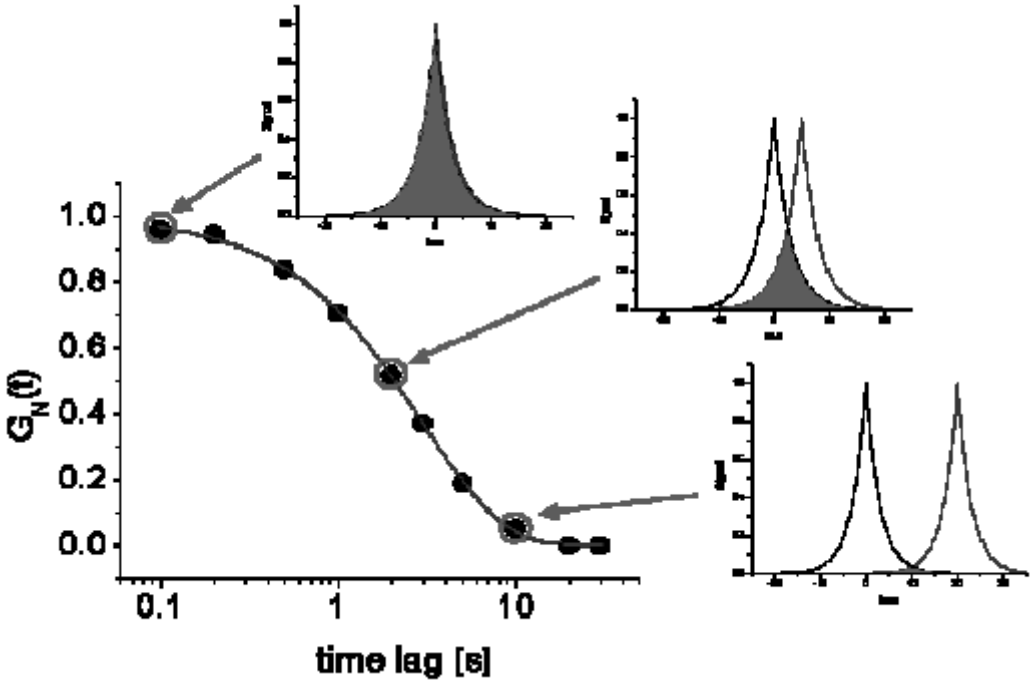


Fig.3.4 The development of an autocorrelation curve. The ACF calculates the self-similarity of fluctuations as a function of time lag. By fitting the curve to a particular model, the diffusion coefficient and concentration of fluorescent dyes in a solution may be calculated.

Most of the systems under study such as polymers do not inherently fluorescence when they are excited by laser. This problem was solved by labeling these polymer molecules with fluorescent dyes. However, these dyes also have a problem that they can not stand high power lasers. Fluorescent dyes emit a limited number of photons before they irreversibly photobleach. In order to solve these problems, more stable dyes have been introduced in the FCS experiments and these dyes can emit larger number of photons before photobleaching.

The FCS experimental set-up composes mainly of the laser source as illustrated in Fig. 3.4. This laser excites the fluorophores within the laser beam focus. There are two kinds of lasers used in FCS experiments: continuous light (one-photon excitation), pulsed laser light (two-

photon excitation). We are using the second one which was used first by Berland *et al*. after the invention of two-photon confocal microscopy by Denk[63].

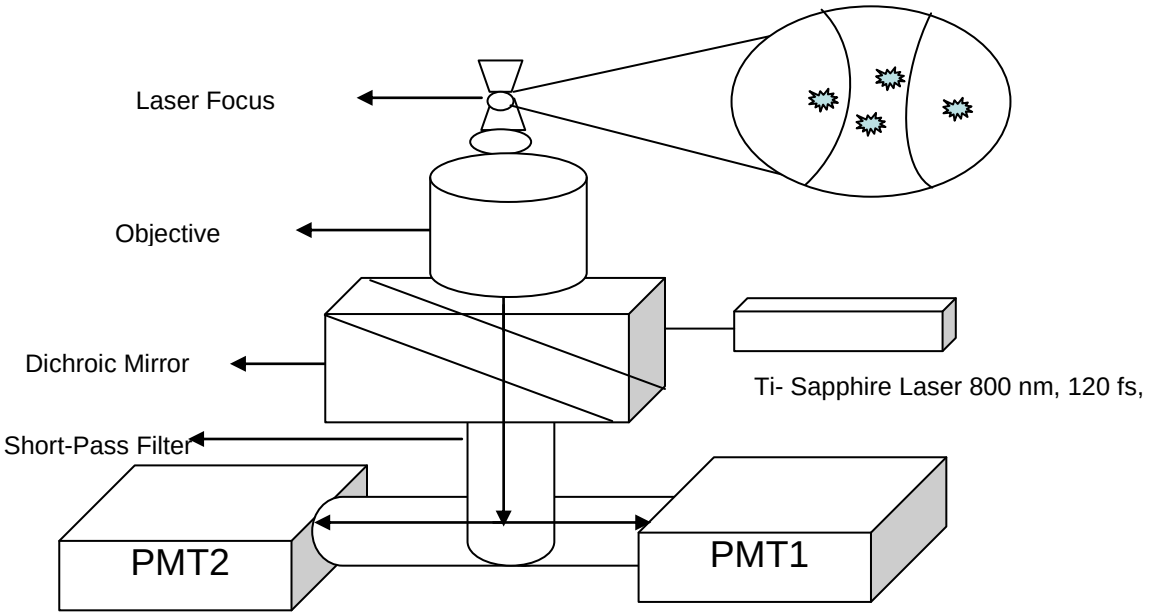


Fig 3.4 Schematical drawing of two-photon FCS setup

In one photon excitation, the incoming laser light is strongly focused by a high numerical aperture objective (ideally NA > 0.9) to a diffraction limited spot. Only the few fluorophores within the illuminated region are excited with one photon. In order to limit the detection volume also in axial direction, a pinhole is introduced in the image plane, which blocks all light not coming from the focal region.

Two-photon excitation requires the absorption of two photons of theoretically double the wavelength usually required for the excitation, within the tiny time interval of about one

femtosecond ($10^{-15}$ s). In order to obtain a reasonable probability of such three-particle events ( two absorbed photons and one emitted photon) the photon flux must be extremely high. This means, a high output power is required, and also pulsed excitation is used, to get an even higher photon density per pulse relative to the average output power. The probability of absorbing two photons per excitation process is proportional to the mean square of the intensity. This allows the laser to excite only the immediate vicinity of the objective's focal spot which receives sufficient intensity for significant fluorescence excitation. Under two-photon excitation, bleaching occurs only in the focal region. In contrast to this, under one-photon excitation, all fluorophores residing in the double cone above and below the focal spot are excited and bleached. Unfortunately, determining the two-photon excitation spectra of different dyes is difficult. As two-photon excitation is a quantum mechanically forbidden process, the selection rules differ greatly from those valid for one-photon processes. In addition, because of the pulsed excitation in two-photon excitation, the maximum number of photons that a dye molecule emits before undergoing photodestruction is significantly lower than that for the one-photon excitation. Moreover, due to the quadratic intensity dependence, the range of applicable powers is much narrower. In spite these experimental difficulties, two-photon excitation combines good signal-to-noise ratio with low invasiveness, especially for sensitive biological applications.

In two-photon setup the high optical resolution is obtained by the use of non- linear two photon absorption. The laser is focused inside the sample using a high power objective[64]. An infrared femtosecond Ti-sapphire (Mai Tai, Spectra physics) laser is being used for two-photon excitation. The laser beam passes through a beam expander which is a telescope consisting of two achromatic lenses separated by a distance equal to the sum of their focal length. The purpose of these lenses is to limit the diffraction in the focus for a beam of width ~ 0.35 μm after it exits

the objective. After that the beam reflects off the dichroic mirror, which is made of a special multilayer dielectric coating. The purpose of this mirror is to transmit the wavelengths above certain value and reflect the wavelength under the same value. So to choose these mirrors, it should be matched with the fluorophores used in the experiment. The laser light is collected by the same objective to focus the beam into the sample. This objective must have a high numerical aperture (NA). The fluorescent light is collected using a photomultiplier tube (PMT) which has the single photon sensitivity. There is a short pass filter in the way between the dichroic mirror and PMT to eliminate the scattered light or light leakage from dichotic mirror.

The fluctuations of fluorescent molecules are recording using data acquisition card where the data is the number of photons being collected by PMT as a function of time. The frequency of acquisition can be altered using computer software. Then these data will be auto correlated using a software package that updates the autocorrelation function during the period of the experiment. Then these ACF will be analyzed using a suitable model.

### 3.1.4 FCS THEORY

FCS is a method for investigating molecular dynamics. The fluorescent beads or molecules are homogenously distributed in the sample container in a rest condition. The excitation light sources focus into the sample container to form a focus spot. Whenever the fluorescent beads or molecules move into the focus spot, they absorb energy and emit fluorescent light. Then, photomultiplier tube (PMT) is used to detect the fluorescent signal. The detected analog signal from PMT is then converted to digital signal (photon counts) by discriminator. The photon counts are stored as the raw data in a sampling time $\Delta T$. thus, the detected fluorescence fluctuation F(t) as a function of t ( $t = i\,\Delta T$, $i = 0$ to M-1, M is the data size) is measured. The average of F(t) is denoted by

$$\langle F(t)\rangle = \sum_{i=0}^{M-1} \frac{F(i\Delta T)}{M} \tag{3.2}$$

where $\Delta T$ is the sampling time and M is the raw data size. The fluctuation of F(t) is given by:

$$\delta F(t) = F(t) - \langle F(t)\rangle \tag{3.3}$$

If only one fluorescent chemical species is present in the sample region, F(t) is given by:

$$F(t) = kQ\int E(r)C(r,t)dr \tag{3.4}$$

where k is a constant, Q is the product of the absorptivity, fluorescence quantum efficiency and experimental fluorescence collection efficiency of the fluorescent molecules, E (r) is the spatial intensity profile of the excitation light, and C(r,t) is the number density at position r and time t. then one can write eq.3.1 as follows:

$$\delta F(t) = F(t) - \langle F(t)\rangle = kQ\int E(r)\delta C(r,t)dr \tag{3.5}$$

where $\delta C(r,t) = C(r,t) - \langle C(r,t)\rangle$, by substituting this equation into equation 3.1 we get:

$$G(\tau) = \frac{\iint E(r)E(r')\langle \delta C(r,t)\delta C(r',t+\tau)\rangle dr dr'}{\left(\langle C\rangle \int E(r)dr\right)^2} \tag{3.6}$$

For the 3D Gaussian model with two photon excitation the spatial intensity profile of the excitation light E(r) is given by:

$$E(r) = E(x, y, z) = E_0 \exp\left( - \frac{4(x^2 + y^2)}{{w_0}^2} - \frac{4z^2}{{z_0}^2} \right) \quad 3.7$$

where $w_0$ is the beam waist and $z_0$ is the length of the beam in the z axis.

For Brownian (translational) diffusion, only the fluctuation δC(r,t) will have characteristic behavior governed by the diffusion equation:

$$\frac{\partial \delta C(r,t)}{\partial t} = D \nabla^2 \delta C(r,t) \quad 3.8$$

where D is the diffusion coefficient. The solution of the above equation is given by:

$$\delta C(r,t) = \frac{\langle C \rangle}{\sqrt{4\pi D t}} \exp\left( - \frac{r^2}{4Dt} \right) \quad 3.9$$

By assuming that the sample is stationary, the following relation holds for translational diffusion in two dimensions:

$$\langle \delta C(r,t).\delta C(r', t+\tau) \rangle = \frac{\langle C \rangle}{\sqrt{4\pi D \tau}} \exp\left( - \frac{(r - r')^2}{4D\tau} \right) \quad 3.10$$

The diffusion coefficient for spherical particles is given by the Stokes-Einstein relation:

$$D = \frac{k_B T}{6\pi\eta R_H} \tag{3.11}$$

where $R_H$ is the hydrodynamic radius of the particle, η is the viscosity of the surrounding fluid, and T is the ambient temperature. By correlating the change in concentration of particles through a sample volume, the diffusion of particles can be determined, as well as the average particle size (for spherical particles). Substituting eq. 3.10 and 3.7 in 3.6, we get:

$$G(\tau) = \frac{2\sqrt{2}}{\pi w_0^{\,2} z_0 \langle C \rangle}\left(1+\frac{8D\tau}{w_0^{\,2}}\right)^{-1}\left(1+\frac{8D\tau}{z_0^{\,2}}\right)^{-\frac{1}{2}} = G(0)\left(1+\frac{8D\tau}{w_0^{\,2}}\right)^{-1}\left(1+\frac{8D\tau}{z_0^{\,2}}\right)^{-\frac{1}{2}} \tag{3.12}$$

where $w_0$ and $z_0$ are the beam width in the lateral and axial directions, D is the diffusion coefficient, and the density of fluorescent particles is:

$$\langle C \rangle = \frac{1}{2VG(0)} = \frac{2\sqrt{2}}{\pi\sqrt{\pi} w_0^{\,2} z_0 G(0)} \tag{3.13}$$

The average number of molecules within the excitation volume may be calculated by multiplying particle density by the area of the laser focus:

$$\langle N \rangle = V\langle C \rangle = \frac{1}{2\sqrt{2}G(0)} \tag{3.14}$$

If an external flow of velocity V is introduced to the system, an exponential term is superposed over the usual autocorrelation function.

$$G(\tau) == G(0)\left(1+\frac{8D\tau}{{w_0}^2}\right)^{-1}\left(1+\frac{8D\tau}{{z_0}^2}\right)^{-\frac{1}{2}}\exp\left(\frac{-\left(V_{flow}\tau\right)^2}{{w_0}^2\left(1+\frac{8D\tau}{{w_0}^2}\right)\left(1+\frac{8D\tau}{{z_0}^2}\right)^{\frac{1}{2}}}\right) \quad 3.15$$

### 3.1.5 CROSS CORRELATION:

In performing an autocorrelation analysis, one effectively compares a measured signal with itself at some later time and looks for recurring patterns. Nevertheless, it may also be useful to find common features in two independently measured signals. Whereas autocorrelation measurements are sensitive only to signal variations within one channel, cross-correlation analysis is used to compare the signals arising from two different channels. Only temporally coordinated fluctuations in both channels give rise to cross-correlation. Phenomena limited to one fluorophore, e.g., triplet blinking, or artifacts in one detector will not show in the cross-correlation curve, because they are not directly related to the other channel. In fact, cross correlation analysis is just the straightforward way to achieve much higher detection specificity. In analogy to equation (3.1), the cross-correlation function is defined as:

$$G_{ij}(\tau) = \frac{\left\langle \delta F_i(t).\delta F_j(t-\tau)\right\rangle}{\left\langle F_i(t).F_j(t)\right\rangle^2} \quad 3.16$$

where i and j are two different measured signals of the fluorescent intensity.

## 3.2 Ellipsometry

### 3.2.1 Introduction

Ellipsometry, introduced by Drude in 1889[65] is a powerful optical technique for the investigation of the structural (thickness) and optical (complex refractive index or dielectric function) properties of thin films. The name "ellipsometry" was introduced in 1945 by Alexandre Rothen[66], and it stems from the most general state of polarization, which is elliptical. According to Azzam and Bashara[67], ellipsometry can be defined as the measurement of the state of polarization of a polarized light wave. It is generally conducted to obtain information about an optical system that modifies the state of polarization. During an ellipsometric experiment, polarized light is allowed to interact with an optical system under investigation. This interaction changes the state of polarization of the incident light wave. Most commonly, ellipsometry is performed in reflection, that is, a light beam of known polarization is reflected by the sample, and the polarization of the reflected beam is measured. The measurement yields the change in polarization upon reflection, which can be used to deduce the optical properties of the sample, and it can yield information about layers that are thinner than the wavelength of the probing light itself, even down to a single atomic layer. Ellipsometry is commonly used to characterize film thickness for single layers or complex multilayer stacks ranging from a few angstroms or tenths of a nanometer to several micrometers with an excellent accuracy. However, there are many other applications of ellipsometry in other areas including chemical deposition, depth gradients and profiles, phase transition temperatures, expansion coefficients, in situ growth monitoring[65, 67, 68].

Ellipsometry is a popular technique because it is used in real time and in-situ. In addition, it is non-penetrating, inexpensive, very sensitive, and it does not require ultra vacuum conditions.

A variety of ellipsometry configurations have been developed over the years as technology has improved. Ellipsometry is usually performed by modulating the polarization state of a light beam. This is achieved by means of optical components such as linear polarizers. The earliest ellipsometers featured polarizers that would be rotated until no reflected light passed through the other side – such devices have been called "null ellipsometers"[69]. In contrast, a phase-modulated ellipsometer continuously shifts a component of a polarized beam of light[70]. Exploitation of phase modulation in ellipsometry allows for sub-angstrom resolution of thin films. Ellipsometric measurements may be performed as a function of wavelength (spectroscopic ellipsometry), as a function of the angle of incidence (variable-angle) or both. On the other hand, monochromatic elipsometry utilizes single wavelength. In addition, considerable amount of information may be obtained from optically anisotropic samples by acquiring ellipsometric data as a function of the polarization state of the light beam incident on the sample.

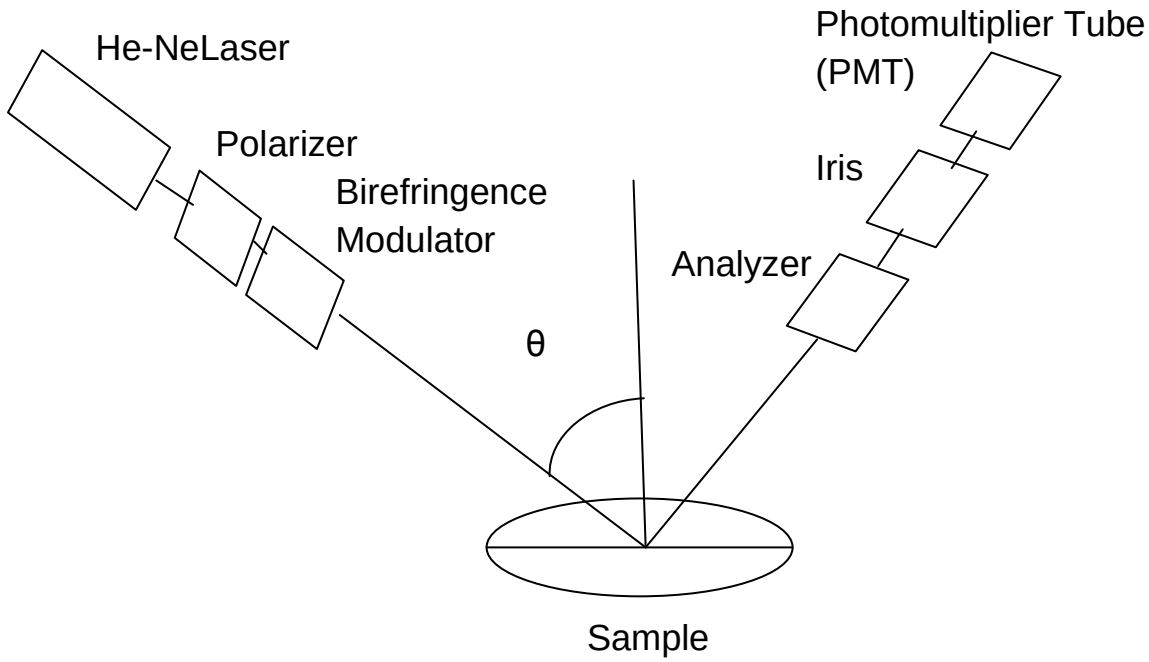


Fig. 3.5 Schematic of phase-modulated ellipsometry setup.

The polarization of the light can be decomposed into s and p components (the s component oscillating perpendicular to the plane of incidence and parallel to the sample surface and p is parallel to the plane of incidence). The optical scheme for a monochromatic, phase-modulated ellipsometer is shown in Fig.3.5 A laser light source (He-Ne laser, $\lambda$ = 632.8 nm, 5 mW) is directed onto a polarizer oriented at $45^0$ to the plane of incidence so that the beam components parallel and perpendicular to the plane of incidence (referred to as s and p components, respectively) are equal in magnitude. The now polarized beam enter a birefringence modulator which is oriented parallel to the plane of incidence. The birefringence modulator consists of a 10 mm thick piece of fused silica, which is set into longitudinal

oscillation of amplitude $\delta_0$ at a fixed frequency of 50 kHz. This oscillation creates a sinusoidally varying phase shift between the s and p components of the laser. After reflection by the sample, the phase modulation of the light beam is converted to an intensity modulation by the analyzer, which is oriented at $+45^0$ or $-45^0$. The light intensity is finally picked up by the photomultiplier tube detector.

### 3.2.2 ELLIPSOMETER THEORY

The polarizer is rotated by $45^0$ relative to the s and p axes. The amplitude of the electric field vector after the light passes through the polarizer is given by:

$$E = E_0 \left(\frac{1}{\sqrt{2}}\hat{s} + \frac{1}{\sqrt{2}}\hat{p}\right) \qquad 3.17$$

where $\hat{s}\ and\ \hat{p}$ are unit vectors along s and p axes. The birefringence modulator modulates the polarization of the light beam passing through it at frequency 50 kHz utilizing the photoelastic effect, which cause glass to become birefringent under strain. The strain is induced by setting an isotropic glass slab (fused silica) of thickness d into longitudinal oscillation at its resonance frequency, driven by the piezoelectric effect. The periodic uniaxial strain $\delta(\omega_0)$ which is produced in the center of the slab results in a periodic change in the refractive index for light polarized parallel to the oscillation direction. This leads to a periodic variation in the refractive index difference for light polarized parallel and perpendicular to the oscillation direction. The dominant change is along the axis. In this direction, the refractive index increases during compression and decreases during expansion [71]. The difference in the refractive index varies sinusoidally with time at the frequency $\omega_0$. This strain-induced birefringence gives a phase shift between the light polarized in the two directions of :

$$\delta(\omega_0) = 2\pi\Delta_n \frac{d}{\lambda} = \delta_0 \sin(\omega_0 t) \tag{3.18}$$

where $\lambda$ is the wavelength of the light beam, $d$ the BM glass slab thickness and $\delta(\omega_0)$ and $\Delta_n(\omega)$ are the periodic uniaxial strain and the periodic variation in the refractive index difference

As in our case the incident light is polarized at $45^0$ to the axis of vibration, after birefringence element the light will be elliptically polarized with an oscillating phase shift between components parallel and perpendicular to the vibration axes. After passing through the birefringence modulator, a sinusoidally varying phase shift is created between the s and p polarizations. The light wave incident on the ambient medium-film surface has the form

$$\vec{E} = E_0\left(\hat{s} + e^{i\delta_0 sin\omega_0 t}\hat{p}\right) \tag{3.19}$$

where $\delta_0$ and $\omega_0$ are the amplitude and the angular frequency of the phase shift. The reflection at the ambient medium-film surface causes a change in the amplitude and the phase shift for the s and p polarizations. The two effects are included in the complex reflection coefficients,

$$r_p = r_{p,0}e^{i\delta_p}$$

$$r_s = r_{s,0}e^{i\delta_s} \tag{3.20}$$

So the amplitude of the electric field vector of the reflected light between the sample cell and the analyzer is given by:

$$\vec{E} = \frac{E_0}{\sqrt{2}}\left(r_{s,0}e^{i\delta_s}\hat{s} + r_{p,0}e^{i\delta_p+\delta_0 sin\omega_0 t}\hat{p}\right) \quad 3.21$$

The analyzer is a linear polarizer that samples the two alternative directions winch are rotated by 45˚ relative to s and p axes. The electric field amplitude for these two directions are:

$$\vec{E} = \frac{E_0}{2}\left(r_{s,0}e^{i\delta_s}\hat{s} \mp r_{p,0}e^{i\delta_p+\delta_0 sin\omega_0 t}\hat{p}\right) \quad 3.22$$

The PMT measure the intensity of light which is proportional to $|E^2|$

$$I \propto |E^2| \propto \left(r_{s,0}^2 + r_{p,0}^2\right)\left[1 \mp \frac{2r_{s,0}r_{p,0}}{r_{s,0}^2 + r_{p,0}^2}\cos(\Delta + \delta_0 sin\omega_0 t)\right] \quad 3.23$$

where $\Delta = \delta_p - \delta_s$. The output current of the PMT is proportional to the intensity $I$ and the gain voltage $V_G$, applied across PMT's dynodes. The electronics supplies a voltage to a lock-in amplifier which is proportional to the ac component of $I_{PMT}$. The lock-in measures the amplitudes of the ac voltage components possessing angular frequencies $\omega_0$ and $2\omega_0$. At Brewster angle $r_{p,0} = 0$ for a surface with a profile thickness of zero. However, for a nonzero thickness $r_{p,0} \neq 0$ at Brewster angle $\theta_B$. In this case, $\theta_B$ is defined as the angle at which $\Delta = \mp\pi/2$. Practically, $\theta_B$ is found by zeroing in on the angle of incidence at which $V_{2\omega_0}$=0. At this angle $V_{\omega_0}$ is proportional to $\bar{\rho}$ and the proportionality constant is determined by the calibration procedure.

In Brewster angle ellipsometry, the quantity $\bar{\rho}$ is measured and defined as the imaginary part of the ratio of the complex components measured at Brewster angle.

$$\overline{\rho} = \mathrm{Im}\left(\frac{r_p}{r_s}\right)\Big|_{\theta_B} \qquad 3.24$$

The nature of dependence of $\bar{\rho}$ on the thickness of the surface makes it ideal for probing the structure of the surface as a function of the distance perpendicular to the surface. For a step surface with zero thickness, $r_p = 0$, so $\rho = 0$. A nonzero surface thickness gives a nonzero value for ρ, which is determined from the Drude equation. For thin profile compared to the wavelength of the light λ,

$$\bar{\rho} = \frac{\pi\sqrt{\epsilon(-\infty)+\epsilon(\infty)}}{\lambda\epsilon(-\infty)-\epsilon(\infty)}\int_{-\infty}^{+\infty}\frac{[\epsilon(z)-\epsilon(+\infty)][\epsilon(z)-\epsilon(-\infty)]}{\epsilon(z)}dz \qquad 3.25$$

where ∈(z) is the optical dielectric constant as a function of z, the depth into the surface, and ∈ (+∞) and ∈ (-∞) are the optical dielectric constants of the bulk incident and reflecting mediums, respectively. As an example, consider as seen in Fig. 3.5, a surface that has the optical dielectric profile is given by :

$$\epsilon(z) = \begin{cases} \epsilon 0, & z < 0 \\ \epsilon 1, & 0 < z < d \\ \epsilon 2, & z > d \end{cases} \qquad 3.26$$

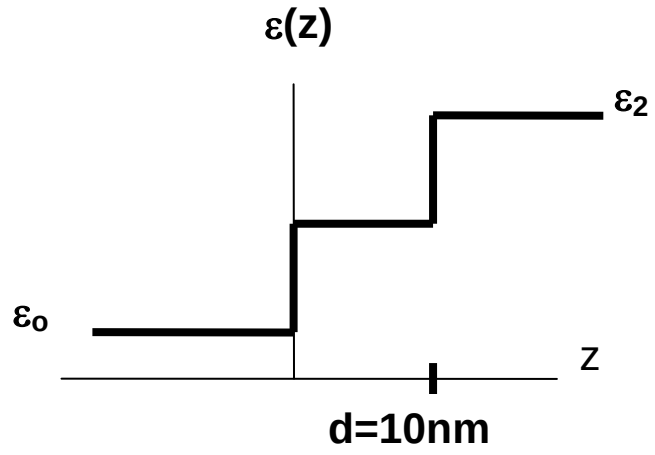


Fig. 3.6. Interface with dielectric profile.

For this profile, the Drude equation is given by:

$$\bar{\rho} = \frac{\pi}{\lambda} \frac{\sqrt{\varepsilon_2 + \varepsilon_0}(\varepsilon_2 - \varepsilon_1)(\varepsilon_1 - \varepsilon_0)}{(\varepsilon_2 - \varepsilon_0)\varepsilon_1} d \qquad 3.27$$

We can see that $\bar{\rho}$ proportional to the thickness of the layer. The minimum resolution of the ellipsometer is $\bar{\rho} \cong 5 \times 10^{-5}$. With $\epsilon_2 \cong \epsilon_1 \cong 2, \epsilon_2 - \epsilon_1 \cong 0.2, \epsilon_0 = 1, and\ \lambda = 633nm,$ this resolution corresponds to d≈ 0.05 nm. So ellipsometry can be used to measure the thickness of monolayers. The maximum sensitivity of $\bar{\rho}$ is seen to occur at $\theta_B$ as shown in Fig. 3.7 below.

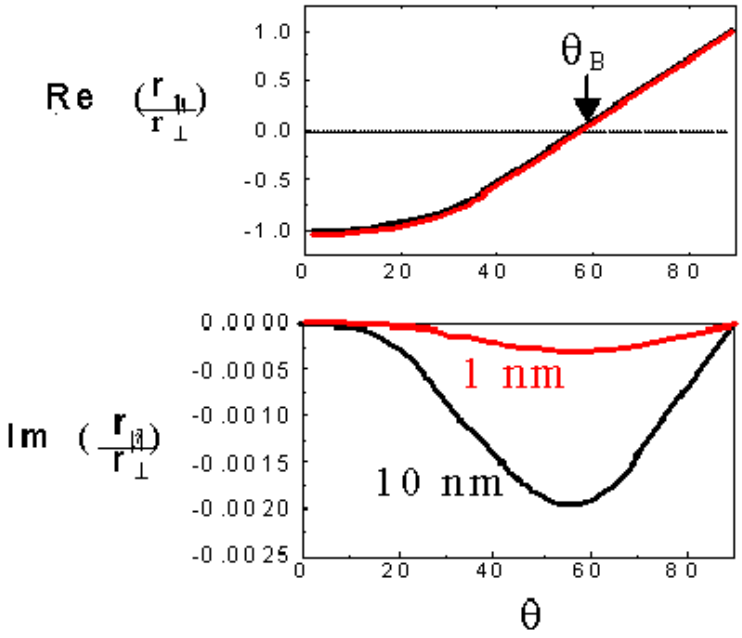


Fig. 3.7 Variation of Re(r) and Im(r) with layer thickness.

# CHAPTER 4

## DIFFUSION OF NANOPARTICLES IN SEMIDILUTE AND ENTANGLED POLYMER SOLUTIONS

*Some parts of the following material were originally published in The Journal of Physical Chemestry B Letters (2009)*[72]

### 4.1 DIFFUSION OF GOLD NANOPARTICLES IN POLYSTYRE-TOLUENE SOLUTIONS

Understanding the transport properties of nano- and micrometer-sized particles in crowded solutions of macromolecules (polymers, proteins, etc.) is important in various problems of medical and technological interests, such as chromatography, electrophoresis, and drug delivery[73-75]. This understanding would also be beneficial to several important fields of studies across disciplines. For example, the diffusional characteristics of tracer particles in crowded solution of flexible and rigid rod macromolecules are important for diverse biological phenomena ranging from metabolism, protein-protein interactions, enzyme reactions and gene therapy. In the field of biophysics, macromolecular crowding dramatically affects cellular processes such as protein folding and assembly, regulation of metabolic pathways, and condensation of DNA. In addition, the modeling of cellular processes, such as enzyme reactions, critically rely on understanding the diffusion of globular proteins in crowded cytoplasmic environments[76, 77].

In the area of polymer physics, the dynamics of particles can provide important information about the local mechanical and viscoelastic properties of the solution, an approach widely used in microrheology [78-81]. Mason and Weitz presented a novel experimental method to measure linear viscoelastic moduli of complex fluids using dynamic light scattering. In their study, they show that the response of the fluid to thermal fluctuations, as probed by the average

motion of small particles dispersed within the fluid, provides a close representation of the response of the bulk fluid to an imposed shear strain. Dynamic light scattering was used to measure the mean square displacement of a probe particle $<\Delta r^2>$, and relate this to the complex shear modulus by describing the motion of the particle with a generalized Langevin equation. The Brownian motion of these particles is strongly influenced by the nature of the surrounding matrix. Albert Einstein derived that the mean square displacement $<\Delta r^2>$ of a particle undergoing Brownian motion in a Newtonian fluid must increase linearly with time. Later, the concepts of Einstein were expressed in a stochastic differential equation of motion by Paul Langevin. Mori and Kubo derived the generalized Langevin equation, in which the constant friction coefficient of the traditional Langevin equation is replaced by a memory function that couples the motion of a particle to the history of its velocity, thus accounting for the viscoelasticity of the medium that surrounds the particles. This has formed the foundation for a field of investigation known as microrheology[78-81]. In microrheology, the thermal displacement of particles is analyzed in terms of the rheological response of the surrounding material.

A large body of experimental work has focused on comparing the experimentally measured translational diffusion coefficient (D) of the particles with the prediction from Stokes-Einstein (SE) relation using the known polymer macroscopic viscosity η[35, 82-84]. The translational diffusion coefficient (D) of the sphere and η is typically related via the Stokes-Einstein relation:

$$D = \frac{k_B T}{6\pi\eta R} \tag{4.1}$$

where R is the radius of the sphere and η is the zero shear-rate viscosity of the medium in which it is suspended. This relation assumes that the medium may be treated as a continuum on the length scale of R. Ullmann *et. al.* have studied the diffusion coefficient of polystyrene latex probe spheres in aqueous solutions of poly (ethy1ene oxide) as a function of the sphere radius R, the polymer concentration c, and the molecular weight M of the polymer. They found that the Stokes-Einstein equation for D fails badly, for D being larger than that predicted from R and the macroscopic shear viscosity η, and the failure increases with increasing polymer concentration.

In the de Gennes models of polymer solutions[85], solution properties depend qualitatively on the polymer concentration c, with properties changing their nature as the polymer concentration passes from one regime to the next, particularly at the overlap concentration c*, which divide the dilute solutions from semidilute solutions. A semidilute polymer solution can be viewed as a transient mesh of polymer chain, the distance between the contact (entanglement) points of the chains giving a scaling length ξ. For high molecular weight polymers, ξ is much less that the total chain length and the entanglement points dominate the polymer dynamics. Moreover, the local properties are predicted to be independent of molecular weight M. In the semidilute regime, the average mesh size ξ decreases with increasing concentration according to $\xi \approx R_g (c/c^*)^{-3/4}$. Here, the overlap concentration is given by $c^* = M_w/(4/3\pi N_A R_g^3)$ and $R_g$ is the radius of gyration of the polymer chains

It is further predicted that polymer solution properties follow scaling laws in which the logarithmic dependence of a property is proportional to a power of the polymer concentration. For example, the following scaling relation gives the diffusion coefficient, D:

$$\frac{D}{D_0} = \exp(-\alpha c^{\nu}) \qquad 4.2$$

where $D_0$ is the limit of low polymer concentration, and α and ν are arbitrary parameters[82].

In another theoretical analysis of probe motion in semidilute solutions, de Gennes and coworkers argue that if R>> ξ, the polymer solution will appear to the probe particle as a continuum. On the other hand, if R ≤ξ, the polymer solution cannot be treated as a continuum anymore and its local viscosity η may change with the length scale at which it is probed.
Theories developed by Odijk[86], following Ogston[87, 88], Philles[89-91], Cukier[92], Altenberger[93], Amsden[94] and de Gennes[95, 96] predicted the same exponential dependence of viscosity on probe size, but they differ in the physical mechanisms that led to such dependence. Mechanisms used as a basis include hydrodynamic drag on the solute molecule, energy barriers to solute jumps, and physical obstruction due to the presence of the polymer chains. Although none of these models is successful at explaining all the experimental observation, all experiments and theoretical calculations showed the same universal stretched exponential dependence of viscosity on the size of nanoprobes and concentration of polymer solutions.

An important advance in the study of the relation between nanoviscosity, probe size and polymer concentration came in 1978 with the experiments of Langevin and Rondelez[97]. They showed that instead of two variables ( probe size and concentration of a polymer), the nano viscosity felt by the nanoprobe is an exponential function of only a single variable, R/ ξ, where R is the size of a probe and ξ is the correlation length which is dependent on concentration, in the semi dilute solution. Following this experimental work, de Gennes[85, 95] developed a theoretical approach to the viscosity of polymer solution. He suggests that a dense polymer solution can be viewed as a transient statistical network of mesh size (correlation length), ξ, in a solvent. This

size also corresponds to the size of the "blob" inside which all monomers belong to the same polymer chain. Moreover, he postulated that the viscosity should depend on R as $\eta(R/\xi)$, as verified by Langevin and Rondelez. Therefore, in this approach, the viscosity experienced by the probe of size $R>>\xi$ should have a constant value equal to the macroscopic viscosity, while for $R<\xi$, the viscosity should depend on R as $\eta(R/\xi)$. Thus, in this model, the crossover length scale, L, is equal to $\xi$. Since $\xi$ decreases with polymer concentration, for any size, R, there is a well-defined concentration, $c(\xi)$, for which a crossover occurs to the macroscopic viscosity. In the first case, when $R>>\xi$, the mobility of the particle is coupled to the chain relaxation; hence, the particles experience the macroscopic zero shear rate viscosity and the particle diffusion satisfies the SE relation[35, 98]. In the opposite case, when $R<\xi$ the particles generally experience the local microscopic viscosity, which is a strong function of the length scale at which it is probed[83]. The local viscosity is generally lower than the macroscopic viscosity of the polymer solution, therefore in this situation the particle mobility is faster compared to SE prediction[35].

In this chapter, we focus on the diffusion of gold particles in semidilute polymer solution of polystyrene (PS) in toluene. The size of the nanoparticles used in our experiments is such that $R\approx\xi$. We have used the methods of fluctuation correlation spectroscopy (FCS), which have high sensitivity and selectivity[99-101].

Unlike traditional FCS, which depends upon fluorescent dyes, we have utilized multiphoton absorption induced luminescence of gold nanoparticles as contrast. This overcomes the problem of finite photochemical lifetime of dyes in probing slow polymer dynamics. In addition, it allows us to measure the dynamics at length scales larger than the size of the dye molecules (≈1 nm). The novelty of this investigation is the use of much lower concentration of particles ($<10^{-4}$ % v/v) which perturbs the system minimally as compared to methods such as

dynamic light scattering (DLS) or fluorescence recovery after photobleaching (FRAP). It also simplifies the interpretation of data as the particle-particle interaction through depletion forces or by the formation of polymer bridges between neighboring particles can be neglected.

Polystyrene (PS) of Mw = 240 kg/mol (Mw/Mn = 1.10, Polymer Sources, Inc.) and a dilute concentration of particles were prepared in toluene by stirring the samples as needed and was kept within a sealed cell to prevent evaporation of solvent during measurements. Gold nanoparticles of radius, R ≈ 2.5 nm were purchased commercially (Microspheres-Nanospheres, Inc.) and their size was verified by transmission electron microscopy (TEM) measurements (Figure 4.1). Control experiments involving the gold particles and polymer conducted over several days yielded no evidence of time dependent changes in diffusion or clumps in the counts vs time data. This implies that there are no strong chemical interactions (e.g., ionic, covalent, etc.) between particle and polymer are present, which would have led to adsorption of polymers onto surfaces.

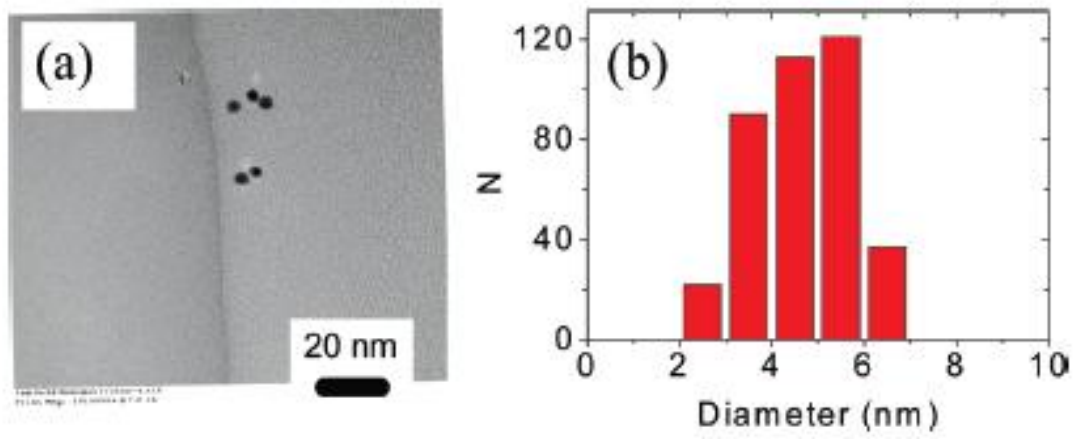


Fig 4.1 (a) TEM of gold colloids deposited on carbon film magnified 800 000×. A JEOL FasTEM 2010 TEM with a LaB6 filament working at 200 kV was employed to capture the image. (b) A histogram obtained from measuring the diameters of gold colloids is displayed. The average diameter measured is 4.7 ±1.1 nm.

A plot of emission intensity vs incident power showed that the excitation of particles is a three photon process[50]. Recent experiments have demonstrated that gold nanoparticles excited by a laser can generate significant local thermal effects in the vicinity of the particle[102]. According to the theory of photothermal heterodyne detection by Berciaud et. al., $\Delta T$ (the surface temperature increment relative to the ambient temperature) are given by $\Delta T=P_{abs}/4\pi\kappa R$, where $P_{abs}$ is the absorbed heating laser power, $\kappa$ is the thermal conductivity of gold nanoparticles, and R is the radius of the nanoparticle. A particle of R = 20 nm excited by a 1 mW laser could have a local temperature 50 K above that of the surrounding liquid medium. As the absorption cross-section has a $R^3$ dependence, the thermal halo effect for R = 2.5 nm size particles has a local temperature $((2.5/20)^3*50)$, which is <0.1 K higher as compared to the surrounding liquid. Therefore, the local thermal effect is not expected to significantly affect the diffusive behavior of particles in our experiments. Samples were prepared with concentrations, c = 0.1, 0.15, 0.27, and 0.33 g/cm$^3$ of PS using a digital balance with a resolution of 1 mg. The overlap concentration (c*), which denotes the onset of the semidilute regime was determined by using the relationship,[14] $c^* = M_w/ (4/3\pi N_A Rg^3)$. Here, $N_A$ is Avogadro's number and the radius of gyration of the polymer chains, Rg ≈ 18 nm was estimated from experimental results of a previous study [103]. We obtained c* = 0.015 g/cm$^3$; so all concentrations studied are above the overlap concentration. In the semidilute regime, the average mesh size, $\xi$ decreases with increasing concentration according to $\xi \approx Rg(c/c^*)^{-0.75}$ and independent of the molecular weight $M_w$ since $Rg\sim M_w^{0.6}$. For the concentration range studied in our experiments, the particle size is comparable to the mesh size; $R/\xi$ ranges from 0.6 (for c = 0.1 g/cm$^3$) to 1.4 (for c = 0.33 g/cm$^3$).

The diffusion coefficient (D) is obtained by the following procedure: $G(\tau) = G(0)/[(1 + S(\tau))(1 + S(\tau)/p2)^{1/2}]$, where G(0) is the autocorrelation function (ACF) magnitude at small time, and p ($\omega_z / \omega_0 \approx 5$) is the ratio of the effective length to width of the ellipsoidal laser focus. $S(\tau) = \tau/\tau_D$ for normal diffusion, where $\tau_D$ is the average residence time of the particles within the focus. D is related with $\tau_D$ through $D = \omega_0^2/8\ \tau_D$, where the half-width of laser focus $\omega_0 \approx 0.2$ μm.

Figure 4.2 displays representative autocorrelation functions for nanoparticles in neat toluene, and PS concentrations of c = 0.1 and 0.33 g/cm$^3$. It is clear from the Figure that as the concentration of polymer is increased, the mean decay time of the correlation functions increases, which can be attributed to the increase of viscosity of the solution. At higher concentrations of polymer, the simple diffusion model fails to fully describe the autocorrelation function. We used a more general functional form for $S(\tau) = (\tau/\ \tau_a)^{\alpha}$, with $\alpha < 1$, which is known as anomalous subdiffusion[76, 104] to fit all autocorrelation functions in Figure 2. In this case, an apparent diffusion coefficient can be defined as $D = \omega_0^2/8\tau_a$, which describes the diffusion coefficient at the length scale of $\omega_0$ and at the time scale of $\tau_a$.[1] Table 4.1 shows the fitting parameter used to fit the autocorrelation function for all concentrations.

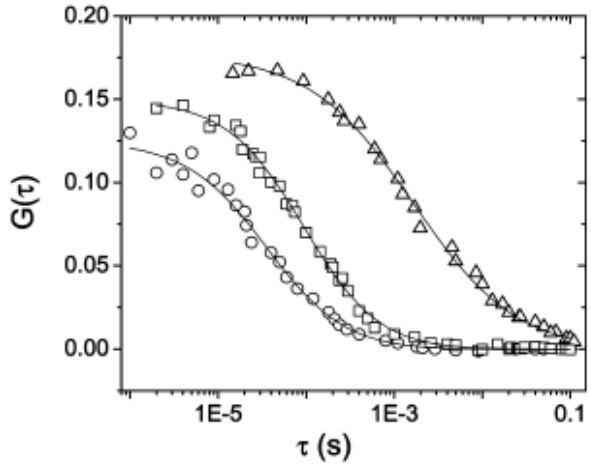


Figure 4.2 Autocorrelation plots of 5 nm gold colloids diffusing through neat toluene (circles), 0.1 g/cm$^3$ PS in toluene (squares), and 0.33 g/cm$^3$ PS in toluene (triangles). All curves were fitted with an anomalous diffusion model, where $D$ = 141 $\mu$ m$^2$/s, α = 0.95 in toluene, $D$ = 53.1 $\mu$ m$^2$/s, α = 1.0 in the 0.1 g/cm$^3$ PS solution, and $D$= 2.98 $\mu$ m$^2$/s, α = 0.73 in the 0.33 g/cm$^3$ PS solution. Typical fitting error for α is ±0.05.

Table 4.1: Fitting parameters of $S(\tau) = (\tau/\tau_a)^{\alpha}$ used to fit the autocorrelation functions

| Concentration (g/cm$^3$) | $\tau_a$ ( $10^{-5}$ sec) | α |
|---|---|---|
| 0.1 | 2.13±0.21 | 0.98±0.05 |
| 0.15 | 16.5±0.17 | 0.93±0.075 |
| 0.27 | 42.1±5.59 | 0.82±0.01 |
| 0.33 | 177.93±39.89 | 0.73±0.01 |

In Figure 4.3, we plot D and α as a function of concentration of PS. As the concentration of polystyrene increases, D decreases monotonically. At neat toluene and lower concentrations, the anomalous exponent α ≈ 1, which suggests that the diffusing particles obey homogeneous dynamics; however, at higher concentrations, the transport behavior of particles becomes clearly subdiffusive. Note that, even for samples with the highest concentration of polymers, the glass transition temperature (Tg) of the mixture was well below the measurement temperature (≈27

°C). For c = 0.33 g/cm$^3$, we estimated Tg ≈ -100 °C by employing the Fox equation[105], $1/T_{g,solution} = x_1/T_{g,toluene} + x_2/T_{g,polystyrene}$, where $T_g$ is the glass transition temperature of the mixture of toluene and polystyrene, and $x_{1,2}$ is the mass fraction of the toluene and the polystyrene, respectively. Table 4.2 shows the calculated value of the glass transition temperatures for PS-toluene solutions of all concentrations. To obtain more insight into the transport process, we studied the diffusion of free dyes (coumarin 480) in polymer solutions with similar concentrations.

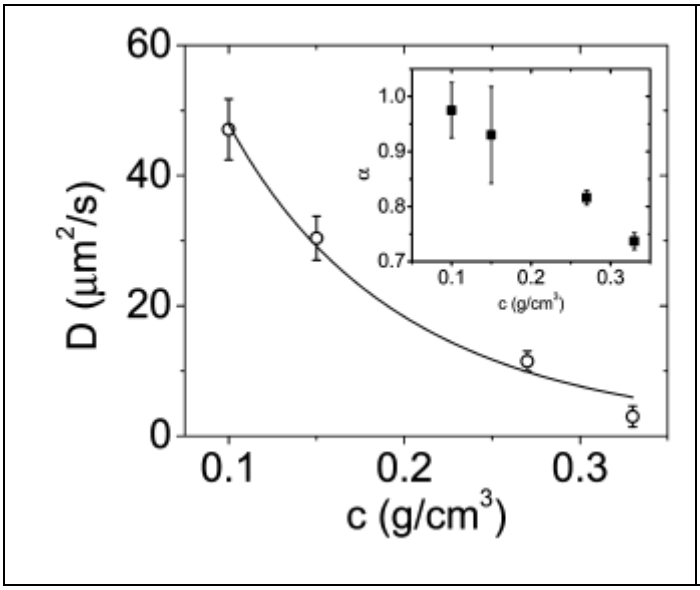


Figure4.3 Concentration dependence on the diffusion coefficient of 5 nm gold colloids at 27$^0$C. The data are fitted (solid line) according to the Phillies' equation with fitting parameters, $D_0 \approx 170$ $\mu$m$^2$/s, $\mu \approx 12$, $v \approx 0.9$. (inset) Anomalous exponent α obtained for gold colloids plotted as a function of concentration.

In Figure 4.4, we present the measured values for D and α as a function of concentration. The diffusion of coumarin is normal within experimental error bars for all concentrations studied. Diffusion data can be fitted reasonably well with the Vrentas-Duda free volume theory[50], which assumes that the friction coefficient is a strong function of concentration due to the dependence of free volume on concentration[106].

Table 4.2: The glass transition temperatures for the PS-toluene solutions.

| Concentration (g/cm$^3$) | $T_g$ ($^0$C) |
|---|---|
| 0.1 | -127 |
| 0.15 | -122 |
| 0.27 | -108 |
| 0.33 | -100 |

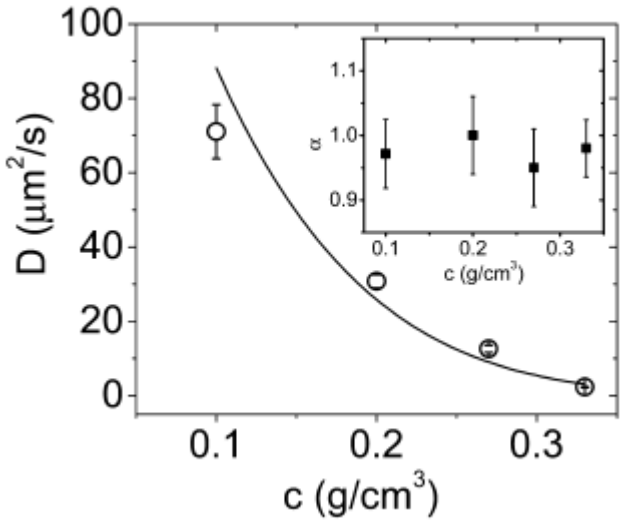


Figure 4.4 Concentration dependence on the diffusion coefficient of coumarin at 27 $^0$C. The data are fitted (solid line) according to the Vrentas-Duda equation. (inset) Anomalous exponent α for coumarin obtained as a function of concentration.

We compared the diffusion coefficient of the particle with the prediction from SE relation. The viscosity information of the PS-toluene solution at various concentrations has been obtained from refs [107, 108]. For all concentrations studied the correlation length, ξ of the polymer solution is comparable to the particle radius. In this case, our results indicated that the measured diffusivity of the particle exceeds the SE-predicted value, when the solution viscosity was used to calculate the predicted value. To be more precise, for c = 0.1 g/cm$^3$, $D/D_{SE} \approx$ 0.3, 2, and 7 when we used solvent viscosity, linear viscosity, and solution viscosity, respectively. The

calculation is shown here for c=0.1g/cm$^3$ and the calculated $D/D_{SE}$ for all concentrations is shown in table 4.3. Firstly, the solvent (Toluene) viscosity is 0.59 cP, so the predicted diffusion from Stokes-Einstein equation for 5 nm gold nano particles would be $D_{SE}$=147 μm$^2$/s and $D/D_{SE}$ =0.3. Secondly, the linear viscosity depends on the concentration through the given relation: $\ln \eta = -5.26 + B_1 c$, where $B_1$=0.4 for Mw=240 kg/mol and c is the concentration. For c=0.1 g/cm$^3$ η=5.5 cP, then the predicted diffusion $D_{SE}$ =15.8 μm$^2$/s and $D/D_{SE}$=2.75. Finally, the solution viscosity is given by: $\ln \eta = -5.26 + B_1 c + B_2 c^2 + B_3 c^3$. For c=0.1 g/cm$^3$, η=13.6 cP and the predicted diffusion $D_{SE}$ =6.4 μm$^2$/s and $D/D_{SE}$=7. In this case, motion of the particle is not completely coupled with the polymer matrix relaxation, and the particle experienced local nanoviscosity. This local viscosity is smaller than the macroscopic viscosity of the polymer solution, but higher than the solvent viscosity. For rigid, spherical particles, it is customary to fit the concentration dependence of diffusion coefficient with a stretched exponential relation, known as Phillies equation: $D(c) = D_0 \exp(-\mu c^{\nu})$, where $D_0$ is the diffusion coefficient in pure solvent and ν is the scaling parameter. Our data in Figure 4.3 can be fitted by a stretched exponential reasonably well with a value of the exponent, $\nu \approx 0.9$, as determined by a nonlinear least -squares fit.

Table 4.3 Comparison between experimental diffusion and prediction from Stokes-Einstein equation

| | $D/D_{SE}$ | | |
|---|---|---|---|
| c (g/cm$^3$) | Solvent viscosity | Linear viscosity | Solution viscosity |
| 0.1 | 0.3 | 2.75 | 7 |
| 0.15 | 0.2 | 1.93 | 13 |
| 0.27 | 0.07 | 1 | 47 |
| 0.33 | 0.03 | 0.34 | 42 |

Let us now discuss the observation of anomalous subdiffusive behavior of nanoparticles at higher concentrations of polymers. This indicates that the mean square displacement (MSD) of the particles, $<r^2(t)>$ increases less than linearly with time. This has been observed previously in complex, heterogeneous environments, such as in gels[96,101] or inside of a cell cytoplasm[76, 77]. Computer simulations also predicted such behavior in the presence of fixed obstacles at high concentrations[109]. Particle tracking microrheology experiments measured an anomalous exponent of $\alpha = 3/4$ for the diffusion of tracer particles in filamentous actin network, when the size of then tracer is larger than the network mesh size[110]. This indicated a coupling between the tracer motions with the transverse thermal fluctuation of the network. However, the entangled network that the concentrated polymer solutions formed in our experiments is temporary. We estimated the volume fraction of polymers at entanglement concentration by using, $\varphi e \approx (M_e/M_w)^{0.76}$. Where $M_e$ is the entanglement molar mass[32]. From the known polystyrene density which is 1.05 g/cm$^3$ and entanglement molecular weight at the melt ($M_e \approx 17$ kg/ mol), we determined $c_e \approx \rho^* \varphi_e = 0.15$ g/cm$^3$. Therefore, the observation of subdiffusion coincides with the onset of the entanglement effect. The entanglement length of the PS solution was estimated to be ≈10 nm at $c = 0.3$ g/cm$^3$, which is comparable to the size of the particles. In this case, an analogy with glass forming colloidal systems can be made, where a tracer particle can be trapped for a long time within a transient cage formed by other particles. In such cases, particle tracking experiments had revealed subdiffusion. A similar situation can arise in our experiments as well, where the mobility of the nanoparticles can become restricted due to transient caging of the particles within the entanglement tube formed by the polymer chains. This also explains why normal diffusion was observed in experiments with dyes. Because of their much smaller size, they are not likely to be caged. In an alternative scenario, nonspecific interactions such as steric or van der Waals

interactions of the particles with the macromolecule in a crowded environment can cause heterogeneities in the frictional drag. These interactions are typically weak and have energies of the order of thermal energy so that the particles could bind and unbind with the macromolecular segment as they move within the focal volume[76]. This may give rise to a spectrum of time scales, resulting in a nonlinear relationship between MSD and time. A definitive microscopic interpretation requires experiments both as a function of polymer molecular weight and particle sizes, which are currently under progress.

In conclusion, we report measurement of translational diffusion coefficient of nanoparticles in semidilute polymer solutions. The focus of this work was to investigate the situation when the size of the particle is comparable to the matrix correlation length. An important finding is the observation of anomalous subdiffusion at entangled polymer solutions. The results will have ramifications in understanding the colloidal transport properties in polymer solutions and in other structured fluids. The approach used here will also be helpful to extend the technique of microrheology at much smaller scales comparable to the molecular dimensions.

## 4.2 DIFFUSION OF NANOPARTICLES PROBES IN SEMIDILUTE POLY(ETHYLENEGLYCOL)-WATER SOLUTION

This work is a continuation of our previous study on probe diffusion of gold nanoparticles in semidilute and entangled polymer solution of polystyrene (PS) in toluene where the radius of the particles was much smaller than the radius of gyration ($R_g$) but comparable to the average mesh size $\xi$ of the fluctuating polymer network. In this work, the diffusion coefficient of gold

nanoparticles in poly(ethy1ene glycol) in water solutions was studied as a function of sphere radius R, polymer concentration c, and polymer molecular weight $M_w$. The radii of the particles are comparable to both $R_g$ and $\xi$ .

The diffusion of hard spheres in linear polymer solutions has been theoretically studied based on different physical models. As discussed earlier, all of these models describe the reduced diffusion coefficient of probe particle in a stretched exponential function of the concentration of the polymer matrix.

$$D/D_0 = \exp(-\mu c^{\nu}) \qquad 4.3$$

where $D_0$ is the diffusion coefficient in pure solvent, $\mu$ is a function of the probe size R, and $\nu$ is a scaling parameter related to the solution properties of the polymers. This phenomenological approach was first introduced by Phillies to describe the self-diffusion behavior of macromolecules over a wide range of concentrations. He generalized a simple scaling equation for optical probes in polymer solutions:

$$D/D_0 = \exp(-ac^{\nu}M_w^{\gamma}R^{\delta}) \qquad 4.4$$

where $M_w$ is the molecular weight of the background polymer, R is the probe radius, and $\nu$, $\gamma$, and $\delta$ are scaling coefficients. Experimentally, $\nu$ = 0.5-1.0, $\gamma$= 0.8 ± 0.1, and $\delta$ = 0.2. These values are substantially inconsistent with theoretical predictions $\gamma$ = 0 and $\delta$ = 1 for probe diffusion in open-coil polymer solutions.

In semidilute concentration regime, where R is of the same order of the correlation length, $\xi$, the diffusion will be dominated by the fluctuation of the mesh size, and an activation energy using scaling analysis be used proportional to R/ $\xi$. Therefore, the diffusion coefficient can be written as:

$$D = D_0 \exp(-\beta(R/\xi)^{\delta}) \quad 4.5$$

Using $\xi = R_g(c/c^*)^{-0.75}$, eq 4.5 can be written as a stretched exponential function of polymer concentration. eq 4.3 In this case, if we assume that $\delta=1$ according to several theoretical predictions, then $\nu = 0.75$.

Poly (ethylene glycol) (PEG) of Mw = 5.4, 37.8, 102 kg/mol (Mw/Mn = 1.08, Polymer Sources, Inc.) and a dilute concentration of particles were prepared in water by stirring the samples as needed. Gold nanoparticles of diameter, D ≈ 5, 10 nm were purchased commercially (Microspheres-Nanospheres, Inc.) and their size was verified by transmission electron microscopy (TEM) measurements. Control experiments involving the gold particles and polymer conducted over several days yielded no evidence of time dependent changes in diffusion or clumps in the counts vs time data. This implies that no strong chemical interactions (e.g., ionic, covalent, etc.) between particle and polymer are present, which would have led to adsorption of polymers onto surfaces.

Poly(ethylene glycol) (PEG) is a flixable polymer and its radius of gyration in water as a function of molecular weight is given by $R_g = 0.02\ M_w^{0.58}$ [nm][111]. Using this relation, we calculated $R_g$ = 2.9 nm (for PEG 5400 g/mol), $R_g$ = 9 nm (for PEG 37 800 g/mol) and $R_g$ = 16.1 for PEG 102 000 g/mol). The average mesh size, $\xi$ is a function of polymer concentration, c, $\xi = R_g(c/c^*)^{-0.75}$, where c* is the polymer overlap concentration at which chains start to overlap.

The overlap concentration depends on the molecular weight of PEG: $c^* = 0.086$ g cm$^{-3}$ (for PEG 5400), $c^* = 0.02$ g cm$^{-3}$ (for PEG 37 800), $c^* = 0.001$ g cm$^{-3}$ (for PEG 102 000). Thus, for example, 8.6 % (w/w %) solution of PEG 5 400 in water, the polymer chains start to overlap. The mesh size, $\xi$, only weakly depends on the molecular weight. All samples were prepared with

concentrations, c=0.1, 0.2, 0.3, and 0.4 g/cm3 (w/w %) of PEG; so all concentration studied here were above the overlap concentration in the semidilute regime and the average mesh size $\xi$ corresponding to these concentrations was 2.6 nm, 1.55 nm, 1.14 nm, and 0.9 nm, respectively. The probe gold nanopartibles have two different sizes: 5 nm, 10 nm and so R/ $\xi$ ranges from 0.86 to 5.43.

Measurements of the diffusion coefficient D of the 5 nm and 10 nm gold nanoparticles are plotted as a function of the polymer concentration in figure 4.5. At each concentration, the average of three different measurements for D was recorded with the standard deviation as the error of the measurement. The behavior exhibited by 5 nm and 10 nm spheres for the three different molecular weights: 5400 g/mol, 37 800 g/mol, and 102 000 g/mol were largely similar. In each PEG-water system, the diffusion coefficients decrease monotonically with increasing polymer concentration; D of the 5 nm nanosphere in pure water was 112 $\mu m^2/s$, which is $D_{0,}$ and it falls to 62 $\mu m^2/s$, 57.7 $\mu m^2/s$ and 49.5 $\mu m^2/s$ in 0.1 $g/cm^3$ solutions of 5400 g/mol, 37 800 g/mol, and 102 000 g/mol polymers, respectively.

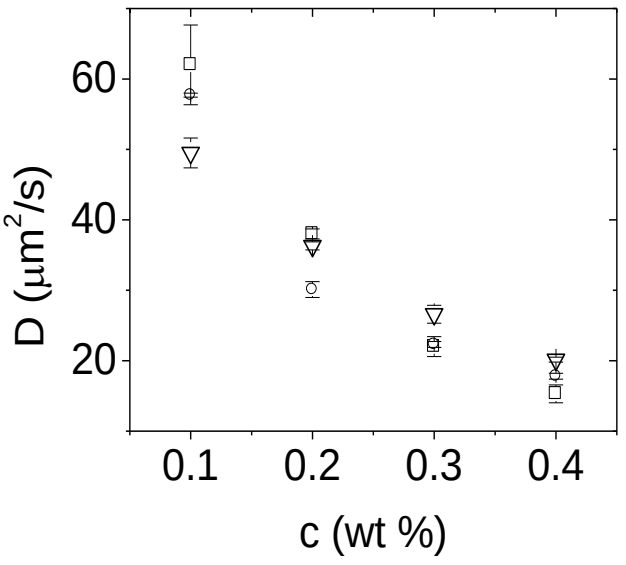


5 nm gold nanparticles

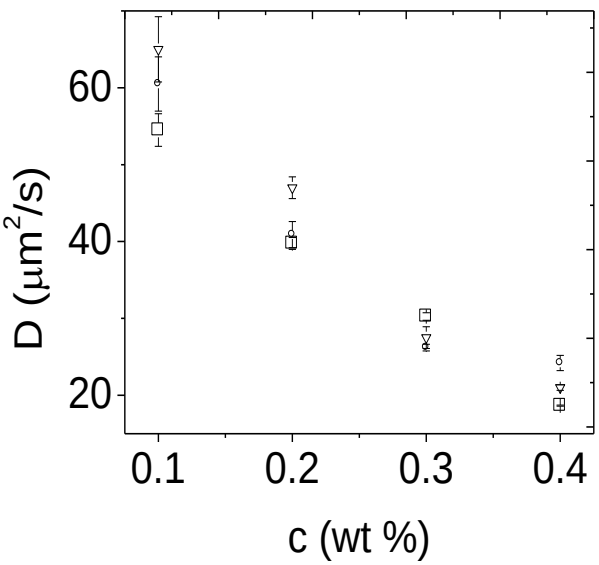


10 nm gold nanoparticles

Fig 4.5 The concentration dependence of the : (a) 5 nm gold nanoparticles in three different Mw: 5.4k g/mol (triangles), 37.8 kg/mol (circles), and 102kg/mol (squares). (b) 10 nm for the same Mw.

All the diffusion measurements was fitted using Phillis stetched exponential $D=D_0 \exp(-\mu c^{\nu})$, where $D_0$ is the diffusion of the nanoparticles in pure water. $D_0$ was measured for both 5nm and 10 nm nanospheres to be 112 $\mu m^2/s$ and 85 $\mu m^2/s$, respectively. The solid line in Fig. 4.5 shows the fit to this equation. The corresponding μ and ν are given in Table 4.4.

| | Molecular weight ( g/mol ) | | | | | |
|---|---|---|---|---|---|---|
| Nanosphere size(nm) | 5,400 | | 37,800 | | 102,000 | |
| | μ | ν | μ | ν | μ | ν |
| 5 | 4.6 | 0.89 | 4.0 | 0.76 | 2.7 | 0.53 |
| 10 | 3.1 | 0.86 | 2.8 | 0.81 | 3.16 | 0.71 |

According to eq. 4.5, we plot ln ($D/D_0$) as a function of $R/\xi$ for 5 nm and 10 nm nanospheres in PEG solutions (Mw =5.4K, 37.8K, and 102K) in Fig. 4.6. Since $R/\xi$ ratio for 10 nm particles is double the ration for 5 nm particles ($\xi$ is the same in both cases), there is a shift in the curve for 10 nm particles to the right. In addition, the larger particles (10 nm) shows slower diffusion compared to the smaller ones (5nm). A master fit of the data gives stretched exponential power of $\delta$=0.96, 1.22 for 5nm and 10nm particles, respectively. The predicted value for $\delta$ is 1 by Cukier and Altenberger *et al*. this value indicates that the diffusion in polymer solution is a single relaxation process. If the particles diffuse in a continuum medium, it should obey Stokes-Einstein relation.

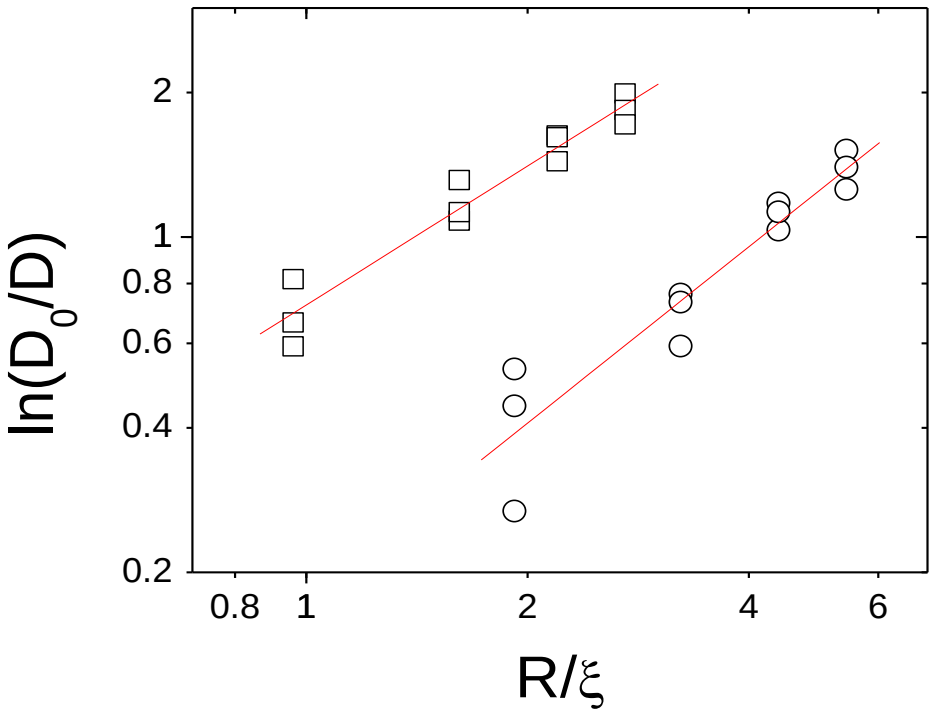

Fig. 4.6 Reduced probe diffusion coefficient vs the ratio of probe radius to mesh size ($R/\xi$) for different probes: 5 nm (squares) and 10 ( circles) for three different molecular weights Mw= 5.4k, 37.8k, and 102 k. the slopes of the fitting lines are 0.96 and 1.22 for the 5nm and 10 nm probes, respectively.

The macro viscosity ($\eta$) of the polymer solution was estimated in two different regimes. In the semidilute regime, where the concentration is greater than the overlap concentration $\varphi^*$ and less than the entanglement concentration $\varphi_e$, the relation $\eta_{sp} \approx (\varphi/\varphi^*)^2$ was used [32]. Here, the specific viscosity ($\eta_{sp}$ ) is given by $\eta_{sp} = (\eta - \eta_s)/\eta_s$ , and from this relation we can calculate $\eta$. In the entanglement regime, $\eta_{sp}$ is given by $\eta_{sp} \approx (\varphi/\varphi^*)^{14/3} N^{2/3}/[N_e]^2$ where N is the Kuhn monomers in the whole chain of polymer which can be calculated using the relation $N = M_w/M_0$, where $M_0$ is the molar mass of PEG Kuhn monomer, and its value for PEG is 137 g/mol. The other quantity, $N_e$ is the Kuhn monomers in an entanglement strand, and its value is 15 for PEG. The calculations are summarized in the following table.

| | Macro solvent viscosity $\eta$ (cP) | | | |
|---|---|---|---|---|
| $c(g/cm^3)$ | Mw=5400 g/mol | Mw=8000 g/mol | Mw=37800 g/mol | Mw=102400 g/mol |
| 0.1 | 2.35 | 3.44 | 26 | $9.17*10^8$ |
| 0.2 | 6.4 | 10.77 | 9425 | $2.3*10^{10}$ |
| 0.3 | 18 | 24 | 62906 | $1.6*10^{11}$ |
| 0.4 | 68 | 366 | 243168 | $6.2*10^{11}$ |

According to de Gennes scaling theory, the reduced diffusion coefficient does not depend on molecular weight $M_w$ whenever c>c*, because the mesh size is a function of only polymer concentration in the semidilute and concentrated regime. Our results indicate that $D/D_0$ depends weakly upon molecular weight $M_w$ in agreement with the theoretical prediction. To compare, we plot (Fig. 4.7) the results of this study with our previous study for diffusion of 5nm gold nanoparticles in 240k PS solutions in toluene.

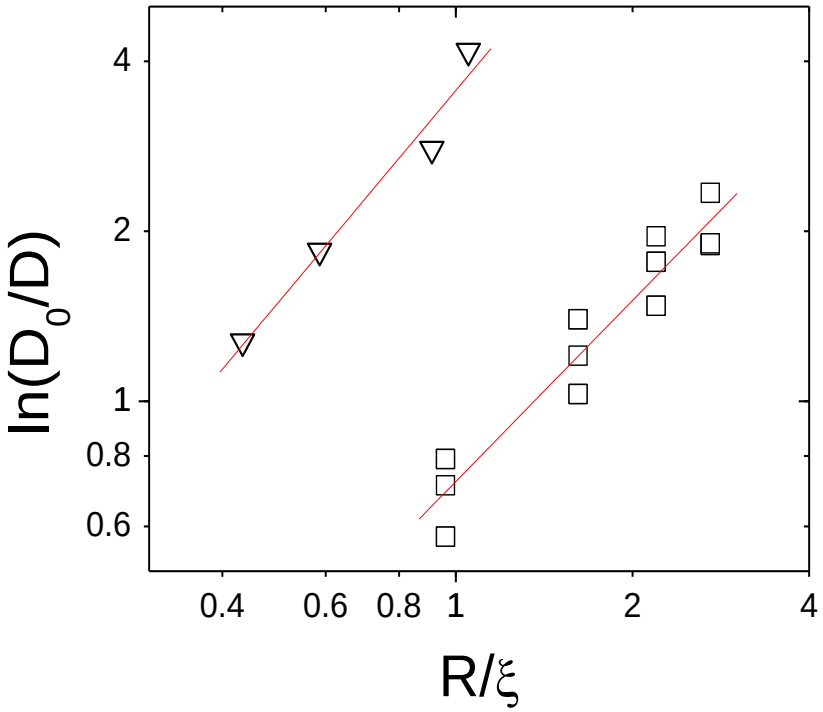


Fig. 4.7 Reduced probe diffusion coefficient vs the ratio of probe radius to mesh size ($R/\xi$) for different probes: 5 nm ( squares) in PEG-Water system (Molecular weight: 5,4k, 37,8k, and 102k) and (triangles) PS-Toluene system. The slopes of the fitting line are: 1.06 and 1.24 for both systems, respectively.

# CHAPTER 5

## CRITICAL ADSORPTION ON SHERICAL NANOPARTICLES

**The following material in a modified form was originally published in Physical Review Letters (2007)**

There has been a great interest recently in colloidal suspensions and the dynamics of colloids. Colloidal dispersions are familiar in everyday life, such as paint, and they are of great fundamental and technological importance. If colloidal particles are immersed in a solvent consisting of a binary liquid mixture, one of the fluid components may preferentially adsorb onto the bodies because of the difference in their affinity for the fluid components. The width of this layer is order of the solvent correlation length, which is a few angstroms. But near the critical point of the liquid mixture, as the correlation length diverges, the layer thickens and its importance in governing the properties of the suspension increases significantly.

As mentioned in chapter 2, the critical adsorption of simple fluids and liquid mixtures at semi-infinite and planar liquid-vapor and liquid solid surfaces in many different systems has been studied in much detail and is well understood. For a spherical particle, critical adsorption is expected to exhibit differences in behavior due to the effect of surface curvature. It has also been demonstrated experimentally that critical adsorption is highly related to thermally-induced reversible colloidal aggregation. This flocculation phenomena is observed in binary liquid mixtures (2,6 lutidine + water, isobutyric acid + water, etc.) in the presence of a small volume fraction of silica or polystyrene colloidal particles[21-23, 112]. Many theoretical and experimental studies have tried to explain this phenomenon; however, none of them can

explain all of the experimental observations[113, 114]. In this regard, a direct study of the critical adsorption onto a single isolated particle will be of great interest.

The colloidal particles used in many of these experiments have surface hydroxyl groups which dissolve in the binary mixture. Therefore, the surface becomes negatively charged. If one of the components of the mixture preferentially adsorbs onto the particles, an adsorbed film of the phase rich in that component can develop onto them. If the phase separation temperature of the liquid mixture is approached, the thickness of the adsorbed layer around the colloidal particles will increase. This leads to wetting films of the preferred phase coating the colloidal particles. These wetting films result in the presence of effective surface fields, which could lead to flocculation in these systems[112, 113]. However, it has also been suggested that if a high concentration of particles is used, the aggregation phenomena observed for the colloidal particles in binary liquid mixtures would be in fact a true phase separation in the ternary mixture.[115]. If the liquid mixture is near the critical demixing point $T_c$, the confinement of critical fluctuations of an order parameter field induces long-ranged forces between the surfaces of the film. This force has been recently called the "critical Casimir force". This is an attractive force, and it has been argued to play an important role to flocculation for a near-critical solvent mixture[42, 43, 116]. It has still not been worked out the roles of these different effects on flocculation. But we believe that the knowledge of the adsorption profiles at the surface of a single sphere near Tc would be useful to understand this phenoemena. This is the first experimental study in which the critical adsorption on spherical particles was measured. The results presented here will help in understanding the interaction of liquids with surfaces possessing geometric structure[26], the phase behavior of multi-component fluids[115, 117], and wetting phenomena[29-31, 112].

**Theoretical background**

The spherical particles with mesoscopic radius $R_0$ immersed in a binary liquid are characterized by the dimensionless variable $R_0/\xi$, where $R_0$ is the radius of the dissolved sphere and $\xi$ is the bulk correlation length. At a distance z from the surface of the sphere, critical adsorption is characterized by a universal scaling function $P(z/\xi, R_0/\xi)$[17]. The curvature dependence of the excess adsorption $\Gamma(t, R_0)$ describes the total enrichment of the preferred component of the fluid near the criticality in the proximity of the sphere, which is also characterized by universal scaling function $G(R_0/\xi)$ obtained from P(x,y) by integrating over $x=z/\xi$. Near $T_c$, the excess adsorption is expected to follow a scaling relation, $\Gamma\ (t\rightarrow 0) \sim t^{-\gamma}$, where t is the reduced temperature, $t=|T-T_c|/T_c$, and $\gamma$ is the bulk susceptibility critical exponent[17]. In this study, we test these scaling relations by measuring the enlarged effective hydrodynamic radius (R) of spherical particles due to critical adsorption.

**Methods**

**Materials and preparation**

The colloidal particles used in this experiment were fluorescently labeled green silica nanospheres purchased from Microspheres-Nanospheres, Inc., of radii approximately 25 nm and 10 nm. The critical mixture used was 2, 6 lutidine + water (LW). LW has an inverted coexistence curve with a lower critical temperature of ~33.9 $^0$C and a critical composition of 28.2% lutidine by weight. These particles possess small surface charges. Lutidine is the prefered solvent as it adsorbs onto the surface of the particles[112]. This was verified by observing that the majority of the particles reside in the lutidine-rich phase in the two-phase

region. To set up the experiment, the sample was prepared by mixing the lutidine with water at the critical composition and then ultrasonicating the mixture. Next, the sample was inserted in a home-built sample cell. Then, the temperature of the sample cell was controlled using a commercial temperature controller (Lakeshore, Inc.) and was regulated ± 3 mK over 1 hour. Finally, measurements were taken within 25 mK of $T_c$, so that the size-ratio $y= R_0/\xi$ was varied by a factor of about 40.

**Experimental technique**

We choose the fluorescence correlation spectroscopy method for investigation because the particle concentration in these experiments is much lower ($< 10^{-5}$ v/v) compared to other traditional methods of particle-size measurements, such as scattering. The sample cell was placed on the stage of a Zeiss inverted microscope. Near-infrared light pulsed from a femtosecond Ti:Sapphire laser was focused through a long working distance objective (63x, NA=0.75) into the liquid mixture. Fluorescence was excited only at the focus of the laser spot, collected through the same objective, and detected by single photon counting modules. The laser power was kept below 1 mW. By utilizing two-photon excitation of the fluorophores at the focus of a laser beam, we could measure diffusion within a tiny focal volume of the order of 0.1 femtoliter (Fig. 1a). Fluctuations in the fluorescence signal was induced by molecules entering and leaving the illuminated region (Fig. 1b). By calculating the autocorrelation function, $G(\tau)$ of this fluctuation (F), $G(\tau)= <\delta F(t)\delta F(t+\tau)>/<F(t)>^2$, and using a suitable model to analyze it, the center-of-mass diffusion coefficient of the particles was obtained. The hydrodynamic radius (R) of the particle was determined from the measured diffusion coefficient by using the Stokes-Einstein (SE) relation: $R=k_BT/6\pi\eta D$, where $k_B$ is Boltzmann's constant, T is the absolute temperature and $\eta$ is

the viscosity of the binary solvent (Fig. 1c inset). All experiments were performed at the one-phase region of the liquid mixture.

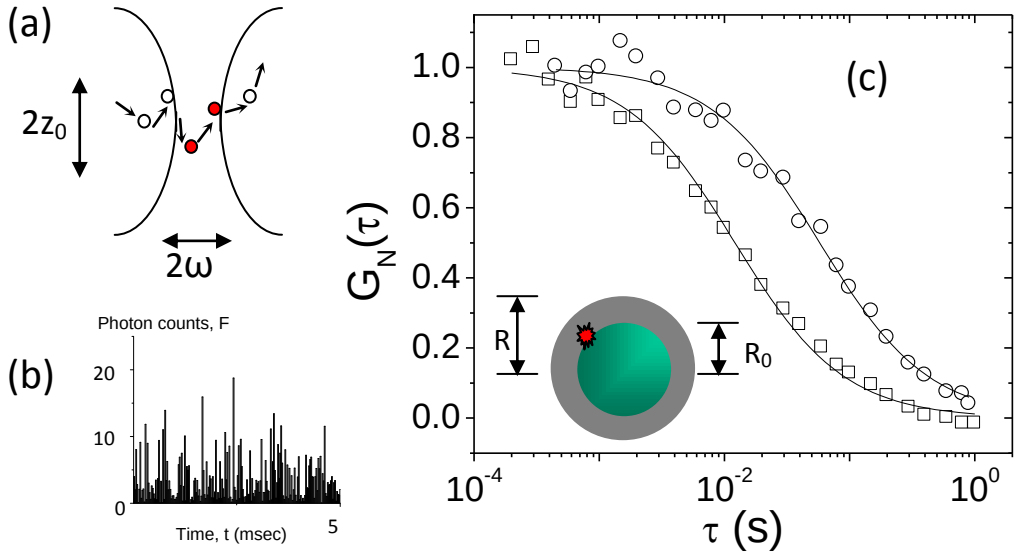


**FIG 1.** Experimental scheme: (a) A focused femtosecond laser caused two-photon excitation of fluorophores within a cylindrical volume of dimensions $\omega_0$~0.4 μm and $z_0$~2 μm. (b) Photon emission counts fluctuate with time, resulting from the diffusion of particles into and out of the focus spot. (c) Normalized intensity-intensity autocorrelation functions $G_N(\tau)$ of $R_0 \approx 25$ nm $SiO_2$ colloids plotted as a function of logarithmic time lag $\tau$ for two temperatures: $\Delta T = T_c - T = 1.125$ K (squares, D = 3.56 $\mu m^2/s$) and $\Delta T = 0.025$ K (circles, D = 0.88 $\mu m^2/s$). The solid lines correspond to single diffusion time fits. (Inset) The schematic of a nanoparticle was attached with a fluorescent dye and an adsorbed liquid layer. $R_0$ is the radius of the solid core and R- $R_0$ is the thickness of the adsorbed film.

## Results and Discussion

Figure 1c shows the autocorrelation functions collected from this experiment at two different temperatures for the particles of the radius, $R_0 \approx 25$ nm. The function is given by, $G(\tau)=G(0)/[(1+ 8D\tau/\omega_0^2)\sqrt{(1+8D\tau/z_0^2)}]$, where $\omega_0$ and $z_0$ are the half-widths of the excitation focus in lateral and axial directions, respectively. We obtained the diffusion coefficient (D) from the fitting of the autocorrelation function (ACF). Far away from $T_c$, by averaging over 3-

4 measurements, we determined D ≈3.5 $\mu m^2/s$ and 8 $\mu m^2/s$ in LW critical mixture for $R_0$=25 and 10 nm particles, respectively. These are close to the expectation from SE relation based on the known viscosity of the solution ($\eta$=2.6 cP) at room temperature[118]. In addition, the ACFs can be fitted with a single diffusion coefficient indicating that the polydispersity of the particles (about 10%) can be neglected

Figure 2 shows the variation of diffusion coefficients for both particles as a function of $\Delta T$ (=$T_c$-T), which decreases as the critical temperature is approached. Each point in the graph is the average, and the error bars are the standard deviation measured in three experiments. The graph shows this trend with different samples. Turbidity of the sample does not present major problem in the range of temperatures, where the experiments were performed. However, because of strongly scattered signal measurements becomes difficult very close to $T_c$ (within 10 mK). By taking into account the temperature dependence of viscosity especially its weak divergence near $T_c$, we have determined the hydrodynamic radius (R)[118]. By subtracting the hard sphere size of the particle ($R_0$), the thickness of the adsorbed layer has been obtained, which was plotted against the reduced temperature (t) in the Fig 2 insets. The results found in this study indicate that there is an enhancement of the adsorbed film thickness as the $T_c$ is approached. We are aware of suggestions that near the critical point, when the growing correlation length becomes larger than the particle size, the SE relation could break down.

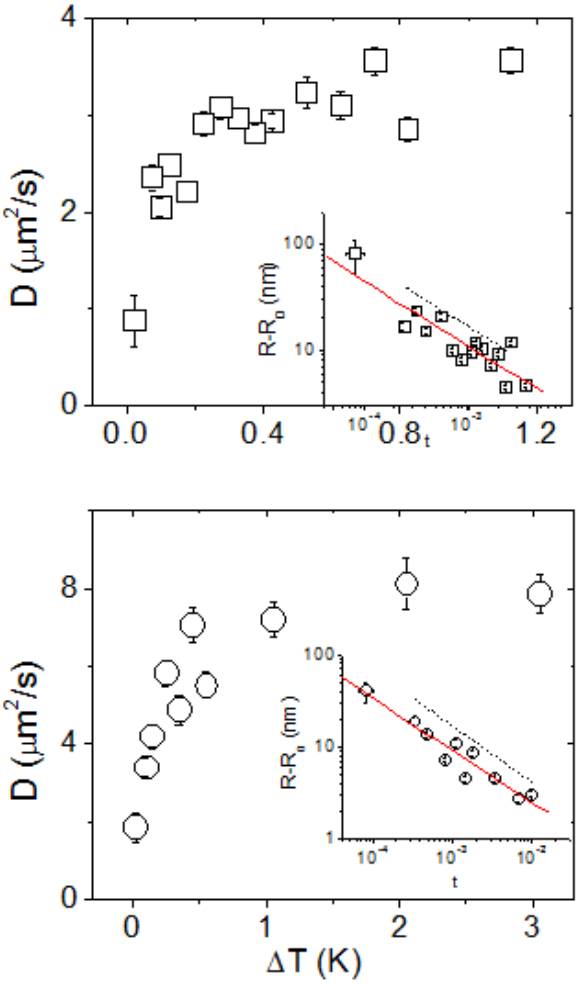


**FIG 2.** Diffusion coefficient of 25 nm (top) and 10 nm (bottom) $SiO_2$ particles plotted against ΔT. (Insets) The thickness of the adsorbed liquid layer on the surface of particles plotted as a function of reduced temperature (t). The solid line is the best fit and the dashed line is the variation of the correlation length (ξ).

However, we have verified through studies of diffusion of fluorescent molecules that SE relation is obeyed even very close to $T_c$[119]. A more direct test of this verification will be to use a liquid-vapor system near the critical point and to study the diffusion of particles to check the validity of SE relation. Nonetheless, within the temperature range in this experiment, the thickness of the adsorbed film follows behavior similar to that of the correlation length, which is given by $\xi = \xi_0 t^-$

$^{\upsilon}$. We obtained $\upsilon$=0.61 and 0.56 for 25 nm and 10 nm particles, compared to literature value of $\upsilon$=0.63[120].

The excess adsorption ($\Gamma$), which describes the total enrichment of the preferred component by volume, was also determined. Assuming that the result of the adsorption is an enlarged sphere, we have used a simple relation to calculate: $\Gamma = 4\pi(R^3 - R_0^3)/3$. To compare our results with theoretical ansatz, we then derived a dimensionless quantity, $\Gamma_e$ as a function of the size ratio $y=R_0/\xi$, where $\Gamma_e = \Gamma/(A_0 M_- \xi_0)$; $A_0=4\pi R_0^2$ is the surface area of the particle, and $M_-$ is the coefficient of the bulk order parameter, which is ≈ 0.9 for LW. As shown in Fig. 3, the results for the two different sized particles indicate that although their functional forms are similar, the excess adsorption per unit area on $R_0$≈10 nm particles is systematically lower compared to $R_0$≈25 nm particles. These results can be compared to currently available theoretical studies[17], according to which, $\Gamma_e$ is governed by a universal scaling function, which in the limit $t\rightarrow 0$ is given by the following: $\Gamma_e(y) = g_+ \frac{t^{\beta-\nu}-1}{\nu-\beta} + t^{\beta-\nu} G(y)$. Here, $g_+$ is a universal number, whose numerical value ≈ 0.6[120]. In Fig. 3 we plotted the theoretical scaling form for the excess adsorption using Ising exponents, $\beta \approx 0.32$, $\nu \approx 0.63$. The functional form of the theoretical prediction for excess adsorption is consistent with the experimental data. Good data collapse is obtained when $\Gamma_e$ is plotted vs. reduced temperature as shown in the Fig. 3 inset. The solid line is a least square fit of the data to a power law. The slope of this line is -0.97 ± 0.12, which is close to the mean field value of the bulk susceptibility exponent. For comparison, we have also plotted in the figure the expectation from the Ising exponent.

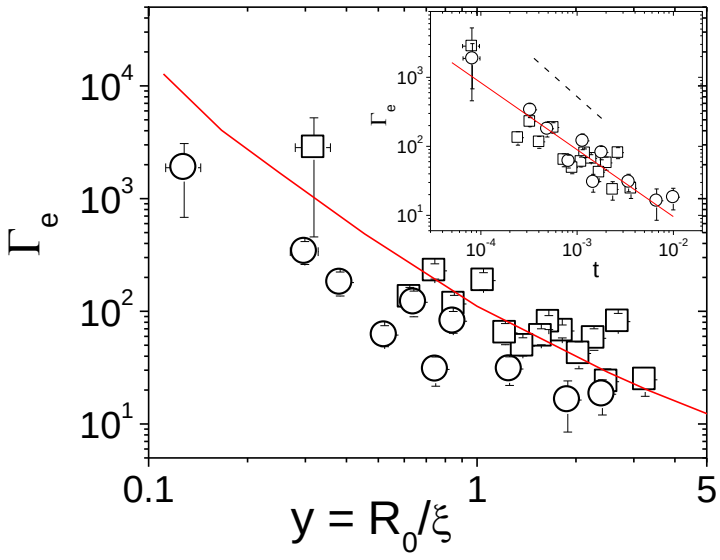


**FIG 3.** The quantity $\Gamma_e$ is plotted as a function of $y= R_0/\xi$ for both particles (squares: 25 nm, circles: 10 nm). The solid line is the theoretical mean-field prediction. (Inset) $\Gamma_e$ vs. t on a log-log scale. The solid line through the data corresponds to the slope of -0.97. The dashed line has a slope of -1.24.

## Conclusion

In summary, we have used the FCS experimental method to study the critical adsorption on particles possessing high surface curvature. These experiments have determined the temperature dependence of excess adsorption near the critical point of a binary liquid mixture. The results from this investigation will be useful in understanding the collective behavior of colloidal suspensions and in situations where fluids interact with structured substrates such as near corners and edges.

# CHAPTER 6

## KINETICS OFADSORPTION OF GOLD NANOPARTICLES ON SOLID/LIQUID INTERFACES

Interactions of macromolecules, colloids and bioparticles such as proteins with solid/liquid interfaces leading to adsorption is of great importance in many practical process such as filtration procedures, electrophoresis, and chromatography. A fascinating new application of colloid adsorption is the “colloid bar coding” technique, which enables the encoding of libraries of a million of compounds by using a fluorescent dyes. Understanding the kinetics and mechanisms of particle adsorption phenomena is relevant for colloid science, biophysics. Moreover, in the field of medicine, one can control protein and cell separation, enzyme immobilization, thrombosis, etc.

The kinetic aspects of adsorption is caused by widely varying transport conditions including diffusion[121-124], forced convection[125], or mixing[126, 127]. Colloid particle adsorption proceeds via more complicated path than molecular adsorption because particle transfer from the bulk to the interface is affected by many interactions differing in magnitude and the characteristic length scale. The diffusion transport mechanism was the dominating one in various experimental studies on colloid and protein adsorption. However, the disadvantage of diffusion controlled transport is its inherent unsteadiness, leading to considerable decrease in adsorption rate with time[128].

Due to the significance of protein adsorption, many works have been carried out to explain mechanisms and kinetics of these processes[129]. The experimental techniques used to quantify the amount of the adsorbed substance include reflectometry[124, 130-132], ellipsometry[133,

[134], and total internal reflection fluorescence (TIRF)[125, 135]. Proteins have the propensity to adsorb to interfaces because they are interfacially active molecules, and they are spontaneously accumulated at interfaces[136]. Physical adsorption at a liquid-solid interface is due to favorable van der Waals, ionic and/or polar interactions. It is important to predict the amount of protein adsorbed to a surface as a function of time and certain protein and surface properties. The protein adsorption kinetics can be mimicked by colloid systems. The advantage of working with colloid systems is that the adsorbed particles can be directly detected and counted by using optical microscopy or AFM.

The adsorption of colloids and proteins is often irreversible, that is, desorption and surface diffusion are slow compared to the rate of adsorption. In these cases, the random sequential adsorption (RSA) model may apply. In this model, particles are represented as rigid objects that deposit sequentially at random positions onto surface. This process continues until no additional particles may be placed on the surface, and the maximum (jamming) coverage $\Theta_{mx}$ is attained. In addition, overlapping with a previously placed particle is rejected and a new place is chosen. The determination of the adsorption kinetics under the diffusion-controlled regime is often used in protein adsorption studies. The adsorption is governed by two parameters: the dimensionless adsorption constant $\overline{k_a}$ and the maximum (jamming) coverage $\Theta_{mx}$. The adsorption rate is governed by the equation:

$$\frac{d\Theta}{d\tau} = \overline{k_a} c \left(1 - \frac{\Theta}{\Theta_{mx}}\right)^n \qquad 6.1$$

In addition, the limiting long-time solution derived from this equation has the form:

$$\Theta = \Theta_{mx}(1 - e^{-\overline{k_a}\tau/\Theta_{mx}}) \qquad 6.2$$

Johnson and Lenhoff determined the kinetics of colloid particles using atomic force microscopy (AFM). They measured the particle adsorption kinetics in a stepwise manner by immersing a mica sheet into the colloid suspension (polystyrene latex of average diameter 116 nm), and the results of their experiments is shown in Fig. 6.1. There is a good agreement between the theoretical and experimental data, which suggest that RSA model can account for colloid adsorption kinetics and can be exploited to predict protein adsorption kinetics.

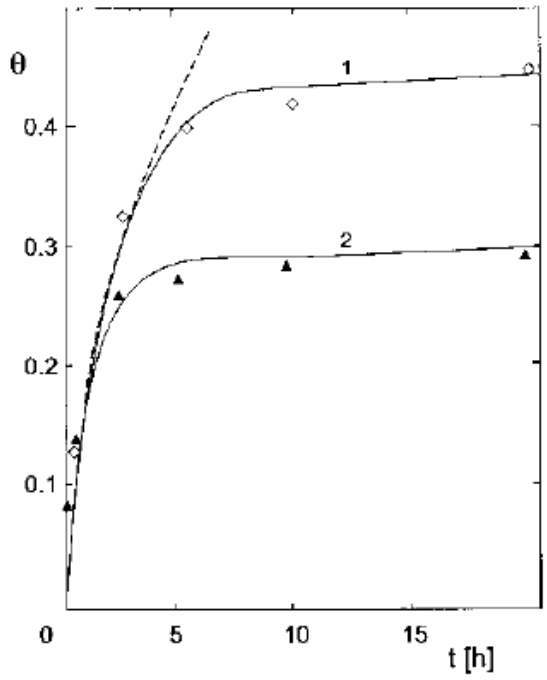


Fig. 6.1 Adsorption kinetics of Latex particles on mica under the diffusion-controlled transport( AFM method); the particle coverage versus the adsorption time t dependence for two different concentrations: curve 1,2. The continuos lines represent the exact theoretical results derived numerically. The continuos line represents the theoritical results of RSA model (Józef Tóth 2002).

In this chapter, the kinetics of gold nanoparticle (of radius 10 nm) adsorption on silicon wafer were investigated as a function of the diffusion of these particles in polymer solution with different concentrations. As found in chapter 4, the diffusion of the probe gold nanoparticles in polymer solutions decreased monotonically with concentration. The thickness of the adsorbed

layer of gold nanoparticles was measured as a function of time using ellipsometry. Understanding the relationship between the adsorption kinetics of these particles and the diffusion is important in protein adsorption studies.

Control experiments have been done using different polymer-liquid combinations to ensure that the polymers do not adsorb on the surface of the silicon wafers. On the other hand, we search for the suitable colloid nanoparticles that adsorb onto the surface of the wafers. Gold nanoparticles was negatively charged citrate-passivated. In this case, the substrate must be positively charged to bind electrostatically the gold nanoparticles. Silicon wafers were immersed in base solution of NaOH for 15 minutes, after that they rinse with deionized (DI) water. The samples have been dried out using argon gas and they exposed to ultraviolet/ozone (UVO) treatment for 30 min in order to generate a large number of surface-bound hydroxl groups, which are required for coupling organosilane. The samples were coated with 3-aminopropyltri ethoxysilane (APTES) using vapor diffusion method. Aqueous solutions of poly vinyl alcohol purchased from Sigma were prepared with different concentrations: 0,1, 2, 3, 4, and 5 % (wt %). The gold nanoparticles were added to these solution in very low concentrations ($<10^{-4}$ % v/v). The silicon wafers were placed in a home-built cell and filled with polymer solutions. A dynamical measurement of the thickness were performed using a phase-modulated ellipsometer (Beaglehole Instruments) whose angle of incident was fixed near the Brewster angle. The data were recorded at equally spaced time interval using lock-in amplifier. Following this, the diffusion of the gold nanoparticles of the same sample was measured using FCS.

The y- lock-in amplifier signal, which is linearly proportional to the ellipticity $\bar{\rho}$ (a quantity proportional to the thickness of the adsorbed layer) is recorded as a function of time. Fig. 3 shows the plot of $\bar{\rho}$ versus time for two different concentrations of PVA-water: 1% and 5

%. The data were fitted using equation 6.2, which is an exponential growth. The two fitting parameters are $\Theta_{mx}$ and $\overline{k_a}$ . If we let $\tau_a = \Theta_{mx}/\overline{k_a}$, then we can fit the data of one parameter $\tau_a$ and $\Theta_{mx}$.

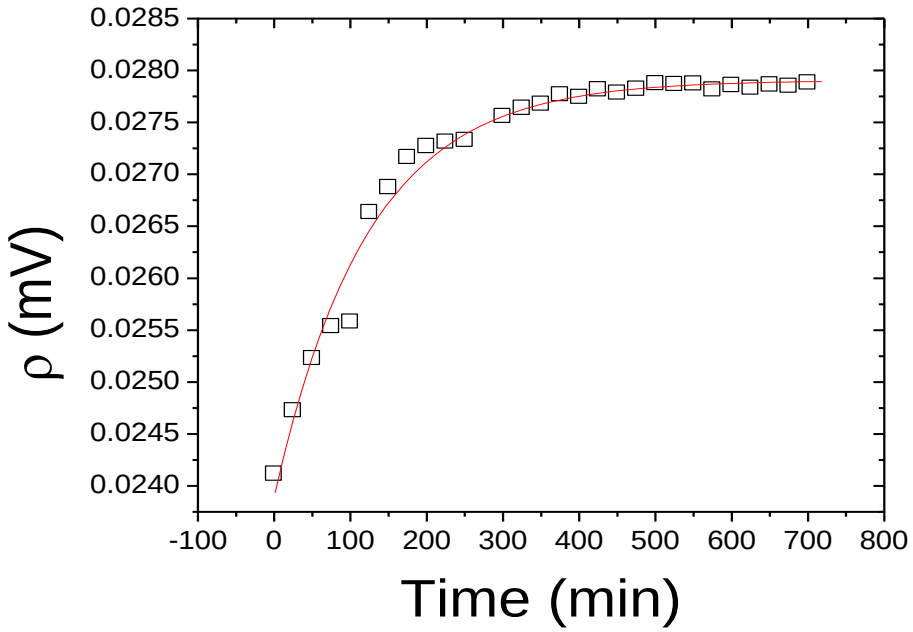


Fig 6. 2. The ellipticty as a function of time for two different concentrations of PVA-water solutions: 2 % (top) and 4 % ( bottom), the solid line is the fit of the data using 31500 s, 3800 s , respectively.

As we see from Fig. 6.3, the time constant is decreased when the concentration of polymer solution is increased. We know from chapter 4 that the diffusion of gold nanoparticles is decreased by increasing the polymer concentration. This means that the time constant is proportional to the diffusion of the goldnanoparticles. A suggested explanation to these observed results is that the faster the nanoparticles the longer time they need to settle down and adsorbed onto the surface. The time constant $\tau_a$ obtained from the fitting line in Fig. 3 is plotted versus concentration in Fig. 6.4

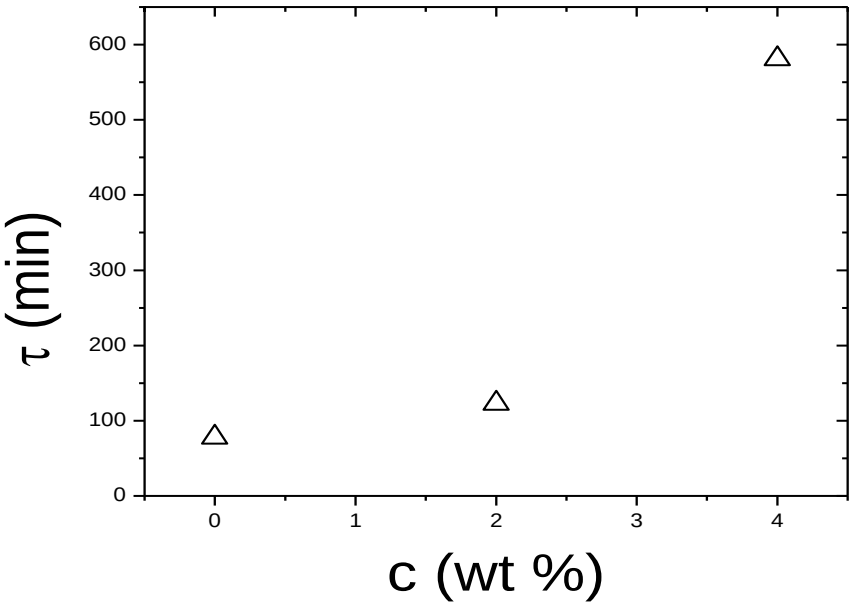


Fig. 6.3. The time constant of the exponential growth of the adsorped layer of gold nanoparticle on silicon wafers. The data of $\tau_a$ is obtained from the fitting parameter to the equation: $\bar{\rho} = \rho_{mx}(1 - e^{-\tau/\tau_a})$

The maximum thickness $\rho_{mx}$ , which is the second parameter of the fitting equation was plotted versus cocncetration. As Fig. 6.5 shows, $\rho_{mx}$ is decreased with concentration

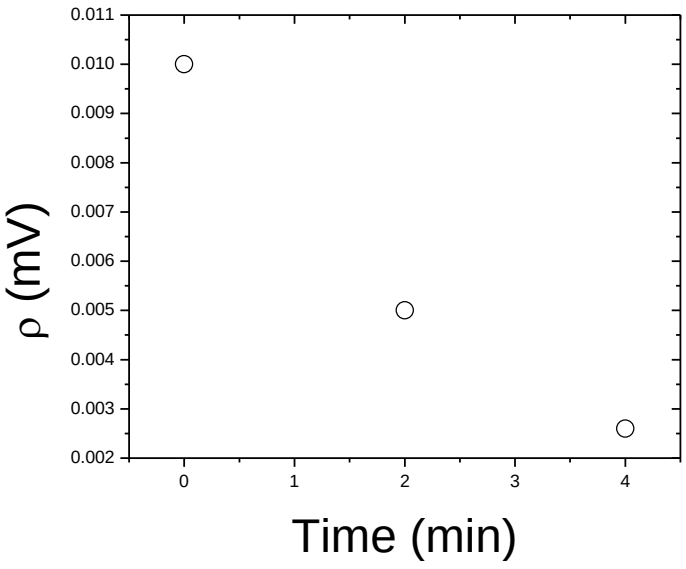


Fig. 6.4 The maximum thickness $\rho_{mx}$ ( y lock-in amplifier signal) versus cocncetration.

In conclusion, we have studied the adsorption kinetics of gold nanoparticles which was controlled by the diffusion using ellipsometry. The thickness of the adsorped layer was measured as a function of time. The time constant of the maximum adsorption was determined by fitting the data with an exponential growth function. The results show that the time constant of adsorption deceases as the diffusion coefficient of the nanoparticle decreases.

# CHAPTER 7

## CONCLUSION AND FUTURE WORK

My experiments in this dissertation have focused on conducting fundamental investigation in the dynamics and kinetics of polymeric-colloidal systems. Understanding the interaction of nanoparticles with macromolecules (polymers, proteins, etc.) is important in numerous problems of technological and medical interests, such as developing high performance polymeric materials, nano-template surfaces, and effective drug delivery vehicles. In the broader context, research in soft matter field has importance for characterization of polymer nanocomposites, multicomponent polymer systems, etc. In our lab, I was doing research using novel spectroscopy techniques called fluorescence correlation spectroscopy (FCS), which can offer structural and dynamical information about these systems with unprecedented spatial and temporal resolution, down to the atomic and molecular scale. This allows us to understand the issue of heterogeneities in soft matter systems. Another technique is ellipsometry, which is generally used to measure the thickness of thin films. In our research, we have been used ellipsometry to investigate the kinetics of adsorption layer of the nanoparticles on liquid/solid interface.

The mesoscopic length scale of soft condensed matter allows them to fluctuate in any thermal environment. They are subjected to random force from surrounding molecules and they undergo Brownian motion. The dynamics observed for polymers, colloids, and fluorescent dyes were all driven by Brownian diffusion. It has been recognized that combinations of these systems, like for example polymers and colloids, exhibit new properties which are found in each system separately. These mixed systems have a higher degree of complexity than the separate systems. An important part of this complexity is the effective interactions between the

macromolecules which, in complex systems, are not limited to the coulomb and quantum-mechanical interactions. Instead, it depends on many degrees of freedom of the solvent, and it is already the result of a thermodynamic average. The optical measurements of FCS and ellipsometry were performed by myself under the supervision and assistance of my advisor, Dr. Ashis Mukhopadhyay. These experiments allowed us to report important observations in Chapters 4 – 6.

Length scales influence the diffusion of colloids in semidilute and entangled polymer solution environments. The Stokes-Einstein (SE) relation was developed for mesoscopic objects surrounded by a homogenous distribution of smaller solvent molecules. Colloids smaller than the polymer mesh of semidilute and entangled network violate this assumption. Our experiments on 5 nm diameter gold colloids in semidilute and entangled solution of polymer with 18 nm radius of gyration illustrate deviation from the SE prediction. The colloids diffused from 7 (at the lower concentration) to 47 ( at the higher concentration) times faster when compared SE theory that employed the solution viscosity. In this case, motion of the particle is not completely coupled with the polymer matrix relaxation, and the particle experienced local nanoviscosity. Moreover, we observe anomalous diffusion behavior of the gold nanoparticles at higher concentration of polymer solution. This indicates that the mean square displacement increase less than linearly with time and shows the importance of heterogeneous environment of the concentrated polymer solutions. If we use smaller probes (free dyes), we observe normal diffusion behavior. A number of questions are still open in this context, including what is the length-scale for which we observe a crossover from solvent viscosity to macroviscosity.

Spherical colloidal nanoparticles immersed in critical binary mixture was studied to determine the critical adsorption profile on the surface of these particles by using FCS. The

temperature dependence of the adsorbed film thickness and excess adsorption was determined from FCS measurements of the enlarged effective hydrodynamic radius of the particles. Our results indicated that the adsorbed film thickness is of the order of correlation length associated with concentration fluctuations. The excess adsorption per unit area increases following a power law in reduced temperature with an exponent of 1, which is the mean-field value for the bulk susceptibility exponent. The volume fraction of the colloidal particles was much lower compared to other traditional methods. Experiments with high volume fraction were also performed, but the data were yet not analyzed. There is expectation that the particles alter the critical behaviors, such as the critical temperature and critical composition. Moreover, we would like to address the effect of changing the interaction between the particles by either adding salt to change the electrostatic interaction or coating the particles with polymers to change the steric interaction.

The kinetics of adsorption gold nanoparticles immersed in polymer solution on silicon wafers were investigated using ellipsometry. The thickness of the film saturates after some time for every sample depending on the concentration of the polymer solution. The saturated value, which is the maximum thickness of the adsorption layer depend inversely on the polymer solution concentration. On the contrary, the time required for saturation increased with polymer concentration. There will be an extension for this study to measure the diffusion of the gold nanoparticles and the results will be analyzed to see if there is a relation between the kinetics of the adsorption and the diffusion.

# REFERENCES


1. R. A. L. Jones, *Soft Condensed Matter*. (Oxford University Press, Oxford, 2006).
2. I. W. Hamley, *Introduction to Soft Matter-Revised Edition*. (John Wiley & Sons, Ltd., Chichester, 2007).
3. C. Park, J. Yoon and E. L. Thomas, Polymer **44**, 6725-6760 (2003).
4. J. K. G. Dhont, G. Gompper, G. Nägele, D. Richter and R. G. Winkler, *Soft matter from synthetic to biological materials*. (Forschungszentrum Jülich GmbH, Jülich, 2008).
5. B. J. Park and E. M. Furst, Langmuir **26**, 10406–10410 (2010).
6. J. A. Lipton-Duffin, J. A. Miwaa, M. Kondratenko, F. Cicoira, B. G. Sumpterd, V. Meunier, D. F. Perepichkab and F. Roseia, Proc. Nat. Acad. Sci. USA **107**, 11200-11204 (2010).
7. G. J. Fleer, M. A. Cohen, J. M. Stuart, H. J. Schjeutjens, T. Cosgrove and B. Vincent, *Polymers at Interfaces*. (Chapman and Hall, London, 1993).
8. J. A. Forrest and R. A. L. Jones, *Polymer Surfaces, Interfaces and Thin Films* (World Scientific, Singapore, 2000).
9. B. Frank, A. P. Gast, T. P. Russell, H. R. Brown and C. Hawker, Macromolecules **29**, 6531-6534 (1996).
10. S. Granick, S. K. Kumar, E. J. Amis, M. Antonietti, A. C. Balazs, A. K. Chakraborty, G. S. Grest, C. Hawker, P. Janmey, E. J. Kramer, R. Nuzzo, T. P. Russell and C. R. Safinya, Polym. Sci., Part B: Polym. Phys. **41**, 2755-2793 (2003).
11. R. A. L. Jones, S. K. Kumar, D. L. Ho, R. M. Briber and T. P. Russell, Nature **400**, 146-149 (1999).
12. H. Kim, A. Ruhm, L. B. Lurio, J. K. Basu, J. Lal, S. G. J. Mochrie and S. K. Sinha, Phys. Rev. Lett. **90**, 068302 (2003).

13. J. Klein, Y. Kamiyama, H. Yoshizawa, J. N. Israelachvili, G. H. Fredrickson, P. Pincus and L. J. Fetters, Macromolecules **26**, 5552-5560 (1993).

14. D. Leckband and J. N. Israelachvili, Q. Rev. Biophys. **34**, 105-267 (2001).

15. M. E. Fisher and P. G. de Gennes, C. R. Acad. Sci., Ser. B **287**, 207 (1978).

16. D. S. P. Smith, B. M. Law, M. Smock and D. P. Landau, Phys. Rev. E **55**, 620 (1997).

17. A. Hanke and S. Dietrich, Phys. Rev. E **59**, 5081-5100 (1999).

18. B. M. Law, M. D. Brown, L. Marchand, L. B. Lurio, W. A. Hamilton, I. Kuzmenko, T. Gog, S. Satija, E. Watkins and J. Majewski, Eur. Phys. J-Spec. Top. **167**, 127-132 (2009).

19. M. P. Gelfand and R. Lipowsky, Phys. Rev. B. **36**, 8725-8735 (1985).

20. D. Beysens and T. Narayanan, J. Stat. Phys. **95**, 997-1008 (1998).

21. V. Gurfein, D. Beysens and F. Perrot, Phys. Rev. A **40**, 2543-2546 (1989).

22. D. Beysens and D. Estève, Phys. Rev. Lett. **54**, 2123-2126 (1985).

23. P. D. Gallagher, M. L. Kurnaz and J. V. Maher, Phys. Rev. A **46**, 7750-7755 (1992).

24. B. M. Law, J.-M. Petit and D. Beysens, Phys. Rev. E **57**, 5782-5794 (1998).

25. R. R. Netz, Phys. Rev. Lett. **76**, 3646-3649 (1996).

26. C. RascÓn and A. O. Parry, Nature **407**, 986-989 (2000).

27. Y. Jayalakshmi and E. W. Kaler, Phys. Rev. Lett. **78**, 1379-1382 (1997).

28. H. Guo, T. Narayanan, M. Sztuchi, M. Schall and G. H. Wegdam, Phys. Rev. Lett. **100**, 188303 (2008).

29. M. C. Stewart and R. Evans, Phys. Rev. E **71**, 011602 (2005).

30. A. J. Archer, R. Evans, R. Roth and M. Oettel, J. Chem. Phys. **122**, 084513 (2005).

31. A. Drzewinski, A. Maciolek, A. Barasinski and S. Dietrich, Phys. Rev. E. **79**, 041145 (2009).

32. M. Rubinstein and R. H. COLBY, *Polymer Physics*. (Oxford University Press, New York, 2003).

33. L. Masaro and X. X. Zhu, Prog. Polym. Sci. **24**, 731-775 (1999).

34. R. Liu, X. Gao, J. Adams and W. Oppermann, Macromolecules (2005).

35. J. Won, C. N. Onyenemezu, W. G. Miller and T. P. Lodge, Macromolecules **27**, 7389 (1994).

36. D. S. P. Smith, B. M. Law, M. Smock and D. P. Landau, Phys. Rev. E **55**, 620-636 (1997).

37. A. Hanke and S. Dietrich, phys. Rev. E **59**, 5081–5100 (1999).

38. B. M. Law, M. D. Brown, L. Marchand, L. B. (Lurio, W. A. Hamilton, I. Kuzmenko, T. Gog, S. Satija, E. Watkins and J. Majewski, J. Special Topics **167**, 127-132 (2009).

39. M. E. Fisher and P. G. de Gennes, C. R. Acad. Sci., Ser. B **287**, 207-209 (1978).

40. R. Garcia, S. Scheidemantel, K. Knorr and M. H. W. Chan, Phys. Rev. E **68**, 056111 (2003).

41. T. J. Sluckin, Phys. Rev. A. **41**, 960-964 (1990).

42. T. W. Burkhardt and E. Eisenriegler, Phys. Rev. Lett. **74**, 3189-3192 (1995).

43. F. Schlesener, A. Hanke and S. Dietrich, J. Stat. Phys. **110**, 981-1013 (2003).

44. J. R. Lakowicz, *Principles of Fluorescence Spectroscopy*. (Kluwer Academic/Plenum Publishers, New York, 1999).

45. M. T. Cicerone, F. R. Blackburn and M. D. Ediger, Macromolecules **28**, 8224-8232 (1995).

46. M. M. Somoza, M. I. Sluch and M. A. M. Berg, **36**, 2721- 2732 (2003).

47. N. J. e. a. Durr, Nano Lett. **7**, 941-945 (2007).

48. M. Lippitz, M. A. van Dijk and M. Orrit, Nano Lett. **5**, 799-802 (2005).

49. R. A. Farrer, F. L. Butterfield, V. W. Chen and J. T. Fourkas, Nano Lett. **5**, 1139-1142 (2005).

50. C. A. Grabowski, B. Adhikary and A. Mukhopadhyay, Appl. Phys. Lett. **94**, 021903 (2009).

51. P. Hinterdorfer and A. van Oijen, *Handbook of Single-Molecule Biophysics*. (Springer Science+Business Media, LLC, London, 2009).

52. A. Einstein, *Investigations on the Theory of the Brownian Movement*. (Dover, NY, 1985).

53. B. J. Berne and R. Pecora, *Dynamic Light Scattering*. (Dover Publication, New York, 2000).

54. P. T. Callaghan, *Principles of Nuclear Magnetic Microscopy*. (Clarendon Press, Oxford, 1991).

55. D. Harvey, *Modern Analytical Chemestry*. (McGraw-Hill, Boston, 2000).

56. W. Liu, T. Cellmer, D. Keerl, J. M. Prausnitz and H. W. Blanch, Biotechnol. Bioeng. **90**, 482-490 (2005).

57. D. E. Madge, E. L. Elson and W. W. Webb, Phys. Rev. Lett. **29**, 705-708 (1972).

58. E. L. Elson and D. E. Madge, Biopolymers **13**, 1-27 (1974).

59. O. Krichevsky and G. Bonnet, Rep. Prog. Phys. **65**, 251–297 (2002).

60. P. Schwille and E. Haustein, *Fluorescence Correlation Spectroscopy: An Introduction to its concepts and applications*. (Biophysics Textbook Online, 2002).

61. S. Maiti, U. Haupts and W. W. Webb, Proc. Nat. Acad. Sci. USA **94**, 11753–11757 (1997).

62. K. M. Berland, P. T. C. So and E. Gratton, Biophys. J. **68**, 694-701 (1995).

63. W. Denk, J. H. Strickler and W. W. Webb, Science **73** (1990).

64. Y. Imanishi, K. H. Lodowski and Y. Koutalos, Biochemistry **46**, 9674-9684 (2007).

65. G. H. Tompkins, *A User's Guide to Ellipsometry*. (Academic Press, Inc., London, 1993).

66. A. Rothen, Rev. Sci. Instruments **16**, 16 (1945).

67. R. M. A. Azzam and N. M. Bashara, *Ellipsometry and Polarized Light*. (Elsevier Science Pub. Co., New York, 1989).

68. H. Arwin, M. Poksinski and K. Johansen, Appl. Optics **43**, 3028-3036 (2004).

69. S. A. Alterovitz, G. H. Buabbud, J. A. Woollam and D. C. Liu, J. Appl. Phys. **54**, 1559-1569 (1983).

70. D. Beaglehole, J. Chem. Phys. **73**, 3366 (1980).

71. Beaglehole, (2003).

72. R. Omari, C. A. Grabowski and A. Mukhopadhyay, J. Phys. Chem. B **113**, 8449–8452 (2009).

73. A. C. Balazs, T. Emrick and T. P. Russell, Science **314**, 1107-1110 (2006).

74. H. Kang, F. A. Detcheverry, A. N. Mangham, M. P. Stoykovich, K. C. Daoulas, R. J. Hamers, M. Muller, J. J. de Pablo and P. F. Nealey, Phys. rev. Lett. **100**, 148303 (2008).

75. Y. Lin, A. Boker, J. B. He, K. Sill, H. Q. Xiang, C. Abetz, X. F. Li, J. Wang, T. Emrick, S. Long, Q. Wang, A. Balazs and T. P. Russell, Nature, 55-59 (2005).

76. D. S. Banks and C. Fradin, Biophysical J. **89**, 2960-2971 (2005).

77. M. Weiss, M. Elsner, F. Kartberg and T. Nilsson, Biophys. J. **87**, 3518–3524 (2004).

78. T. G. Mason and D. A. Weitz, Phys. ReV. Lett. **74**, 1250 (1995).

79. V. Pryamitsyn and V. Ganesan, Phys. ReV. Lett. **100**, 128302 (2008).

80. M. J. Solomon and Q. Lu, Curr. Opin. Colloid Interface Sci. **6**, 430 (2001).

81. J. Sprakel, J. van der Gucht, M. A. Cohen Stuart and N. A. M. Besseling, Phys. ReV. Lett. **99**, 208301 (2007).

82. G. S. Ullmann, K. Ullmann, R. M. Lindner and G. D. J. J. Phillies, Phys. Chem. **89**, 692 (1985).

83. X. Ye, P. Tong and L. J. Fetters, Macromolecules **31**, 5785 (1998).

84. C. N. Onyenemezu, D. Gold, M. Roman and W. G. Miller, Macromolecules **26**, 3833 (1993).

85. P. G. de Gennes, Macromolecules **9**, 587 (1976).

86. T. Odijk, Biophys. J. **79**, 2314–2321 (2000).

87. A. G. Ogston, B. N. Preston and J. D. Wells, Proc. R. Soc. London Ser. A **333**, 297–316 (1973).

88. A. G. Ogston, Trans. Faraday Soc. **54**, 1754–1757 (1958).

89. G. D. J. J. Phillies, W. Brown and P. Zhou, Macromolecules **25**, 4948 (1992).

90. G. D. J. J. Phillies and D. Clomenil, Macromolecules **26**, 167 (1993).

91. G. D. J. phillies, J. Non-Cryst. Solids. **612**, 131–133 (1991).

92. R. I. M. Cukier, 1984, 17, 252, Macromolecules **17**, 252 (1984).

93. A. R. Altenberger and M. Tirrell, J. Chem. Phys. **80**, 2208 (1984).

94. B. Amsden, Polymer **43**, 1623 (2002).

95. P. G. de Gennes, *Scaling concept in polymer physics.* (Cornell University Press, 1979).

96. F. B. Wyart and P. G. de Gennes, Eur. Phys. J. E, 93–97 (2000).

97. D. Langevin and F. Rondelez, Polymer **19**, 875–882 (1978).

98. P. Tong, X. Ye, B. J. Ackerson and L. J. Fetters, Phys. rev. Lett. **79**, 2363 (1997).

99. T. Cherdhirankorn, A. Best, K. Koynov, K. Peneva, K. Muellen and G. Fytas, Macromolecules **113**, 3355 (2009).

100. J. Liu, D. Cao and L. Zhang, J. Phys. Chem. C **112**, 6653-6661 (2008).

101. H. Zettl, W. Hafner, A. Boker, H. Schmalz, M. Lanzendorfer, A. H. E. Muller and G. Krausch, Macromolecules **37**, 1917 (2004).

102. R. Radunz, D. Rings, K. Kroy and F. Cichos, J Phys. Chem. A **113**, 1674 (2009).

103. F. Hamada, S. Kinugasa, H. Hayashi and A. Nakajima, Macromolecules **18**, 2290 (1985).

104. H. Sanabria, Y. Kubota and M. N. Waxham, Biophys. J. **92**, 313 ( 2007).

105. T. G. Fox and S. Loshaek, J. Polym. Sci. **15**, 371 (1955).

106. B. P. Chekal and J. M. Torkelson, Macromolecules **35**, 8126 (2002).

107. A. A. Grishcuk and Y. I. Estrin, Russ. J. Appl. Chem. **80**, 1940 (2007).

108. J. Brandrup, E. H. Immergut, E. A. Grulke, A. Abe and D. R. Bloch, *Polymer Handbook 4th ed*. (John Wiley & Sons, New York, 2005).

109. M. Saxton, Biophys. J. **66**, 394 (1994).

110. F. Amblard, A. C. Maggs, B. Yurke, A. N. Pargellis and S. Leibler, Phys. ReV. Lett. **77**, 4470 (1996).

111. K. Devanand and J. C. Selser, Macromolecules **24**, 5943–5947 (1991).

112. D. Beysens and T. Narayanan, J. Stat. Phys. **95**, 997-1008 (1999).

113. B. M. Law, J.-M. Petit and D. Beysens, Phys. Rev. E **57**, 5782-5794 (1998).

114. R. R. Netz, Phys. Rev. Lett. **76**, 3646-3649 (1996).

115. Y. Jayalakshmi and E. W. Kaler, Phys. Rev. Lett. **78**, 1379-1382 (1997).

116. A. Hanke, F. Schlesener, E. Eisenriegler and S. Dietrich, Phys. Rev. Lett. **81**, 1885-1888 (1998).

117. H. Guo, T. Narayanan, M. Sztuchi, P. Schall and G. H. Wegdam, Phys. Rev. Lett. **100**, 188303 (2008).

118. E. Gülari, A. F. Collings, R. L. Schmidt and C. J. Pings, J. Chem. Phys. **56**, 6169 (1972).

119. C. Grabowski and A. Mukhopadhyay, Phys. Rev. Lett. **98**, 207801 (2007).

120. D. S. P. Smith, B. M. Law, M. Smock and D. P. Landau, Phys. Rev. E **55**, 620 (1997).

121. H. J. Vanenckevort, D. V. Dass and A. G. Langdon, J. Colloid Interface Sci. **98**, 138-143 (1984).

122. B. R. Young, B. R. Pitt and S. L. Cooper, J. Colloid Interface Sci. **124**, 28-43 (1988).

123. P. Vandlum and W. Norde, J. Colloid Interface Sci. **91**, 248-255 (1983).

124. W. Norde and J. Lyklema, Colloids Surf. **38**, 1-13 (1989).

125. C. T. Shibata and A. M. Lenhoff, J. Colloid Interface Sci. **148**, 485-507 (1992).

126. A. V. Elgersna, R. L. J. Zsom, W. Norde and J. Lyklema, Colloids Surf. **54**, 89-101 (1991).

127. J. Yoon, H. Y. Park and J. H. Kim, J. Coll. Interface Sci. **177**, 613-620 (1996).

128. J. Tóth, (Marcel Dekker, Inc., New York, 2001).

129. Z. Adamczyk, J. Coll. Interface Sci. **229**, 477–489 (2000).

130. J. Buijs, P. A. W. vandenBerg, J. W. T. Lichtenbelt, W. Norde and J. Lyklema, J. Colloid Interface Sci. **178**, 594-605 (1996).

131. J. Buijs, D. D. White and W. Norde, Colloids Surf. B **8**, 239-249 (1997).

132. W. Norde, M. Giesbers and H. Pingsheng, colloids Surf. B **5**, 255-263 (1995).

133. C. G. Golander and E. Kiss, J. Colloid Interface Sci. **121**, 240-253 (1988).

134. M. Wahlgren, T. Arnebrant and I. Lundstrom, J. Colloid Interface Sci. **175**, 506-514 (1995).

135. V. Hlady, D. R. Reincke and J. D. Andrade, J. Colloid Interface Sci. **111**, 555-569 (1986).

136. V. Hlady, J. Buijs and H. P. Jennissen, Methods Enzymol. **309**, 402-429 (1999).

# ABSTRACT

## DYNAMICS OF NANOPARTICLES IN COMPLEX FLUIDS

by

**RAMI A. OMARI**

August 2011

**Advisor**: Dr. Ashis Mukhopadhyay

**Major**: Physics

**Degree**: Doctor of Philosophy

Soft matter is a subfield of condensed matter including polymers, colloidal dispersions, surfactants, and liquid crystals. These materials are familiar from our everyday life- glues, paints, soaps, and plastics are examples of soft materials. Many phenomena in these systems have the same underlying physical mechanics. Moreover, it has been recognized that combinations of these systems, like for example polymers and colloids, exhibit new properties which are not found in each system separately. These mixed systems have a higher degree of complexity than the separate systems. In order to understand their behavior, knowledge from each subfields of soft matter has to be put together. One of these complex systems is the mixture of nanoparticles with macromolecules such as polymers, proteins, etc. Understanding the interactions in these systems is essential for solving various problems in technological and medical fields, such as developing high performance polymeric materials, chromatography, and drug delivery vehicles.

The author of this dissertation investigates fundemental soft matter systems, including colloid dispersions in polymer solutions and binary mixture.

The diffusion of gold nanoparticles in semidilute and entangled solutions of polystyrene (PS) in toluene were studied using fluorescence correlation spectroscopy (FCS). In our experiments, the particle radius ($R \approx 2.5$ nm) was much smaller compared to the radius of gyration of the chain but comparable to the average mesh size of the fluctuating polymer network. The diffusion coefficient (D) of the particles decreased monotonically with polymer concentration and it can be fitted with a stretched exponential function. At high concentration of the polymer, a clear subdiffusive motion of the particles was observed. The results were compared with the diffusion of free dyes, which showed normal diffusive behavior for all concentrations. In another polymer solution, poly ethylene glycol (PEG) in water, the diffusion of the gold nanoparticles depends on the dimentionlesss length scale $R/\xi$, where R is the radius of the nanoparticle and $\xi$ is the average mesh size of the fluctuating polymer network.

FCS were used to study the critical adsorption on curved surfaces by utilizing spherical nanoparticles immersed in a critical binary liquid mixture of 2,6 lutidine + water. The temperature dependence of the adsorbed film thickness and excess adsorption was determined from FCS measurements of the enlarged effective hydrodynamic radius of the particles. Our results indicated that the adsorbed film thickness is of the order of correlation length associated with concentration fluctuations. The excess adsorption per unit area increases following a power law in reduced temperature with an exponent of -1, which is the mean-field value for the bulk susceptibility exponent.

The kinetics of adsorption of gold nanoparticles in polymer solutions on silicon substrate was studied using ellipsometry by measuring the thickness of the adsorbed layer versus time. The data showed an exponential growth with relaxation time constants, which is proportional to the diffusion of the gold nanoparticles in polymer solution.

## AUTOBIOGRAPHICAL STATEMENT

**Education:**

- 2006-2011, Wayne State University, Detroit MI: Doctor of Philosophy in Condensed Matter Physics
- 1998-2002, Yarmouk University, Irbid, Jordan: Master of Science in Physics
- 1994-1998, Yarmouk University, Irbid, Jordan: Bachelor of Science in Physics

**Publications:**

1. Omari, R. A.; Grabowski, C. A.; Mukhopadhyay, A. Effect of Surface Curvature on Critical Adsorption, Phys. Rev. Lett. 103, 225705 (2009).

2. Omari, R. A.; Aneese, A. M.; Grabowski, C. A.; Mukhopadhyay, A. Diffusion of nanoparticles in semidilute and entangled polymer solutions, J. Phys. Chem. B. 113 8449-52 (2009).

3. Abumurad, K. M.; Omari, R. A. Indoor radon levels in irbid and health risk from internal doses, Radiation Measurements 43 S389–S391 (2008)

4. Omari, R. A.; Mukhopadhyay, A. Diffusion of nanoparticles probes in semidilute poly(ethylene glycol)-water solution, in preparation to submit to Macromolecules in April 2011

5. Omari, R. A.; Kohli, I.; Mukhopadhyay, Kinetics of the adsorption of gold nanoparticles on solid/liquid interfaces. In preparation to submit to Physical Review E in May 2011